UNIVERSITY OF CALIFORNIA SAN DIEGO

Improving and Assessing Monosynaptic Rabies Tracing as a Tool for Cortical Circuit Tracing

A dissertation submitted in partial satisfaction of the requirements for the degree

Doctor of Philosophy

in

Neurosciences

by

Maribel Patiño

Committee in Charge:

Professor Edward Callaway, Chair
Professor Brenda Bloodgood, Co-Chair
Professor Christina Gremel
Professor Byungkook Lim
Professor Eran Mukamel

2022

The dissertation of Maribel Patiño is approved, and it is acceptable in quality and form for publication on microfilm and electronically.

University of California San Diego

2022

DEDICATION

Dedicated to my parents, Amalia and Esteban Patiño, who multiple times uprooted their lives to provide me with the opportunity to pursue an education.

EPIGRAPH

Pero los centros nerviosos, órganos de complicadísima arquitecturas,
han resistido durante muchísimos años a la curiosidad de los sabios,
pudiendo afirmarse que solo recientemente,
y merced a la invención de métodos analíticos ingeniosísimos,
nos van entregando progresivamente el ansiado secreto de su intima estructura.

Santiago Ramón y Cajal
Textura del Sistema Nervioso del Hombre y de los Vertebrados

TABLE OF CONTENTS

Dissertation Approval Page iii

Dedication iv

Epigraph v

Table of Contents vi

List of Abbreviations viii

List of Figures ix

Acknowledgements x

Vita xii

Abstract of the Dissertation xiii

Introduction 1

Chapter 1. Single-cell transcriptomic classification of rabies-infected cortical neurons 13
- Abstract 13
- Introduction 13
- Results 16
- Discussion 31
- Methods 36
- Appendix 42
- Acknowledgements 44
- References 45

Chapter 2. Laminar connectivity of mouse primary visual cortex examined using Single Transcriptome Assisted Rabies Tracing (START) 50
- Abstract 50
- Introduction 51
- Results 52
- Discussion 60
- Methods 61
- Appendix 66
- Acknowledgements 67
- References 68

Chapter 3. Quantification of monosynaptic rabies tracing efficiency 73
- Abstract 73
- Introduction 73
- Results 75

Discussion 84
Methods 86
Appendix 89
Acknowledgements 90
References 91

LIST OF ABBREVIATIONS

RVdG	glycoprotein-deleted rabies virus
scRNA-seq	Single-cell RNA sequencing
snRNA-seq	Single-nucleus RNA sequencing
Sst	Somatostatin
Pvalb	Parvalbumin
Vip	Vasoactive intestinal peptide
L2/3, L4, etc.	Layers 2/3, 4, etc. of the cerebral cortex
V1	Primary visual cortex

LIST OF FIGURES

Figure 1.1 Rabies infection induces global transcriptional changes in mouse V1 14

Figure 1.2 Rabies-infected nuclei can be transcriptomically classified de novo despite changes in gene expression 18

Figure 1.3 Preexisting cell type annotations can be transferred to rabies-infected nuclei 21

Figure 1.4 Cell-type specific rabies-induced transcriptional changes 23

Figure 1.5 Rabies infection differentially affects expression of inhibitory marker genes 25

Figure 1.6 Rabies infection differentially affects expression of excitatory marker genes 34

Figure 1.S1 Details on rabies-infected fluorescence-activated nuclei sorting 45

Figure 1.S2 Cell type composition of datasets 46

Figure 2.1 Transcriptomic characterization of rabies labeled input cells 64

Figure 2.2 Transcriptomic inputs to L2/3 excitatory neurons of mouse V1 67

Figure 2.3 Transcriptomic inputs to L6 CT excitatory neurons of mouse V1 70

Figure 2.S1 Details on rabies-labeled presynaptic input nuclei sorting, ... 107

Figure 3.1 RVdG-PSD95GFP-SynPhRFP allows simultaneous fluorescent labeling of pre and postsynaptic densities 108

Figure 3.2 Efficiency of transsynaptic spread from excitatory L4 Nr5a1+ starter cells to excitatory inputs 109

Figure 3.3 Efficiency of transsynaptic spread from inhibitory starter cells to excitatory inputs 110

Figure 3.S1 Schematic illustration of experimental design and timeline for control experiments without glycoprotein 111

ACKNOWLEDGEMENTS

I would like to acknowledge and thank all members of the Callaway lab for fostering a supportive and fun learning environment. I thank my advisor Professor Ed Callaway for his mentorship throughout my graduate training and for encouraging both my scientific and DEI endeavors. I thank Dr. Euiseok Kim and Dr. Celine Vuong for their discussions, thoughtful input, and guidance. I also thank all the amazing graduate students for their support spanning from technical help of minutia to emotional support. I also want to recognize and thank Paula Miyazaki, Will Lagos, and Neelakshi Patne who helped significantly with the work described in this dissertation. I also thank my thesis committee for their critical input and constructive feedback regarding this work.

I am grateful to my family and friends for providing an incredible support network while I pursued my PhD. Thank you to my parents Amalia and Esteban who offered endless encouragement, my brother Jorge, and all my friends. I also thank Christian Cazares for his boundless confidence in my ability to accomplish any feat and for encouraging me to constantly challenge myself. I also thank Kira and L the cats for their emotional support and amusing distractions.

Finally, I would like to thank all the diversity initiatives that have supported me throughout my academic career including the UC Berkeley Biology Fellows Program, UC Berkeley Bergeron Scholars Program, NSF – California Alliance for Minority Participation, NIH PREP, the Paul and Daisy Soros Fellowship for New Americans, and the SFN Neuroscience Scholars Program.

Chapter 1, in full, is a reprint of the material as it appears in: Patiño M, Lagos WN, Patne N, Tasic B, Zeng H, & Callaway EM (2022). Single-cell transcriptomic classification of rabies-infected cortical neurons. *Proceedings of the National Academy of Sciences*, *117* (23), 13066. The dissertation author was the primary investigator and author of this paper.

Chapter 2, in full, is currently being prepared for submission for publication and will include Marley Rossa, Will N. Lagos, and Neelakshi Patne, as co-authors and Professor Edward Callaway as the senior author. The dissertation author will be the first author of this work.

Chapter 3, in full, is currently being prepared for submission for publication and will include Will N. Lagos, and Neelakshi Patne, as co-authors and Professor Edward Callaway as the senior author. The dissertation author will be the first author of this work.

VITA

2014	Bachelor of Arts, Molecular and Cell Biology University of California Berkeley, Berkeley, CA, USA
2022	Doctor of Philosophy, Neurosciences University of California San Diego, La Jolla, CA, USA
2024	Doctor of Medicine University of California San Diego, La Jolla, CA, USA

PUBLICATIONS

Patiño, M., Lagos, W. N., Patne, N., Tasic, B., Zeng, H., & Callaway, E. M. (2022). Single-cell transcriptomic classification of rabies-infected cortical neurons. *Proceedings of the National Academy of Sciences*, *119* (22), e2203677119. https://doi.org/10.1073/pnas.2203677119.

Cali, C. P., **Patiño, M.**, Tai, Y. K., Ho, W. Y., McLean, C. A., Morris, C. M., Seeley, W. W., Miller, B. L., Gaig, C., Vonsattel, J. P. G., White, C. L., Roeber, S., Kretzschmar, H., Troncoso, J. C., Troakes, C., Gearing, M., Ghetti, B., Van Deerlin, V. M., Lee, V. M.-Y., … Lee, E. B. (2019). C9orf72 intermediate repeats are associated with corticobasal degeneration, increased C9orf72 expression and disruption of autophagy. *Acta Neuropathologica*, *138*(5), 795–811. https://doi.org/10.1007/s00401-019-02045-5

ABSTRACT OF THE DISSERTATION

Improving and Assessing Monosynaptic Rabies Tracing as a Tool for Cortical Circuit Tracing

by

Maribel Patiño

Doctor of Philosophy in Neurosciences

University of California San Diego, 2021

Professor Edward Callaway, Chair
Professor Brenda Bloodgood, Co-Chair

The mammalian cerebral cortex is composed of a diversity of neuronal cell types with distinct morphology, molecular composition, and electrophysiological properties. These neurons connect to one another to form complex microcircuits that underlie brain cortical processing. Thus, deciphering the precise input and output connectivity patterns of different neuronal cell types is conducive to understanding their functional roles in cortical processing. To this end

monosynaptic rabies tracing has been widely used for cortical circuit tracing studies and has had great impact on the understanding of neural circuit organization. Still, the advent of single-cell genomic technologies has unveiled that the extent of neuronal diversity may be much greater than originally imagined, raising new questions about the connectivity patterns of these more precisely defined cell subtypes. Our understanding of cortical circuit organization could benefit from higher throughput methods of assigning inputs to neuronal cell types and the ability to assign cells to finer subtypes. Chapter 1 explores the feasibility of combining monosynaptic rabies tracing with single-nuclei RNA-sequencing (snRNAseq) to identify the transcriptomic cell types that provide presynaptic inputs to defined populations of neurons. We found that, despite global and cell-type-specific rabies-induced transcription changes, rabies-infected cortical cells can still be classified according to established transcriptomic cell types when utilizing transcriptome-wide RNA profiles. In Chapter 2, we characterize the interlaminar synaptic connectivity of mouse primary visual cortex (V1) at the transcriptomic level using the newly developed method Single Transcriptome Assisted Rabies Tracing (START). We found that START generates results consistent with established circuit models validating the utility of START as a circuit tracing tool. More importantly, with the improved cell type granularity achieved with transcriptomic characterization of inputs, we were able to uncover subtypes of somatostatin and parvalbumin interneurons that provide input to L2/3 and L6 CT excitatory neurons. Finally, Chapter 3 describes the efficiency of rabies transsynaptic spread from starter cells to input neurons. We found that about 40% of inputs are labeled transsynaptically. Altogether, this dissertation reveals how transcriptomically defined cell-types are organized in V1 and introduces a novel circuit tracing technique that will expand the repertoire of tools available to neuroscientists.

Introduction

The neocortex is evolutionarily the newest addition to the mammalian brain and is responsible for the processing power that ultimately gives rise to higher order functions such as sensory perception, motor planning, attention, and language. It is composed of distinct, interconnected functional areas each containing complex neuronal microcircuits organized into columns and layers of distinct neuronal types. Many aspects of cortical organization and structure are conserved across functional areas and species [1], suggesting that canonical circuits and their underlying principles play a critical role in cortical function. Indeed, the functional properties of a neuron are largely derived from its excitatory and inhibitory inputs. Thus, mapping the detailed connectivity patterns of cortical circuits has been of great interest in the neuroscience field. To this end, the field has invested a plethora of time and resources towards the development of tools to facilitate this overarching goal[2] and much progress has been made in linking neuronal types, circuits, and behavior across multiple organisms[3]. However, the recent explosion of genomics technologies for characterizing neuronal types has profoundly altered our views of the numbers and diversity of genetically defined cell types in the mammalian brain [4], raising important questions about circuit organization at the level of these cell types. In this dissertation I introduce a new tool for deciphering cortical connectivity at transcriptomic resolution and apply it to elucidate interlaminar connectivity in mouse primary visual cortex.

Cortical neuron diversity and their contributions to cortical function

The mammalian cortex contains two major classes of neurons, glutamatergic excitatory pyramidal neurons and GABAergic inhibitory interneurons. While excitatory neurons are responsible for propagating signals, inhibitory interneurons gate signal flow and sculpt network

dynamics. Although inhibitory interneurons represent a minority of cortical neurons, dense axonal arborization allows them to balance and shape excitatory neuron activity, maintaining a fine-tuned excitation-inhibition balance throughout the cortex[5]. Importantly, human and animal studies indicate that subtle perturbations in excitatory-inhibitory balances are implicated in multiple psychiatric conditions[6]. Thus, deciphering the connectivity patterns between excitatory and inhibitory neurons is critical for obtaining an understanding of how the brain functions in both health and disease.

Cortical interneurons are a diverse population that have diverse morphological, molecular, and electrophysiological properties. In addition to these intrinsic characteristics, each neuron's function is shaped by its connectivity patterns. Cortical interneurons can be organized into several major groups based on their expression of selective markers: parvalbumin (Pvalb), somatostatin (Sst) and serotonin receptor 5HT3aR. Morphological and electrophysiological analysis of interneurons expressing these markers has revealed some of their general functions and connectivity patterns. Pvalb+ basket cells, the largest group of cortical interneurons, exhibit fast-spiking firing properties and their basket-shaped axonal boutons preferentially target the perisomatic region of their innervation target[5]. The majority of Sst+ interneurons, termed Martinotti cells, are characterized by an ascending axon that arborizes in layer 1 and targets the distal dendritic compartments of neurons[5]. The 5HT3aR+ interneurons population, the most heterogeneous group, includes vasoactive intestinal peptide (Vip)+ interneurons that are characterized by irregular burst spike firing properties and bipolar morphology[5]. Furthermore, connectivity studies[7–9] have shown that Pvalb + interneurons not only provide pyramidal neuron inhibition, but also selectively inhibit one another. In contrast, Sst+ interneurons inhibit all inhibitory populations, except themselves. Vip+ interneurons preferentially inhibit Sst+

interneurons and provide little input to pyramidal neurons. Importantly, with the emergence of tools to manipulate and monitor activity of defined cell types in vivo, specific inhibitory populations have become implicated in specific circuit functions. Studies across multiple cortical areas have implicated Pvalb + interneurons in gain control, Sst + interneurons in the suppression of lateral and top-down interactions, and Vip + interneurons in cortical disinhibition via the inhibition of Sst+ interneurons[10].

Despite advances in the understanding of inhibitory networks, much remains unknow largely due to the enormous diversity of inhibitory cell types. For example, within the Pvalb+ neuron group, a small population of neurons, termed chandelier cells, exhibit a distinct morphological axonal arborization pattern from basket cells, contact the axonal compartment of their target rather than the perisomatic area, and differ in spatial laminar location[5]. Within the 5HT3aR+ IN population, a small group of neurons expressing neuropeptide cholecystokinin (CCK), synapse on the soma of pyramidal neurons and are localized in distinct lamina from Vip+ cells[5]. In vitro[11] and in vivo[12] connectivity studies have also demonstrated highly specific local connections onto and from distinct inhibitory neuron subtypes. One study[13] of note highlighted the importance of separating major classes into more distinct cell type when studying the role of inhibitory neurons in cortical function. Here an Sst-Cre mouse line was used to conduct in vivo channelrhodopsin assisted patching from Sst+ inhibitory neurons in mouse S1 barrel cortex. Single cells were functionally assayed for modulation of their activity during active whisking and each cell was concurrently anatomically labeled for post-hoc dendritic and axonal processes reconstruction. This study revealed five distinct subtypes of Sst+ interneurons, each with unique morphology, connectivity, and whisking modulated activity. Interestingly, it also revealed a subpopulation of Sst+ interneurons with increased activity during active behavioral states and

decreased Vip+ interneuron synaptic input, a finding that is at odds with canonical Vip+/Sst+ circuit connectivity. It is now evident that inhibitory cell types have greater diversity than what can be captured with just three groups and that most inhibitory circuits cannot be defined with generalizable patterns.

Like inhibitory neurons, excitatory neurons in the primary visual cortex have diverse projection properties, morphology, and intrinsic physiology. They can be divided into three main groups according to their axonal projection patterns: intratelencephalic (IT) neurons, extratelencephalic (ET) neurons, and corticothalamic (CT) neurons. IT excitatory neurons are found across layers (L) 2-6 of the cortex and project to other neurons within the telencephalon including the striatum, amygdala, claustrum and ipsilateral and contralateral cerebral cortices[14]. ET neurons, also known as pyramidal tract (PT) neurons in certain cortical areas, project to subcortical destinations such as the brainstem, spinal cord, and thalamus. ET neurons are large pyramidal neurons found primarily in L5b[14]. CT neurons are found in L6 and project primarily to the ipsilateral thalamus.

Regarding the input patterns to excitatory neurons, basic connectivity principles shared across areas have been proposed. In the “canonical circuit” model information from thalamus is relayed to L4 IT cells from core thalamic cells[15]. Matrix cells from higher order thalamic nuclei project to L1 cortical cells and largely avoid L4[15]. Despite their extensive input to L2/3 and L5, L4 IT neurons do not receive comparable reciprocal input from these layers. Unlike L4 IT neurons which are specialized for processing extrinsic inputs, IT neurons in other layers primarily integrate signals from other cortical inputs. Therefore, their connectivity with each other tends to be bidirectional. Specifically, L2/3 IT neurons receive and send input to L5 IT neurons. L6 IT neurons are the least studied IT group, but studies[16] suggest that they receive

input primarily from other deep layer neurons. ET neurons function as integrators of local cortical and thalamic inputs to relay information to distal subcortical structures. Therefore, they receive extensive input from IT neurons in all cortical layers, especially from L2/3 IT neurons. L6 CT neurons lack substantial local input from other cortical layers and instead receive most of the inputs from higher order cortical areas[14].

Transcriptional characterization of inhibitory and excitatory cortical neurons

Although much work has been done to elucidate principles of cortical connectivity, detailed understanding of the specialized connectivity patterns underlying cortical networks remain largely incomplete and many aspects of cortical circuit organization remain unknown. Single-cell sequencing technologies have only recently begun to expose the full extent of cortical cell type diversity. Recent studies utilizing scRNAseq to study cortical cell type diversity across cortical areas, have found large numbers of clusters corresponding to putative cell types. In one study[17], scRNAseq data from more than 23,000 neurons from primary visual cortex (V1) and the anterior lateral motor cortex (ALM) revealed 133 distinct transcriptomic cell types: 61 inhibitory types, 56 glutamatergic, and 16 non-neuronal types. The transcriptomic inhibitory cell types identified included 20 Sst+, 10 Pvalb+, 16 Vip+, and 13 5HTR3A+/Vip- clusters, subdividing the major established inhibitory cell classes into a multitude of cell subtypes. Importantly, transcriptomic correlates of electrophysiological and morphological diversity within and across excitatory and inhibitory neuron have already begun to be established in multiple studies [17–19]. For example, using a binary intersectional approach to target a transcriptomic cluster in vivo, it was found that a VIP receptor expressing cluster of Pvalb+ neurons proves to correspond to chandelier cells[17]. Albeit relying on in vitro strategies, correlation was also established between

other transcriptomic clusters and morphological and electrophysiological distinct cell types in studies using PatchSeq to simultaneously conduct single-cell characterization of gene expression and electrophysiology in the same cell[18,20]. Together, these studies demonstrate that this recently identified transcriptomic diversity is real and that transcriptomic characterization of neurons can be beneficial in untangling the precise circuit connections underlying cortical processing.

Monosynaptic rabies tracing for cortical connectivity tracing

Monosynaptic rabies tracing using glycoprotein (G)-deleted rabies virus (RVdG) has been widely used for circuit tracing studies throughout the central and peripheral nervous systems and has had great impact on the understanding of neural circuit organization. This approach allows identification of the direct presynaptic inputs to specific cell types or to single neurons of interest, across the whole brain[21–23]. This is possible because rabies virus spreads selectively between synaptically connected neurons and then travels exclusively in the retrograde direction to label synaptic inputs. This method involves removing the rabies virus glycoprotein, an envelope protein necessary for transsynaptic spread, from the rabies genome and replacing it with a fluorescent reporter gene. RVdG is then pseudotyped with the avian sarcoma leucosis virus glycoprotein, EnvA, to allow genetic targeting of the primary infection. As EnvA pseudotyped RVdG (EnvA+ RVdG) requires the EnvA receptor, TVA, which is not expressed in mammalian cells, for entry, only mammalian cells engineered to express TVA can be infected by EnvA+ RVdG. Trans-complementation with rabies glycoprotein (G) allows the virus to spread retrogradely from the initially infected neurons, termed starter cells, and label their direct inputs. Retrograde spread is halted at the input neurons because they lack the glycoprotein required for further spread.

One of the most common applications of monosynaptic rabies tracing is to label the presynaptic inputs to a cell type that expresses Cre-recombinase in a mouse line [24]. To label the inputs to Cre+ neurons, Cre-dependent expression of TVA and rabies G in the desired starter neuron population is required. This can be achieved by infecting the desired started cell location with Cre-dependent helper AAVs expressing TVA and G. Following adequate time for expression of gene products, EnvA+ RVdG expressing a fluorescent reporter gene is injected in the same location resulting in the selective infection of the TVA expressing starter cells. Following adequate time for transsynaptic spread, viral replication, and labeling of input cells, the results can be analyzed. This approach has been used in previous studies investigating the inhibitory inputs to layer specific excitatory neurons[25], local interlaminar connectivity[26], and the brain-wide inputs to cortical inhibitory neurons[8] and excitatory neurons[27]. However, these studies fail to characterize the cell type identity of most inputs, limiting analysis to regional distribution of inputs. While one study[25] was designed to allow some characterization of input cell type identity, determination of cell type was only made at the subclass level and distinctions were limited to general Sst+, Vip+, and Pvalb+ subclasses and not the more refined subtypes.

Although monosynaptic rabies tracing is a well-developed and proven research tool, there is uncertainty about the efficiency of transsynaptic spread. In most cases RVdG only retrogradely labels a proportion of total inputs. For example, one study using electroporation into single pyramidal L2/3 starter cells found that only about 14 – 97 input cells per starter were labeled. Different studies using either tTA/TRE to drive expression of G[28] or transfection via whole-cell recording[29] observed about 250 or 500 inputs per starter neurons respectively. Although the true number of inputs onto a single starter neuron is unknown, electron microscopy data and Golgi studies suggest the amount labeled with rabies virus is far less than the total. Many factors have

been found to affect the efficiency of retrograde spread including the expression level of glycoprotein in the starter cells, time available for spread, initial number of rabies particles entering the starter cells, the use of different rabies virus strains[30], and the use of chimeric rabies glycoproteins[31]. While studies quantifying inputs onto single neurons have provided some insight into the efficiency of spread, the total proportion of inputs labeled across conditions remains unknown.

This dissertation seeks to assess the efficiency of and build upon monosynaptic rabies tracing, a widely used tool in neuroscience research that has led to a greater understanding of cortical connectivity across a multitude of brain areas. As our understanding of the diversity of cell types that make up the mammalian neocortex grows, it is imperative to investigate connectivity patterns at the level of these much more granular classifications. Chapter 1 describes the feasibility of combining monosynaptic rabies tracing with single cell transcriptomics to generate a novel tool for investigating connectivity at the level of cell types defined by their gene expression patterns. By sequencing large numbers of rabies-infected mouse primary visual cortical neurons, we show that they can be reliably transcriptomically classified with the use of transcriptome-wide RNA profiles despite rabies-induced changes in gene expression. In Chapter 2, we apply Single Transcriptome Assisted Rabies Tracing (START) to investigate local interlaminar connectivity in mouse primary visual cortex and provide compelling evidence that START can facilitate the discovery of new cortical circuit motifs. Finally, in Chapter 3 we assess the efficacy of retrograde input cell labeling of monosynaptic rabies tracing. Altogether this dissertation aims to expand the toolkit available to neuroscientists for exploring the complex connectivity patterns of the mammalian brain and help generate hypotheses about the functional role of distinct cortical neurons in both health and disease.

References

1. Douglas RJ, Martin KAC. Neuronal circuits of the neocortex. *Annu Rev Neurosci*. 2004;27:419-451. doi:10.1146/annurev.neuro.27.070203.144152

2. Koroshetz W, Gordon J, Adams A, Beckel-Mitchener A, Churchill J, Farber G, Freund M, Gnadt J, Hsu NS, Langhals N, Lisanby S, Liu G, Peng GCY, Ramos K, Steinmetz M, Talley E, White S. The State of the NIH BRAIN Initiative. *J Neurosci*. 2018;38(29):6427-6438. doi:10.1523/JNEUROSCI.3174-17.2018

3. Luo L, Callaway EM, Svoboda K. Genetic Dissection of Neural Circuits: A Decade of Progress. *Neuron*. 2018;98(2):256-281. doi:10.1016/j.neuron.2018.03.040

4. Armand EJ, Li J, Xie F, Luo C, Mukamel EA. Single-Cell Sequencing of Brain Cell Transcriptomes and Epigenomes. *Neuron*. 2021;109(1):11-26. doi:10.1016/j.neuron.2020.12.010

5. Tremblay R, Lee S, Rudy B. GABAergic Interneurons in the Neocortex: From Cellular Properties to Circuits. *Neuron*. 2016;91(2):260-292. doi:10.1016/j.neuron.2016.06.033

6. Marín O. Interneuron dysfunction in psychiatric disorders. *Nat Rev Neurosci*. 2012;13(2):107-120. doi:10.1038/nrn3155

7. Pfeffer CK, Xue M, He M, Huang ZJ, Scanziani M. Inhibition of inhibition in visual cortex: the logic of connections between molecularly distinct interneurons. *Nat Neurosci*. 2013;16(8):1068-1076. doi:10.1038/nn.3446

8. Wall NR, De La Parra M, Sorokin JM, Taniguchi H, Huang ZJ, Callaway EM. Brain-Wide Maps of Synaptic Input to Cortical Interneurons. *J Neurosci*. 2016;36(14):4000-4009. doi:10.1523/JNEUROSCI.3967-15.2016

9. Xu H, Jeong HY, Tremblay R, Rudy B. Neocortical Somatostatin-Expressing GABAergic Interneurons Disinhibit the Thalamorecipient Layer 4. *Neuron*. 2013;77(1):155-167. doi:10.1016/j.neuron.2012.11.004

10. Kepecs A, Fishell G. Interneuron cell types are fit to function. *Nature*. 2014;505(7483):318-326. doi:10.1038/nature12983

11. Dantzker JL, Callaway EM. Laminar sources of synaptic input to cortical inhibitory interneurons and pyramidal neurons. *Nat Neurosci*. 2000;3(7):701-707. doi:10.1038/76656

12. Hafner G, Witte M, Guy J, Subhashini N, Fenno LE, Ramakrishnan C, Kim YS, Deisseroth K, Callaway EM, Oberhuber M, Conzelmann KK, Staiger JF. Mapping Brain-Wide Afferent Inputs of Parvalbumin-Expressing GABAergic Neurons in Barrel Cortex Reveals Local and Long-Range Circuit Motifs. *Cell Reports*. 2019;28(13):3450-3461.e8. doi:10.1016/j.celrep.2019.08.064

13. Muñoz W, Tremblay R, Levenstein D, Rudy B. Layer-specific modulation of neocortical dendritic inhibition during active wakefulness. *Science*. 2017;355(6328):954-959. doi:10.1126/science.aag2599

14. Harris KD, Shepherd GMG. The neocortical circuit: themes and variations. *Nat Neurosci*. 2015;18(2):170-181. doi:10.1038/nn.3917

15. Jones EG. The thalamic matrix and thalamocortical synchrony. *Trends in Neurosciences*. 2001;24(10):595-601. doi:10.1016/S0166-2236(00)01922-6

16. Vélez-Fort M, Rousseau CV, Niedworok CJ, Wickersham IR, Rancz EA, Brown APY, Strom M, Margrie TW. The Stimulus Selectivity and Connectivity of Layer Six Principal Cells Reveals Cortical Microcircuits Underlying Visual Processing. *Neuron*. 2014;83(6):1431-1443. doi:10.1016/j.neuron.2014.08.001

17. Tasic B, Yao Z, Graybuck LT, Smith KA, Nguyen TN, Bertagnolli D, Goldy J, Garren E, Economo MN, Viswanathan S, Penn O, Bakken T, Menon V, Miller J, Fong O, Hirokawa KE, Lathia K, Rimorin C, Tieu M, Larsen R, Casper T, Barkan E, Kroll M, Parry S, Shapovalova NV, Hirschstein D, Pendergraft J, Sullivan HA, Kim TK, Szafer A, Dee N, Groblewski P, Wickersham I, Cetin A, Harris JA, Levi BP, Sunkin SM, Madisen L, Daigle TL, Looger L, Bernard A, Phillips J, Lein E, Hawrylycz M, Svoboda K, Jones AR, Koch C, Zeng H. Shared and distinct transcriptomic cell types across neocortical areas. *Nature*. 2018;563(7729):72-78. doi:10.1038/s41586-018-0654-5

18. Gouwens NW, Sorensen SA, Baftizadeh F, Budzillo A, Lee BR, Jarsky T, Alfiler L, Baker K, Barkan E, Berry K, Bertagnolli D, Bickley K, Bomben J, Braun T, Brouner K, Casper T, Crichton K, Daigle TL, Dalley R, de Frates RA, Dee N, Desta T, Lee SD, Dotson N, Egdorf T, Ellingwood L, Enstrom R, Esposito L, Farrell C, Feng D, Fong O, Gala R, Gamlin C, Gary A, Glandon A, Goldy J, Gorham M, Graybuck L, Gu H, Hadley K, Hawrylycz MJ, Henry AM, Hill D, Hupp M, Kebede S, Kim TK, Kim L, Kroll M, Lee C, Link KE, Mallory M, Mann R, Maxwell M, McGraw M, McMillen D, Mukora A, Ng L, Ng L, Ngo K, Nicovich PR, Oldre A, Park D, Peng H, Penn O, Pham T, Pom A, Popović Z, Potekhina L, Rajanbabu R, Ransford S, Reid D, Rimorin C, Robertson M, Ronellenfitch K, Ruiz A, Sandman D, Smith K, Sulc J, Sunkin SM, Szafer A, Tieu M, Torkelson A, Trinh J, Tung H, Wakeman W, Ward K, Williams G, Zhou Z, Ting JT, Arkhipov A, Sümbül U, Lein ES, Koch C, Yao Z, Tasic B, Berg J, Murphy GJ, Zeng H. Integrated Morphoelectric and Transcriptomic Classification of Cortical GABAergic Cells. *Cell*. 2020;183(4):935-953.e19. doi:10.1016/j.cell.2020.09.057

19. Naka A, Veit J, Shababo B, Chance RK, Risso D, Stafford D, Snyder B, Egladyous A, Chu D, Sridharan S, Mossing DP, Paninski L, Ngai J, Adesnik H. Complementary networks of cortical somatostatin interneurons enforce layer specific control. Svoboda K, Colgin L, Yu J, Petersen CC, eds. *eLife*. 2019;8:e43696. doi:10.7554/eLife.43696

20. Gouwens NW, Sorensen SA, Berg J, Lee C, Jarsky T, Ting J, Sunkin SM, Feng D, Anastassiou CA, Barkan E, Bickley K, Blesie N, Braun T, Brouner K, Budzillo A, Caldejon S, Casper T, Castelli D, Chong P, Crichton K, Cuhaciyan C, Daigle TL, Dalley R, Dee N, Desta T, Ding SL, Dingman S, Doperalski A, Dotson N, Egdorf T, Fisher M, de Frates RA, Garren E, Garwood M, Gary A, Gaudreault N, Godfrey K, Gorham M, Gu H, Habel C, Hadley K, Harrington J, Harris JA, Henry A, Hill D, Josephsen S, Kebede S, Kim L, Kroll M, Lee B, Lemon T, Link KE, Liu X, Long B, Mann R, McGraw M, Mihalas S, Mukora A, Murphy GJ, Ng L, Ngo K, Nguyen TN, Nicovich PR, Oldre A, Park D, Parry S, Perkins J, Potekhina L, Reid D, Robertson M, Sandman D, Schroedter M, Slaughterbeck C, Soler-Llavina G, Sulc J, Szafer A, Tasic B, Taskin N, Teeter C, Thatra N, Tung H, Wakeman W, Williams G, Young R, Zhou Z, Farrell C, Peng H, Hawrylycz MJ, Lein E, Ng L, Arkhipov A, Bernard A, Phillips JW, Zeng H, Koch C. Classification of electrophysiological and morphological neuron types in the mouse visual cortex. *Nat Neurosci*. 2019;22(7):1182-1195. doi:10.1038/s41593-019-0417-0

21. Wickersham IR, Finke S, Conzelmann KK, Callaway EM. Retrograde neuronal tracing with a deletion-mutant rabies virus. *Nat Methods*. 2007;4(1):47-49. doi:10.1038/nmeth999

22. Wickersham IR, Lyon DC, Barnard RJO, Mori T, Finke S, Conzelmann KK, Young JAT, Callaway EM. Monosynaptic Restriction of Transsynaptic Tracing from Single, Genetically Targeted Neurons. *Neuron*. 2007;53(5):639-647. doi:10.1016/j.neuron.2007.01.033

23. Callaway EM, Luo L. Monosynaptic Circuit Tracing with Glycoprotein-Deleted Rabies Viruses. *J Neurosci*. 2015;35(24):8979-8985. doi:10.1523/JNEUROSCI.0409-15.2015

24. Wall NR, Wickersham IR, Cetin A, Parra MDL, Callaway EM. Monosynaptic circuit tracing in vivo through Cre-dependent targeting and complementation of modified rabies virus. *PNAS*. 2010;107(50):21848-21853. doi:10.1073/pnas.1011756107

25. Yetman MJ, Washburn E, Hyun JH, Osakada F, Hayano Y, Zeng H, Callaway EM, Kwon HB, Taniguchi H. Intersectional Monosynaptic Tracing for Dissecting Subtype-Specific Organization of GABAergic Interneuron Inputs. *Nat Neurosci*. 2019;22(3):492-502. doi:10.1038/s41593-018-0322-y

26. DeNardo LA, Berns DS, DeLoach K, Luo L. Connectivity of mouse somatosensory and prefrontal cortex examined with trans-synaptic tracing. *Nat Neurosci*. 2015;18(11):1687-1697. doi:10.1038/nn.4131

27. Kim EJ, Juavinett AL, Kyubwa EM, Jacobs MW, Callaway EM. Three Types of Cortical Layer 5 Neurons That Differ in Brain-wide Connectivity and Function. *Neuron*. 2015;88(6):1253-1267. doi:10.1016/j.neuron.2015.11.002

28. Miyamichi K, Amat F, Moussavi F, Wang C, Wickersham I, Wall NR, Taniguchi H, Tasic B, Huang ZJ, He Z, Callaway EM, Horowitz MA, Luo L. Cortical representations of olfactory input by trans-synaptic tracing. *Nature*. 2011;472(7342):191-196. doi:10.1038/nature09714

29. Rancz EA, Franks KM, Schwarz MK, Pichler B, Schaefer AT, Margrie TW. Transfection via whole-cell recording in vivo: bridging single-cell physiology, genetics and connectomics. *Nat Neurosci*. 2011;14(4):527-532. doi:10.1038/nn.2765

30. Reardon TR, Murray AJ, Turi GF, Wirblich C, Croce KR, Schnell MJ, Jessell TM, Losonczy A. Rabies Virus CVS-N2cΔG Strain Enhances Retrograde Synaptic Transfer and Neuronal Viability. *Neuron*. 2016;89(4):711-724. doi:10.1016/j.neuron.2016.01.004

31. Kim EJ, Jacobs MW, Ito-Cole T, Callaway EM. Improved Monosynaptic Neural Circuit Tracing Using Engineered Rabies Virus Glycoproteins. *Cell Reports*. 2016;15(4):692-699. doi:10.1016/j.celrep.2016.03.067

Chapter 1. Single-cell transcriptomic classification of rabies-infected cortical neurons

Abstract

Cortical circuit tracing using modified rabies virus can identify input neurons making direct monosynaptic connections onto neurons of interest. However, challenges remain in our ability to establish the cell type identity of rabies-labeled input neurons. While transcriptomics may offer an avenue to characterize inputs, the extent of rabies-induced transcriptional changes in distinct neuronal cell types remains unclear and whether these changes preclude characterization of rabies-infected neurons according to established transcriptomic cell types is unknown. We used single-nucleus RNA sequencing to survey the gene expression profiles of rabies-infected neurons and assessed their correspondence with established transcriptomic cell types. We demonstrated that when using transcriptome-wide RNA profiles, rabies-infected cortical neurons can be transcriptomically characterized despite global and cell-type-specific rabies-induced transcriptional changes. Notably, we found differential modulation of neuronal marker gene expression, suggesting that caution should be taken when attempting to characterize rabies-infected cells with single genes or small gene sets.

Introduction

Monosynaptic rabies tracing using glycoprotein (G)-deleted rabies virus has been widely adopted for circuit tracing studies throughout the central and peripheral nervous systems and has had great impact on the understanding of neural circuit organization [1,2]. This approach allows for identification of the direct presynaptic inputs to specific cell types [3] or to single neurons of interest [4] across the whole brain. Recent advances in single-cell transcriptomics have profoundly

altered our views of the numbers and diversity of genetically-defined cell types [5], raising important questions about circuit organization at the level of these cell types and introducing new challenges for determining the identity of retrogradely labeled input cells. While some studies have successfully used rabies tracing to identify the cell-type-specific inputs to specific types of cortical neurons [6,7], classification of inputs relied either on antibody staining or intersectional methods using Cre-Flp intersectional fluorescent reporters. The former approach drastically limits the cell types that can be characterized because their identification relies on antibody availability and specificity and may also be subject to artifacts from the translation-inhibiting properties of rabies M protein [8]. The latter, while not subject to similar artifacts, are cumbersome, allowing for interrogation of only one cellular input type per experimental animal and requiring multiple experiments and Cre mouse lines to determine the identity of all input cells. Overall, connectivity tracing using rabies virus could benefit from higher throughput methods of assigning inputs to neuronal cell types and the ability to assign cells to finer subtypes.

One way to achieve these goals is to combine single-cell transcriptomics with monosynaptic rabies circuit tracing. Single-cell RNA sequencing (scRNA-seq) technologies have begun to expose the full extent of cortical cell type diversity and findings suggest that previously defined cell types may be composed of multiple distinct types. Studies utilizing scRNAseq to study neuronal cell type diversity across cortical areas have found large numbers of clusters corresponding to putative cell types [9,10]. In one study [11], scRNAseq data from more than 23,000 neurons from primary visual cortex (V1) and the anterior lateral motor cortex (ALM) revealed 133 distinct transcriptomic cell types: 61 inhibitory, 56 glutamatergic, and 16 non-neuronal types. Transcriptomic analyses revealed that each of the major cortical neuronal inhibitory

classes could be further divided into multiple inhibitory cell subtypes, including 20 somatostatin (Sst), 10 parvalbumin (Pvalb), 16 vasoactive intestinal peptide (Vip), and 13 ionotropic serotonin receptor (HTR3A)+/VIP- clusters (belonging to Lamp5 and Sncg subclasses). Furthermore, multiple studies are beginning to establish the transcriptomic correlates of functional, electrophysiological, and morphological diversity within and across excitatory and inhibitory neurons [12–14]. Together, these studies demonstrate that this transcriptomic diversity is meaningful and that transcriptomic characterization of neurons can be beneficial in untangling the precise circuit connections underlying cortical function.

Monosynaptic rabies tracing combined with single-cell transcriptomics could be a more efficient and precise method for determining the cell type identity of inputs to populations of interest than current methods. However, rabies virus infection is known to cause changes in host cellular transcription. Studies show that a major effect of rabies infection in the mouse brain is the global downregulation of gene expression and upregulation of genes involved in immune responses [15–17]. However, these studies were either performed on bulk tissue and could not investigate differential effects of infection across different cell types or they focused their scRNAseq analysis on non-neuronal cells at the infection site rather than on confirmed rabies-infected neurons. Therefore, the extent of transcriptional changes induced in distinct neuronal cell types and whether these changes preclude characterization of rabies-infected neurons according to established transcriptomic cell types remains unknown. Here, we used single-nucleus RNA sequencing (snRNA-seq) to assess the correspondence between rabies-infected and uninfected neuronal nuclei and investigated the effects of rabies infection on neuronal marker genes. We found that, despite global and cell-type-specific rabies-induced transcription changes, both neuronal and non-neuronal rabies-infected cells can still be classified according to

established transcriptomic cell types. Furthermore, we show that rabies differentially affects expression of neuronal marker genes, with certain marker genes being upregulated or downregulated and others remaining unperturbed. Of note, the canonical cortical inhibitory interneuron marker genes *Sst*, *Pvalb*, and *Vip* were strongly downregulated in rabies-infected nuclei. Our findings suggest that rabies tracing is compatible with transcriptomic characterization of input cells when utilizing transcriptome-wide RNA profiles, such as those obtained with snRNA-seq. We further illustrate that caution should be taken when attempting to characterize rabies-labeled cells with single marker genes or proteins. Finally, we have made our dataset of rabies-infected nuclei publicly available to serve as a resource to determine which genes may be most suitable for establishing rabies-labeled input identities with methods that rely on single genes or discrete gene sets, such as spatial transcriptomics or RNA fluorescence in situ hybridization (FISH).

Results

Rabies infection induces global transcriptional changes in mouse V1

To investigate the transcriptional response to rabies infection, we compared the transcriptomes of rabies-infected nuclei from mouse V1 with those from uninfected controls. Rabies-infected nuclei were collected from V1 of wild-type C57BL/6 mice (n=3, 2 females and 1 male) injected with unpseudotyped SAD-B19 G-deleted rabies virus expressing nuclear-localized mCherry (G+RVdG.H2B.mCherry) at P60-P75. Because excitatory neurons comprise about 80% of all cortical neurons [18], the majority of nuclei obtained with this approach were from excitatory neurons. To enrich for rabies-infected inhibitory neurons, Gad2-Cre mice were crossed to R26-LSL-TVA-LacZ mice [19] to express TVA in inhibitory neurons. These transgenic mice (n=8, 5

females and 3 males) were then injected with EnvA-pseudotyped G-deleted rabies virus expressing nuclear-localized mCherry (EnvA+RVdG.H2BmCherry) at P65-P85, which resulted in direct and selective rabies infection of the targeted inhibitory cell class (Figure 1.1A). The biased samples allowed more complete coverage of the rarer but more diverse inhibitory neuron types. 10 days after injection, V1 containing mCherry+ rabies-labeled nuclei was dissected and single-nucleus suspensions were prepared from dissected tissue for fluorescence-activated nuclei sorting (FANS) to collect mCherry+ nuclei (Figure 1.1A and Figure 1.S1A, 1.S1B). snRNA-seq of FANS sorted rabies-infected nuclei was performed using the 10X Genomics 3' Kit v3.1. The rabies dataset was compared to an independent snRNA-seq dataset composed of uninfected nuclei collected from V1 of control uninjected mice acquired using the 10X Genomics 3' Kit v3. The uninfected control dataset contained cell type annotations established according to the Allen Institute for Brain Science (AIBS) cell type taxonomy [11]. Following quality control filtering, principal-component analysis (PCA), and unsupervised graph-based clustering of 8,745 rabies-infected and 9,508 uninfected control nuclei, we applied Uniform Manifold Approximation and Projection (UMAP) to visualize gene expression relationships across infection status. The resulting UMAP plot illustrates that nuclei were grouped primarily by their infection status, with infected and uninfected neurons forming clearly separated clusters (Figure 1.1B). To examine the global response to rabies infection and identify possible gene expression differences between rabies-infected and uninfected nuclei, we performed differential expression (DE) analysis using Model-based Analysis of Single-Cell Transcriptomics (MAST) [20]. Upregulated differentially expressed genes (DEGs; adjusted $p < 0.05$; $\log2FC > 0.25$) (Figure 1.1C) included interferon response genes, such as *Stat1* and *Stat2*, involved in JAK-STAT signaling pathways, a pathway implicated in antiviral and innate immune responses. To better understand the possible functions

of upregulated and downregulated genes in rabies-infected nuclei we performed gene set enrichment analysis (GSEA). GSEA using Gene Ontology (GO) revealed that upregulated DEGs were highly enriched in viral response, innate immunity, and inflammatory pathways such as type 1 interferon signaling, cytokine production and response, and nuclear factor kappa B (NF-κB) signaling (Figure 1.1D). Downregulated genes were predominantly involved with cellular respiration, metabolic pathways, and cellular homeostasis. Additionally, downregulated genes were also enriched for genes encoding proteins involved in synaptic and somatodendritic compartments. These findings are consistent with prior bulk and single-cell RNA-seq studies exploring global or non-neuronal transcriptional changes following rabies infections [15,16,21].

Rabies-infected nuclei can be transcriptomically classified despite changes in gene expression

To characterize rabies-infected nuclei according to established transcriptomic cortical cell types, we used computational strategies for integrated analysis of snRNA-seq datasets that have been shown to enable comparisons of heterogeneous tissue across different experimental conditions [22,23]. Anchor-based data integration was used to identify anchors representing cells in similar biological states across datasets, which were used to guide the merging of the rabies-infected and uninfected control datasets. UMAP visualization of the integrated datasets confirmed that nuclei cluster according to biological cortical cell types and not by infectious status (Figure 1.2A). Clustering analysis segregated nuclei into 22 clusters (Figure 1.2B). Based on known marker genes for major neuronal and non-neuronal classes we identified 6 inhibitory neuron clusters that express GABAergic inhibitory interneuron markers *Gad1* and *Gad2*, 13 excitatory neuron clusters that express *Slc17a7*, which encodes the vesicular glutamate transporter VGLUT1,

Figure 1.1 Rabies infection induces global transcriptional changes in mouse V1. (A) Schematic of experiment workflow. C57BL/6 mice (n = 3, 2 females and 1 male) and Gad2Cre/+; R26LSL-TVA/+ (n = 8, 5 females and 3 males) were injected with unpseudotyped G+RVdG. H2B.mCherry and pseudotyped EnvA+RVdG.H2BmCherry, respectively. At 10 days after injection, V1 was dissected and mCherry+ nuclei collected using FANS. snRNA-seq of FANS–sorted rabies-infected nuclei was performed using the 10× Genomics platform. Scale bar: 500 μM. (B) UMAP of 8,745 rabies-infected nuclei (red) and 9,508 AIBS uninfected control nuclei (blue) merged without integration analysis. (C) Scatter plot displaying gene expression differences in rabies-infected nuclei versus AIBS uninfected control. The light-blue line indicates a perfect correlation. Genes with log2FC of >0.25 are highlighted in blue, and genes most up-regulated in the rabies-infected group are labeled. Values were averaged log normalized across all cells in each condition. (D) Dot plot of the top GO gene sets significantly (padj < 0.05, Benjamini–Hochberg correction) activated (Left) or suppressed (Right) in the rabies-infected dataset compared with AIBS uninfected control.

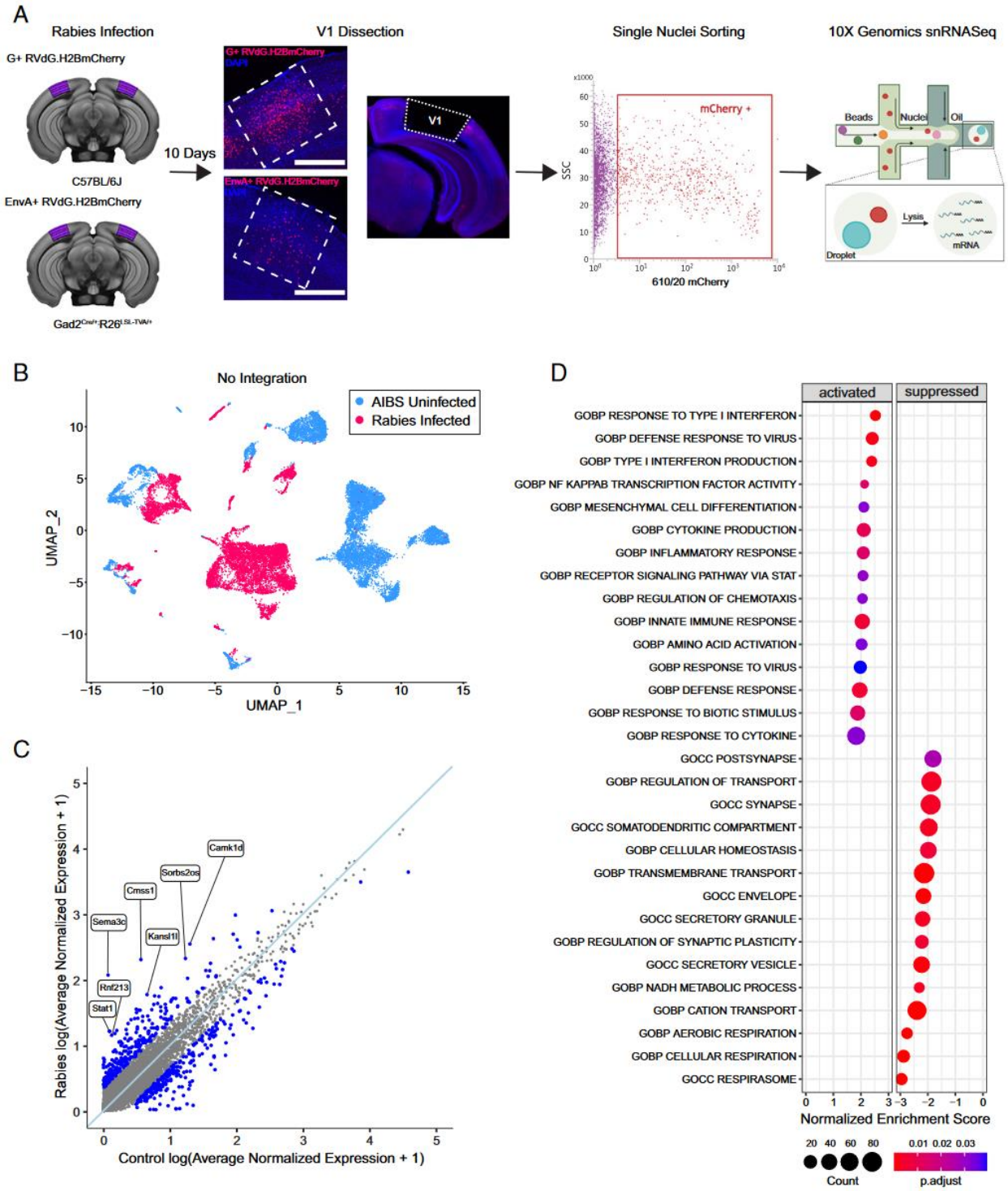
A
Rabies Infection
V1 Dissection
Single Nuclei Sorting
10X Genomics snRNASeq
G+ RVdG.H2BmCherry
10 Days
C57BL/6J
EnvA+ RVdG.H2BmCherry
Gad2Cre/+:R26LSL-TVA/+
V1
mCherry +
SSC
610/20 mCherry
Beads
Nuclei
Oil
Lysis
mRNA
Droplet
B
No Integration
AIBS Uninfected
Rabies Infected
UMAP_2
UMAP_1
C
Rabies log(Average Normalized Expression + 1)
Control log(Average Normalized Expression + 1)
Camk1d
Sorbs2os
Cmss1
Sema3c
Kansl1l
Rnf213
Stat1
D
activated
suppressed
GOBP RESPONSE TO TYPE I INTERFERON
GOBP DEFENSE RESPONSE TO VIRUS
GOBP TYPE I INTERFERON PRODUCTION
GOBP NF KAPPAB TRANSCRIPTION FACTOR ACTIVITY
GOBP MESENCHYMAL CELL DIFFERENTIATION
GOBP CYTOKINE PRODUCTION
GOBP INFLAMMATORY RESPONSE
GOBP RECEPTOR SIGNALING PATHWAY VIA STAT
GOBP REGULATION OF CHEMOTAXIS
GOBP INNATE IMMUNE RESPONSE
GOBP AMINO ACID ACTIVATION
GOBP RESPONSE TO VIRUS
GOBP DEFENSE RESPONSE
GOBP RESPONSE TO BIOTIC STIMULUS
GOBP RESPONSE TO CYTOKINE
GOCC POSTSYNAPSE
GOBP REGULATION OF TRANSPORT
GOCC SYNAPSE
GOCC SOMATODENDRITIC COMPARTMENT
GOBP CELLULAR HOMEOSTASIS
GOBP TRANSMEMBRANE TRANSPORT
GOCC ENVELOPE
GOCC SECRETORY GRANULE
GOBP REGULATION OF SYNAPTIC PLASTICITY
GOCC SECRETORY VESICLE
GOBP NADH METABOLIC PROCESS
GOBP CATION TRANSPORT
GOBP AEROBIC RESPIRATION
GOBP CELLULAR RESPIRATION
GOCC RESPIRASOME
Normalized Enrichment Score
Count
p.adjust

and 3 non-neuronal clusters corresponding to microglia, astrocytes, and oligodendrocytes expressing *Ctss*, *Slc1a3*, and *Mog* respectively. The proportion of excitatory (uninfected = 85.57% vs rabies = 75.38%), inhibitory (uninfected = 13.66% vs rabies = 20.86%), and non-neuronal nuclei (uninfected = 0.76% vs rabies = 3.76%) was similar across experimental groups (Figure 1.S2A) with a slightly higher proportion of inhibitory neurons in the rabies dataset, likely resulting from interneuron enrichment. We used DEGs (Figure 1.2C) and previously reported cell type markers (Figure 1.2B) to further annotate clusters into cell subclasses. We identified four inhibitory neuronal clusters derived from the medial ganglionic eminence (MGE), expressing *Lhx6*/*Sox6*, and two clusters derived from the caudal ganglionic eminence (CGE), expressing *Adarb2*/*Prox1*. MGE-derived clusters included one Pvalb and three Sst clusters. CGE-derived clusters included one Vip and one *Lamp5*$^{+}$ neurogliaform cluster. For glutamatergic neurons, we identified major subclasses previously reported [11], including L2/3, L4, L5, and L6 intratelencephalically (IT) projecting clusters, expressing a combination of markers including *Cux2*, *Fam19a1*, *Rorb*, and *Deptor*. Additional glutamatergic clusters included L5 near projecting (NP), L5 extratelencephalically (ET) projecting, L6b, and L6 corticothalamic (CT). The distribution of rabies-infected and uninfected nuclei in each cluster (Figure 1.S2B) show a larger proportion of rabies-infected nuclei compared to control in MGE-derived clusters, possibly as a result of interneuron enrichment using Gad2-Cre; R26-LSL-TVA mice which would bias rabies infection to inhibitory neurons, 40% of which are Pvalb and 18% of which are Sst [24] (Xu et al., 2010). Additionally, there was an enrichment of L4 and L5 rabies-infected neurons which may be the result of infection biases arising from injecting rabies at a cortical depth of 0.5 mm (Figure 1.1A).

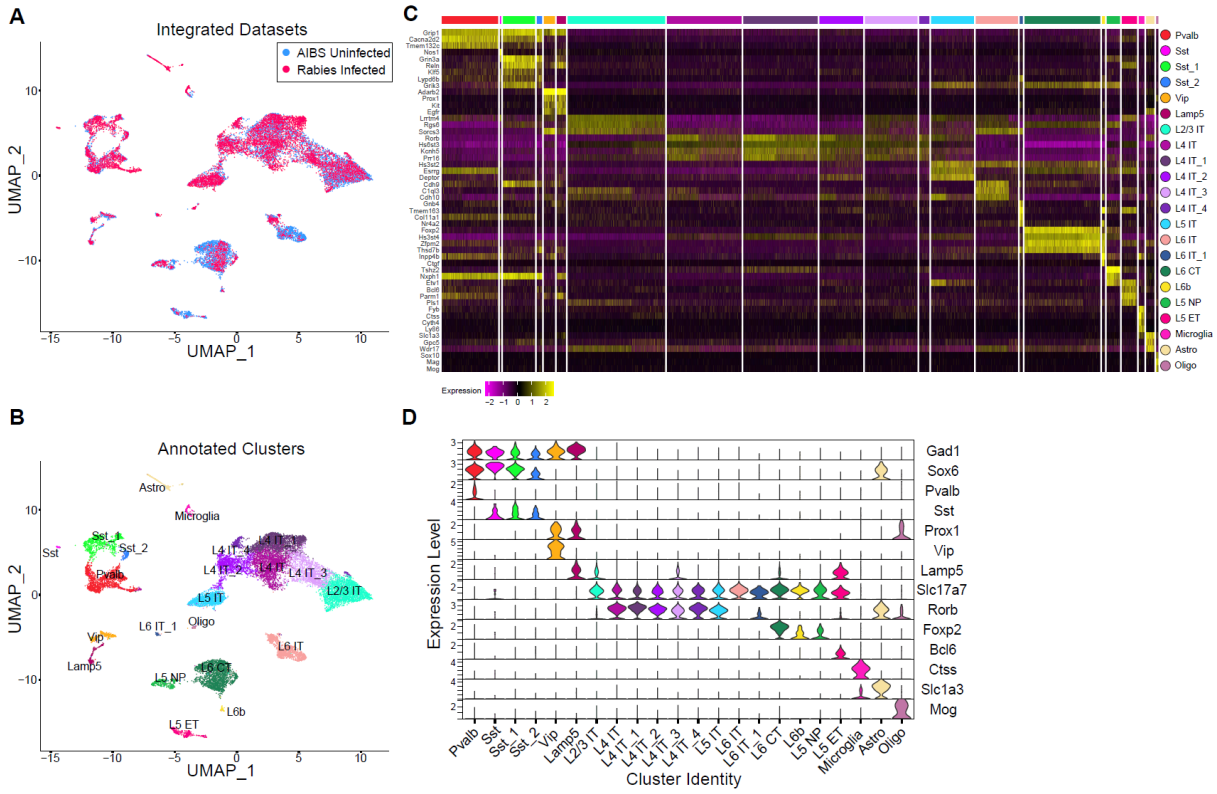

Figure 1.2 Rabies-infected nuclei can be transcriptomically classified de novo despite changes in gene expression. (A) UMAP of 8,745 rabies-infected nuclei (red) and 9,508 AIBS uninfected control nuclei (blue) after anchor-based data integration. (B) UMAP of anchor-based integrated rabies-infected and AIBS uninfected control nuclei colored by de novo cell subclass annotations. (C) Heatmap showing normalized and scaled expression level of DEGs for each cluster in B compared with all other clusters. Clusters are color coded according to B and delineated by white vertical lines. (D) Violin plots illustrating normalized expression level of canonical marker genes for each cluster, which are composed of both infected and AIBS uninfected control nuclei.

In addition to transcriptomically classifying rabies-infected nuclei *de novo* using unsupervised graph-based clustering, we also examined whether the AIBS taxonomy cell type labels could be transferred from the reference snRNA-seq dataset of uninfected cells to the rabies-infected nuclei using a weighted vote classifier derived from the reference cell identities. This approach provides a quantitative score, ranging from 0 to 1, for each predicted cell type classification, with high-confidence cell type predictions being those greater than 0.5 [23]. We tested the transfer of reference class (Figure 1.3A), subclass (Figure 1.3B), and subtype (Figure 1.3C) labels. At the class level 100% of rabies-infected nuclei were classified with a prediction score > 0.5 (Figure 1.3D). The ability to confidently assign cell type predictions decreased at finer cell type granularities, but overall was successful, with 95% and 75% of rabies-infected nuclei having prediction score > 0.5 at the subclass and subtype level (Figure 1.3D). At the subtype level, the distributions of prediction scores varied considerably between subtypes (Figure 1.3C). This variability likely results from variability in the sample size for each subtype in the reference, with some subtypes being underrepresented in the reference. Thus, it may be possible to improve subtype assignment of rabies-infected cells provided that there is a large enough reference sample.

Cell-type specific rabies-induced transcriptional changes

To explore whether rabies infection induces cell-type-specific transcriptional changes we performed DE analysis separately for each of the identified clusters. We observed DEGs in each cluster (adjusted $p < 0.05$; $\log_2 FC > 1$), with non-neuronal cells containing a higher number of DEGs compared to neuronal cells (Figure 1.4A). Of these DEGs, only 7 and 3 were upregulated and downregulated respectively across all clusters (Figure 1.4B, 1.4C). The

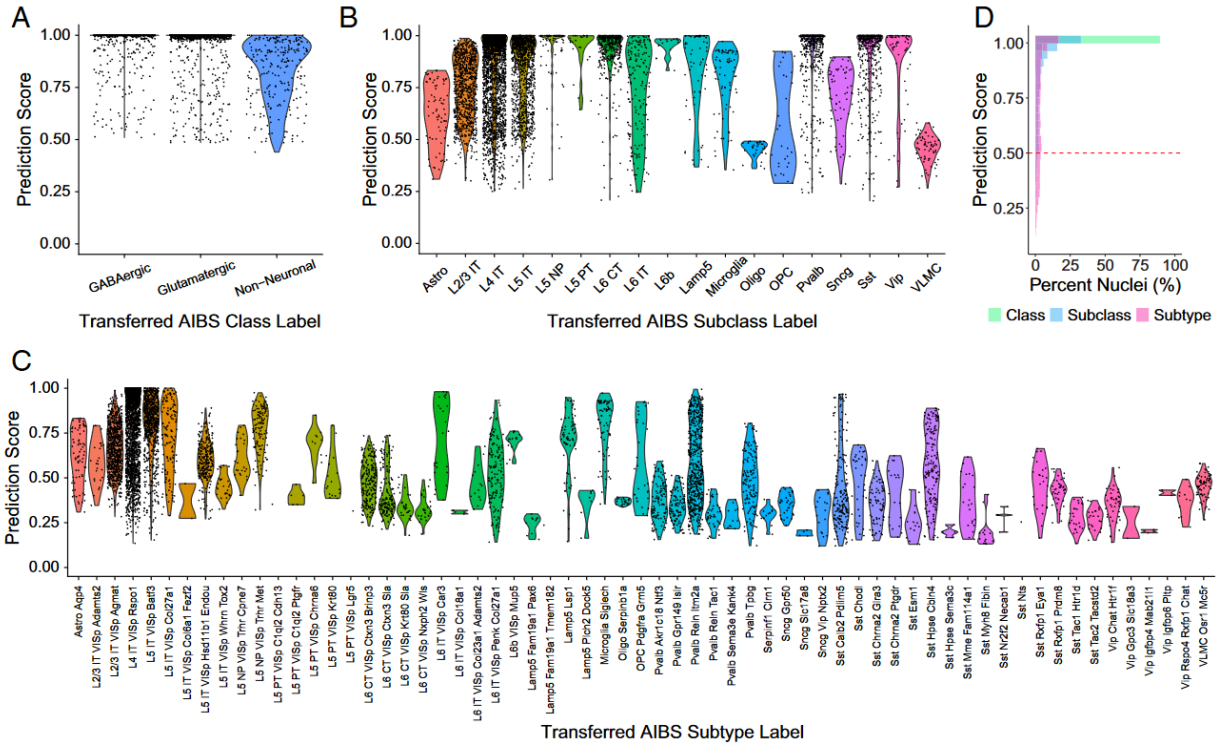

Figure 1.3 Preexisting cell type annotations can be transferred to rabies-infected nuclei. (A) Violin plots of prediction classification scores obtained when transferring AIBS class labels to rabies-infected nuclei. (B) Violin plots of prediction classification scores obtained when transferring AIBS subclass labels to rabiesinfected nuclei. (C) Violin plots of prediction classification scores obtained when transferring AIBS subtype labels to rabies-infected nuclei. (D) Distribution of cell type prediction scores, ranging from 0 to 1, for rabies-infected nuclei at different granularities. Dashed line indicates high-confidence predictions (score of >0.5).

overwhelming majority of DEGs were differentially expressed only in subsets of clusters or single clusters. Genes that shared expression upregulation across all clusters included genes involved in antiviral and immune responses, such as *Xrcc6* which acts as a cytosolic viral sensor and mediates downstream immune responses [25,26] and *Fgfr2* which regulates RIG-1-mediated antiviral signaling [27] (Figure 1.4D). We also observed a global upregulation of *Sema3c*, which encodes Semaphorin 3C (Sema3c), a soluble axonal chemoattractant [28]. *Sema3c* has been reported to be selectively expressed in neurogliaform inhibitory interneurons [29] and serves as a neuronal marker for this subclass [30]. Indeed, in control nuclei only the *Lamp5*$^{+}$ neurogliaform cluster shows expression of *Sema3c*, however selective expression is lost and upregulation is observed in all clusters for rabies-infected nuclei (Figure 1.4D). Genes downregulated in most clusters included those involved in Golgi vesicle transport, such as *Arf5*, and cellular transmembrane transport, such as *Rab3a* and *Spag5*. Although some DEGs were part of a global response across all clusters, other genes were differentially expressed only in specific clusters or classes (Figure 1.4E). For example, *Tek*, *Fntb*, and *Itgl1* were selectively upregulated in neuronal clusters. Similarly, *Grip1os2* was selectively upregulated in inhibitory and L6b neurons and *Xirp2* in IT excitatory clusters.

Effects of rabies infection on neuronal marker genes

We next focused analysis on examining rabies effects on genes commonly used to define neuronal cell types. Expression of select marker genes, such as *Gad1* and *Gad2*, used to distinguish inhibitory neurons from excitatory neurons and nonneuronal cells were unperturbed by rabies infection. However, *Slc32a1*, expressed selectively in interneuron clusters, was downregulated in rabies-infected nuclei (Figure 1.5A). MGE marker genes, *Lhx6*, *Sox6*,

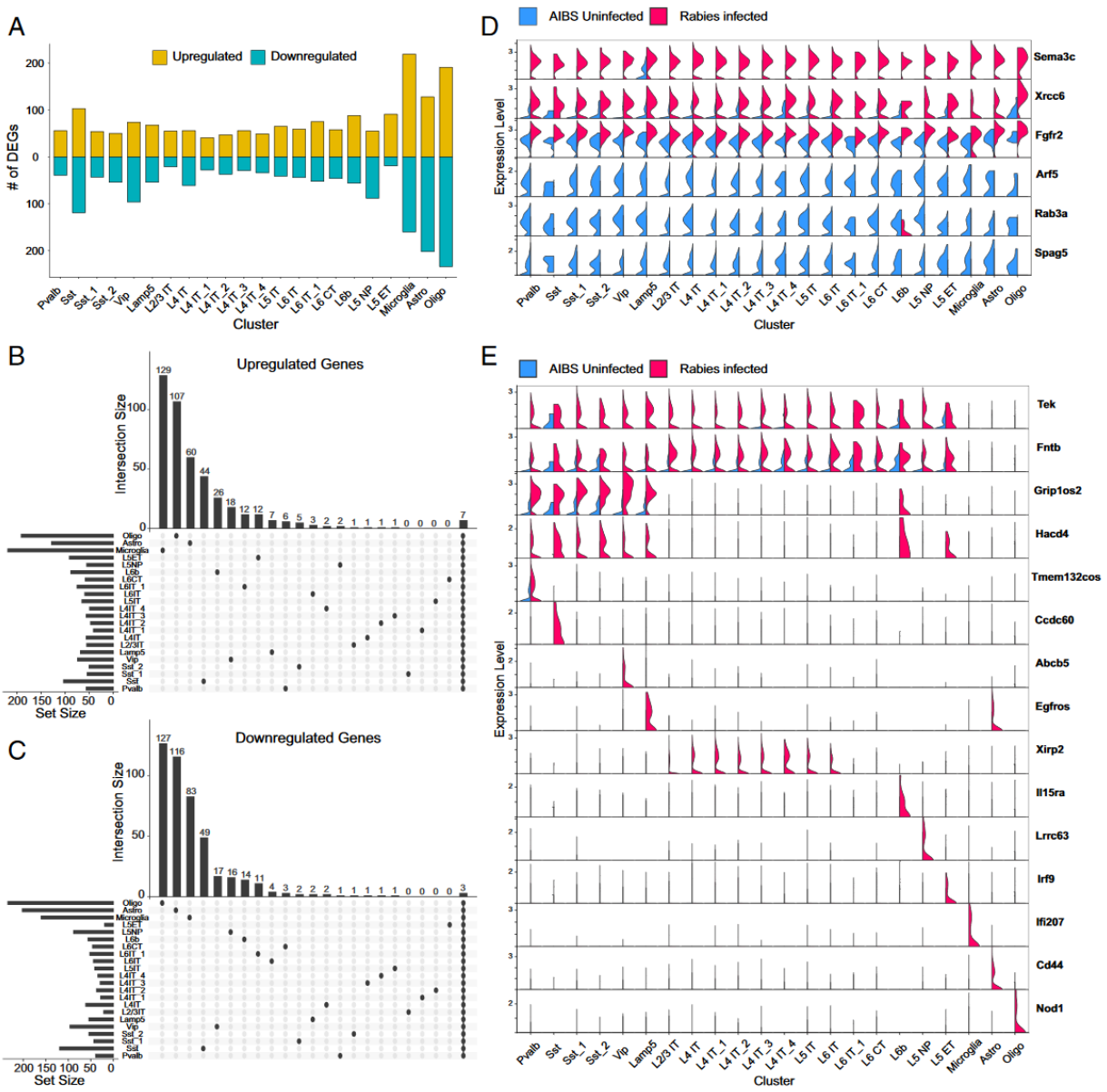

Figure 1.4 Cell-type–specific rabies-induced transcriptional changes. (A) Bar plot showing the number of DEGs that are up-regulated (yellow) or down-regulated (blue) in each cluster in rabies-infected nuclei compared with AIBS control. (B and C) Upset plots of up-regulated (B) and down-regulated (C) DEGs in rabies infected versus AIBS control. Horizontal bars represent the number of DEGs detected in each cluster, and vertical bars represent the number of unique DEGs in that cluster or in selected intersections between clusters indicated below the bars. (D) Violin plots displaying normalized expression of select DEGs in rabies-infected nuclei and AIBS control nuclei in each cluster. Top three genes are up-regulated in rabies-infected nuclei across all clusters and bottom three genes are down-regulated in rabies-infected nuclei across all clusters. (E) Violin plots displaying normalized expression of select DEGs in rabiesinfected nuclei and AIBS control nuclei in each cluster. Genes are differentially expressed in neuronal clusters (top two rows), mainly inhibitory clusters (third row), or in unique clusters.

Cacna2d2, and Kcnip1 were not differentially expressed (Figure 1.5B). Similarly, some marker genes of CGE neurons were unaffected such as *Adarb2*, *Prox1*, and *Kit*, whereas *Pnoc* and *Rgs10* were downregulated (Figure 1.5C). Importantly, *Pvalb* and *Sst*, crucial marker genes of inhibitory interneurons, were strongly downregulated in rabies-infected nuclei (Figure 1.5B, 1.5D). However, other marker genes differentially expressed between Pvalb and Sst subclasses remained unchanged, such as *Tmem132c* and *Grin3a* respectively. Similar to class and subclass markers, rabies differentially affected markers of neuronal subtypes. The Sst-Chodl neuron subtype corresponds to long range projecting inhibitory neurons commonly found in cortical layer 5 and 6 that express high levels of nitric oxide synthase (*Nos1)* [11,30]. Within this cluster, rabies downregulated expression of the unique marker *Chodl*, but did not affect expression of *Nos1*. Expression of *Vip* was also downregulated, but *Lamp5*, *Car4* and *Nxph4* were unaffected. Interestingly, neurogliaform marker gene *Sema3c* was upregulated not only within the *Lamp5*$^{+}$ cluster, but also in clusters that do not typically express it.

Although rabies infection downregulated expression of a variety of interneuron marker genes, *Sst* was selected for further validation with hybridization chain reaction RNA fluorescence *in situ* hybridization (HCR RNA-FISH). Prior studies characterizing rabies-labeled input cells have found conflicting results regarding the ability of rabies virus to infect Sst interneurons [6,7]. Therefore, *Sst* was selected for *in vivo* validation to attempt to address this inconsistency and investigate whether rabies induced *Sst* expression downregulation may be an artifact leading to detection failure. To allow for identification of Sst interneurons after rabies infection without relying on methods possibly subject to expression artifacts, Sst-Cre mice were first crossed to R26R-CAG-loxp-stop-loxp-Sun1-sfGFP-Myc [31] mice to produce Sst-Cre; INTACT, resulting in nuclear sfGFP expression in Sst interneurons. These mice were injected

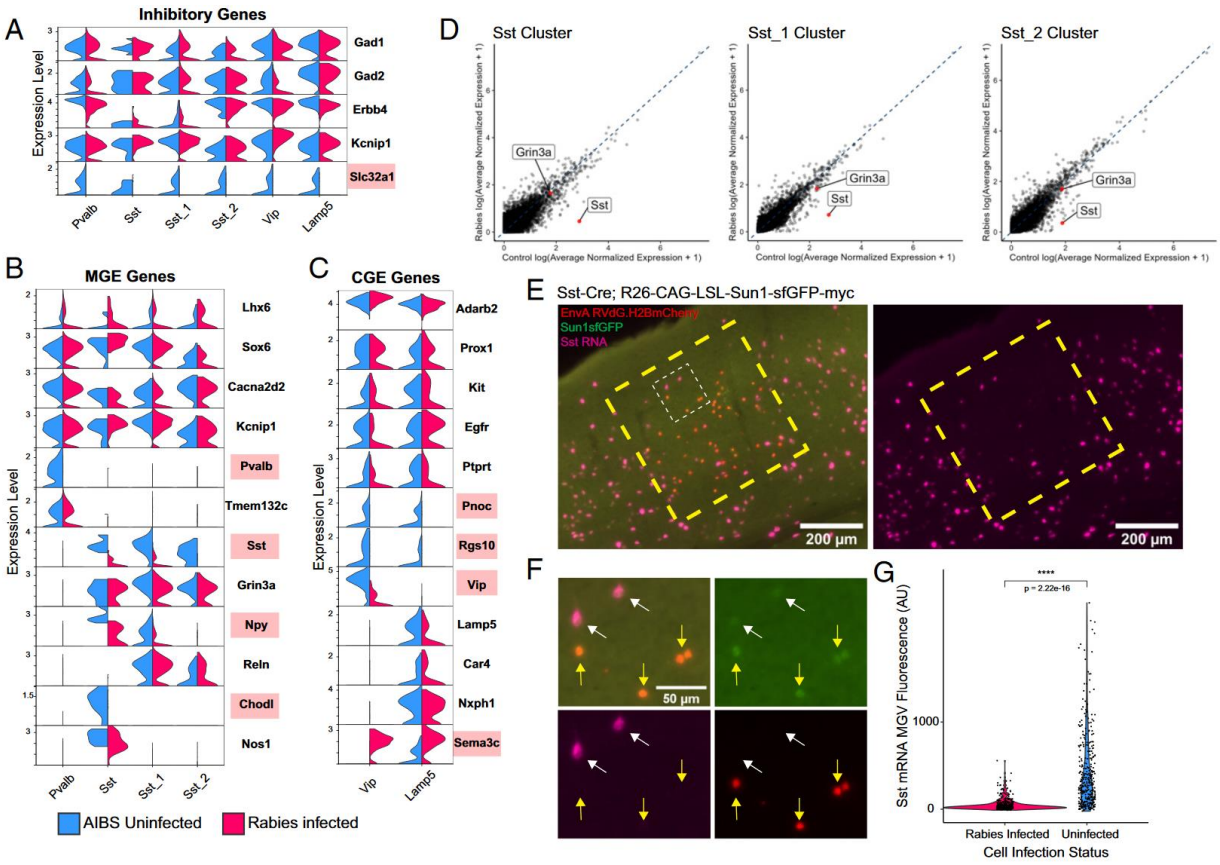

Figure 1.5 Rabies infection differentially affects the expression of inhibitory marker genes. (A–C) Violin plots displaying normalized expression of select inhibitory (A), MGE (B), or CGE (C), marker genes in rabies-infected nuclei and AIBS control nuclei in each cluster. Marker genes up-regulated or down-regulated in rabies-infected compared with AIBS control are highlighted in red. (D) Scatter plot displaying expression differences in rabies-infected nuclei versus AIBS control in Sst clusters, with Sst and Grin3a labeled in red. The dashed blue line indicates perfect correlation. Values were averaged log normalized across cells in each condition in that cluster. (E) Representative images of HCR labeling for Sst transcripts (magenta) in V1 of Sst Cre;R26-CAG-LSL-Sun1-sfGFP-myc mice injected with EnvA RVdG.H2BmCherry. Uninfected Sst neurons are Sun1sfGFP+, mCherry, and rabies-infected Sst neurons are Sun1sfGFP+, mCherry+. Large dashed yellow box indicates a region containing rabies-infected Sst neurons. The small dashed white box indicates the region shown in F with higher magnification. Scale bar: 200 µm. (F) Higher magnification of dashed white box region in E. White arrows indicate uninfected Sst neurons (Sun1sfGFP+, mCherry,) and yellow arrows indicate rabies-infected Sst neurons (Sun1sfGFP+, mCherry+). Sst transcripts labeled with HCR are in magenta. Scale bar: 50 µm. (G) Violin plots displaying MGV intensity of Sst transcript fluorescence. A total of 356 rabies-infected and 347 uninfected Sst neurons across 2 animals were analyzed. P values were determined by Wilcoxon rank-sum test. ****$P \leq 0.0001$.

with AAV to express Cre-dependent TVA followed by EnvA+RVdG-H2BmCherry to restrict rabies infection to Sst interneurons. Importantly, this experimental design makes it possible to quantify and compare *Sst* RNA in uninfected and rabies-infected Sst interneurons in the same mouse and tissue section (Figure 1.4E, 1.4F). In agreement with our snRNA-seq data, we found that *Sst* RNA detection by HCR RNA-FISH is significantly reduced in rabies-infected versus uninfected Sst interneurons (Figure 1.5G).

Similar to its effects on inhibitory marker genes, rabies infection differentially affected excitatory neuronal markers (Figure 1.6). Important excitatory marker genes downregulated in rabies-infected nuclei included *Slc30a3* and *Rspo1*, marker genes for pan-IT neurons and L4 IT neurons respectively (Figure 1.6A). Layer-specific IT marker genes not altered included *Cux2*, a L2/3 IT marker gene, and *Deptor*, a L5 IT maker gene. The L6 IT Car3 subclass is transcriptomically distinct from other excitatory IT subclasses [11] and Car3+ L6 cells have been shown to exhibit distinct projection patterns compared to other IT-projecting neurons [32]. We found that previously reported marker genes for this subclass, *Car3*, *Oprk1* and *Nr2f2*, are all downregulated in rabies-infected nuclei within this cluster (Figure 1.6B). However, *Gnb4*, a marker also unique for the Car3 subclass, and *Cux2*, a gene expressed in L6-IT-Car3, but absent in other L6-IT neurons, remain unchanged. Within the L6 CT subclass, canonical marker gene *Foxp2* was not affected by rabies expression along with *Thsd7b*,*Syt6*, and *Ephb* (Figure 1.6C). L6b neurons share marker genes such as, *Cplx3*, *Nxph3*, and *Ctgf*, of which the latter is downregulated in rabies-infected nuclei. L5NP neurons project only to neighboring areas and express distinct markers such as *Slc17a8*, *Tshz2*, and *Lypd1*. Like other clusters, rabies downregulated certain genes (*Slc17a8*, Lypd1), while having no effect on others (*Tshz2*, *Lcp1*). Within the L5 ET subclass, we found downregulation of *Npr3* and *Chst8* and no change in the

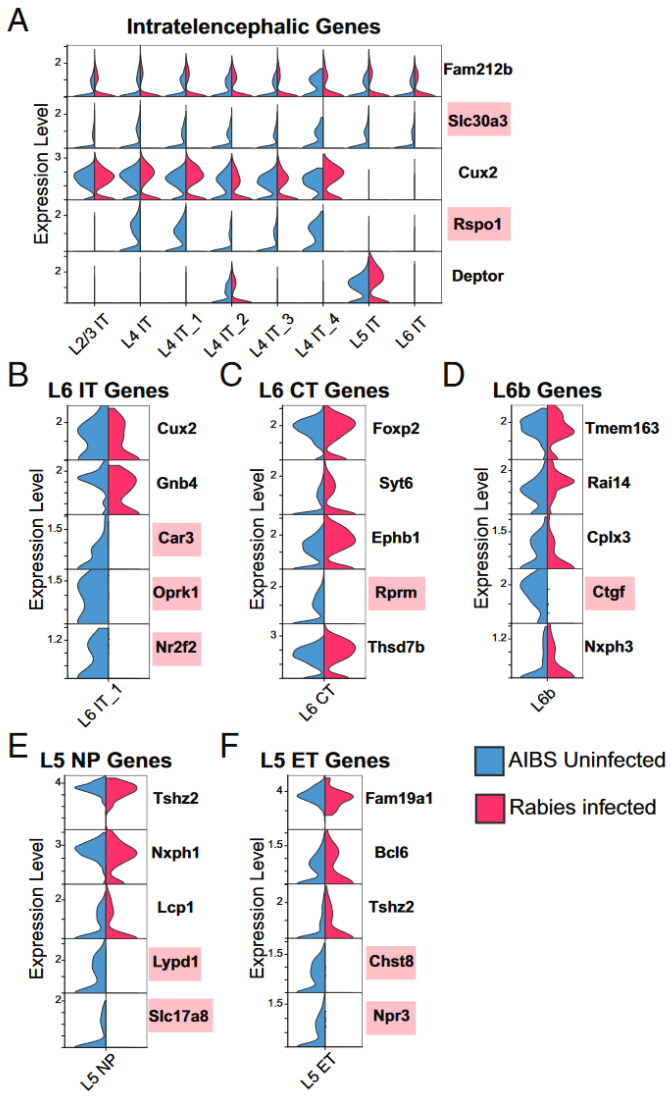

Figure 1.6 Rabies infection differentially affects the expression of excitatory marker genes. (A–F) Violin plots displaying normalized expression of select excitatory IT (A), L6 IT (B), L6 CT (C), L6b (D), L5 NP (E), and L5 ET (F) marker genes in rabies-infected nuclei and AIBS control nuclei in each cluster. Down-regulation of select marker genes (red) is observed in rabies-infected nuclei.

expression of *Bcl6*, *Fam19a1*, and *Tshz2*. Overall, we found that rabies infection can alter expression of certain neuronal marker genes, while others are unchanged. Furthermore, when gene expression is altered, the most common effect observed is gene expression downregulation, although upregulation of some marker genes was also present.

Discussion

Monosynaptic rabies tracing is a valuable tool for unraveling neural connectivity, yet challenges remain in the ability to characterize rabies-labeled input cells to populations of interest. Here we investigated whether single-cell transcriptomics could be used to characterize rabies-infected cells according to established cell types and examined how rabies infection alters host cells' transcriptional landscape. Using snRNA-seq to examine the transcriptomes of large numbers of rabies-infected neurons, we found that despite global and cell-type-specific rabies-induced transcriptional changes, rabies-infected neuronal profiles retain sufficient similarities to control profiles to allow for their classification. Furthermore, we examined the effects of rabies infection on neuronal marker genes and found that rabies differentially impacts host genes, with some showing downregulation or upregulation of expression and others remaining unperturbed. Therefore, while our study supports the use of rabies tracing in combination with snRNA-seq to determine input cell identity, it also suggests that caution should be taken when attempting to determine rabies-labeled cell identity with methods that rely on single or few genes. Finally, our dataset can serve as a resource for other researchers to utilize while designing gene probes for spatial transcriptomics on rabies-infected cortical tissue.

The wide adoption of genetically modified rabies virus to study neural connectivity can be attributed to its ability to overcome the challenge of precisely labeling presynaptic partners

regardless of distance, with EnvA-pseudotyped rabies virus having the additional advantage of targeting initial infection to a genetically accessible population of interest. However, circuit connectivity analysis using this viral tool is largely restricted to characterizing inputs according to the cortical area they reside in and/or their laminar spatial location [33–35]. While some studies have used immunostaining or intersectional approaches to determine the identity of rabies-labeled cortical inputs to populations of interest, studies have yielded conflicting results. For example, a study using rabies tracing to detect inputs to interneurons in mouse V1 used Sst RNA probes and antibodies to establish the identity of rabies-labeled inputs [6]. Using this method, they found no Sst-positive inputs to Pvalb interneurons, despite functional studies describing extensive Sst innervation of Pvalb neurons [29]. A plausible explanation is that Sst interneurons are resistant to retrograde infection by rabies virus. However, this seems unlikely given that rabies-labeled Sst inputs can be detected using a Cre/Flp recombinase-dependent intersectional labeling method where mice with a Cre/Flp-dependent dual RFP reporter and a Cre gene inserted into an interneuron subtype-specific gene locus are used in tandem with a pseudotyped rabies viruses expressing Flp [7]. Given our finding that rabies infection can downregulate *Sst* gene expression, along with reports that rabies can also decrease translation of host proteins, it is likely that the inability to detect Sst inputs is an artifact of using immunostaining and RNA FISH for a gene that is downregulated in rabies-infected cells.

Despite the strong downregulation of certain neuronal marker genes, gene expression of many other marker genes was unaltered. This suggests that rabies infection differentially affects distinct host genes and that some genes may be more vulnerable to transcriptional modulation than others. Nonetheless, when using whole transcriptome information and defining cell types based on expression levels of thousands of genes, the majority of rabies-infected neurons were

accurately classified at the class (100%), subclass (95%), and subtype (75%) level using supervised classification to a reference data set. It is possible that the accuracy of assignment to particular subtypes may be further improved by increasing the size of the reference sample, particularly for rare cell types, as some subtypes were not well represented in the reference.

The ability to characterize rabies-infected cells based on their gene expression profiles can have large implications for future cortical connectivity studies. A multitude of studies using single-cell transcriptomics have already shown that major neuronal classes are composed of multiple genetically distinct subclasses. This has corroborated earlier studies describing distinct subtypes of interneuron classes each with unique morphology, connectivity, and functional activity [14]. Thus, single-cell transcriptomics as a tool to characterize rabies-labeled inputs is not only less liable to technical artifacts, but also has the additional benefit of providing a more precise way to study cortical connectivity since inputs can be identified based on more refined subtypes. Furthermore, emerging genomic technologies, such as multiplexed error-robust FISH (MERFISH), sequential FISH (seqFISH), and spatial barcoding, can transcriptomically profile many cells while retaining spatial information and may thus be valuable tools for relating molecular profiles, spatial locations, and projection patterns when used in combination with rabies tracing. However, these techniques do not yet yield deep transcriptomic information, but instead rely on expression of discrete gene sets and may therefore be more liable to artifacts induced by rabies infection. Here we have shown that rabies differentially affects neuronal marker genes and have provided examples of genes downregulated or upregulated by rabies infection. Importantly, rabies-induced changes in gene expression make certain marker genes unsuitable for the accurate characterization of rabies infected cells if used in isolation. For example, *Sst* RNA probes will not accurately label rabies infected Sst neurons due to

downregulation of the gene. Similarly, using probes against the neurogliaform marker gene *Sema3c* would likely lead to the mischaracterization of neurons, as its global upregulation would make it detectable in non-neurogliaform neurons. Therefore, we encourage investigators to independently validate the utility of reagents that detect single genes for characterization of rabies-infected neurons. Additionally, we have provided examples of neuronal marker genes for major classes, subclasses, and select subtypes that are unperturbed by rabies and may thus serve as suitable genes to include in gene sets to be used for spatial transcriptomics following rabies tracing. For example, while *Pvalb* may not be suitable for identifying the Pvalb interneuron subclass due to its downregulation in rabies-infected nuclei, *Tmem132c* can serve as an alternative gene that is unaffected. Similarly, *Nos1* can be used to distinguish the *Chodl* Sst subtype as *Chodl* may not be a suitable candidate. Previous studies have demonstrated the viability of rabies-infected neurons for functional studies (Wickersham 2007, Osakada 2011, Wertz Science 2015, Reardon 2016). While rabies-infected neurons remain viable during the 10 day survival times that we have assessed with our transcriptomic analyses, the changes in gene expression that we have observed, including down-regulation of genes related to synaptic function and metabolic processes, reiterate the need for caution when interpreting such studies.

Here, we present and make publicly available a large snRNA-seq dataset of rabies-infected neurons consisting of 8,497 neuronal profiles. However, it is important to highlight several limitations of the study. First, prior bulk RNAseq studies have shown that different rabies virus strains induce distinct global transcriptional changes [36]. Thus, it is possible that other strains used for monosynaptic rabies tracing, such as CVS-N2c [37], may induce different cell-type specific neuronal transcriptional changes from the ones observed using the SAD-B19 strain. Future studies should examine the compatibility of other stains not included in this study with

transcriptomic characterization. Second, this study only focused on investigating the effects of rabies infection at a time point of 10 days post-infection. This time point was chosen since circuit tracing experiments express rabies at a range of 7-10 days and we wanted to ensure that transcriptomic characterization was still possible even at the longest expression time. However, studies are needed to investigate how rabies impacts gene expression across neuronal cell types at different infection timepoints and whether our observations reflect a steady-state or transient state of cells. ScRNA-seq studies [10,11] have shown that transcriptomically defined excitatory and inhibitory neuronal types are generally shared across mouse cortical areas and hippocampal formation and exhibit conserved molecular signatures. Therefore, it is likely that rabies modulation of gene expression in homologous neuronal cell types across cortical regions will not vary significantly from what we have observed in V1. However, transcriptomic cell type identification of rabies-infected cells from other brain regions would necessitate collection and analysis of new data from those brain regions of interest. Finally, while we provide evidence that rabies modulates expression of distinct genes differently, the cellular and/or viral mechanisms that lead to these differential gene expression effects remain unknown. In summary, this study shows that rabies-infected neurons can be accurately classified according to transcriptomic cell types, identifies global and cell-type specific rabies-induced modulation of host genes, and provides access to the transcriptomic profiles of rabies-infected cortical neurons through a publicly accessible dataset.

Methods

Mouse transgenic lines

All experimental procedures were approved by the Salk Institute Animal Care and Use Committee. C57BL/6J mice were used as wild-type. Homozygous Gad2-Cre and R26-LSL-TVA-LacZ (Seidler et al., 2008) mice were bred to produce Gad2-Cre; R26-LSL-TVA-LacZ. For HCR RNA-FISH experiments, the knock-in mouse line, R26R-CAG-loxp-stop-loxp-Sun1-sfGFP-Myc (INTACT) was maintained on a C57BL/6J background and bred with Sst-Cre mice to produce Sst-Cre; INTACT. Mice were housed with a 12-hour light and 12-hour dark cycle and *ad libitum* access to food and water. Both male and female mice were used for RNA sequencing experiments. Only female mice were used for HCR experiments.

Virus preparation

AAV8-nef-AO-66/71-TVA950 (5.25E+13 GC/mL), EnvA+RVdG-H2BmCherry (1.09E+08 IU/ml and) and G+RVdG-H2BmCherry (9.59E+09 IU/ml) were produced by the Salk GT3 Viral Core.

Animal surgery for virus injection

Mice were initially anesthetized with 2% isoflurane and maintained at 1.5% isoflurane after placement on a stereotax (David Kopf Instruments, Model 940 series) for surgery and stereotaxic injections. A small craniotomy was made with a mounted drill over the primary visual cortex of the left hemisphere using the following coordinates: 3.4 mm posterior and 2.6 mm lateral relative to bregma. To collect large numbers of rabies-infected neurons for transcriptomic experiments, 150 nl of unpseudotyped G+RVdG-H2BmCherry (9.59E+09 IU/ml)

was injected into the center of V1 of P60-P75 C57BL/6 mice 0.5–0.7 mm ventral from the pia using a pulled glass pipette with a tip size of 30 um connected to a 1ml syringe with 18G tubing adaptor and tubing. To prevent backflow, the pipette was left in the brain for 5 minutes after injection. To bias infection to inhibitory neurons 150 nl of EnvA+RVdG-H2BmCherry (1.09E+08 IU/ml) was injected into P65-P85 Gad2-Cre; R26-LSL-TVA mice. For HCR experiments 100 nl of diluted AAV8-nef-AO-66/71-TVA950 (5.25E+11 GC/mL) was injected into V1 of Sst-Cre; INTACT mice. Two weeks after AAV helper virus injection, 200 nl of EnvA+RVdG-H2BmCherry (7.43E+07 IU/ml) was injected into the same site in V1. After recovery, mice were given water with ibuprofen (30mg/kg) and housed for 10 days before tissue harvest to allow for fluorescent protein expression.

Brain dissection and single nuclei isolation

Ten days after rabies injection, animals were euthanized with an overdose of isoflurane. Brains were extracted and immediately submerged in ice-cold slicing solution (2.5mM KCl, 0.5mM CaCl2, 7mM MgCl2, 1.25mM NaH2PO4, 110mM sucrose, 10mM glucose and 25mM NaHCO3) that was bubbled with carbogen. Coronal brain slices (400um thick) were cut using VF-300 Compresstome^{TM} (Precisionary Instruments, Greenville,NC) and submerged in ice-cold slicing solution. Subregions of V1 containing mCherry+ nuclei in brain slices were micro-dissected out under a fluorescent dissection microscope (Olympus SZX6) and transferred to microcentrifuge tubes and immediately frozen in dry ice, and subsequently stored at -80°C. The remaining brain slices after dissection were collected, fixed with ice-cold 4% PFA overnight, stained with DAPI, and scanned with a 10x objective to validate correct V1 dissection using an Olympus BX63 Microscope.

Single nuclei preparations were performed following a published protocol [38] with modification. In summary, the frozen brain tissues were transferred to pre-chilled dounce homogenizers with 1ml NIM buffer (0.25M sucrose, 25mM KCl, 5mM MgCl2, 10mM Tris-HCl (pH7.4), 1mM DTT (Sigma 646563), 10ul of protease inhibitor (Sigma P8340), 1.5ul of RNasin Plus RNase inhibitor (Promega, N2611)), 0.1% Triton X-100, and 10 uM DAPI, and gently homogenized on ice with ice-cold pestles 10 - 15 times. The homogenate was transferred to pre-chilled microcentrifuge tubes and centrifuged at 3000 rpm for 8 min at 4°C to pellet the nuclei. The supernatant was aspirated, the pellet gently resuspended in ice-cold 1ml NIM buffer, and again centrifuged at 3000 rpm for 8 min at 4°C. The pellet was then resuspended in 450ul of nuclei storage buffer (0.25M sucrose, 5mM MgCl2, 10mM Tris-HCl (pH7.4), 1mM DTT, 9ul of Protease inhibitor), and filtered through a 40μM cell strainer. The sample was incubated with 50ul of nuclease-free BSA to prevent nuclei clumping.

Fluorescence-activated nuclei sorting of single nuclei was performed using a BD Influx sorter with a 70 μM nozzle at 22.5 PSI sheath pressure. DAPI+/mCherry+ rabies-infected nuclei were sorted into 1.5ml Eppendorf tubes and immediately loaded onto the 10X Genomics Chromium Controller.

10x Chromium RNA-sequencing

For 10x processing, we used Chromium Next GEM single-cell 3' Kit v3.1 (10x Genomics, PN-1000128). We followed the manufacturer's instructions for single-cell capture, barcoding, reverse transcription, cDNA amplification, and library construction. We targeted sequencing depth of 100,000 reads per cell. Libraries were sequenced on Illumina NovaSeq6000 and raw read (fastq) files were aligned to the mouse pre-mRNA reference transcriptome (mm10)

using the 10x Genomics CellRanger pipeline (version 5.0.). Intronic reads were included in expression quantification using the *include-introns* parameter.

RNA-seq data quality control and clustering

Reference data used in this study includes 10x v3 single nucleus RNA-seq from primary visual cortex obtained from the Allen Institute for Brain Science (AIBS). Reference 10x v3 nuclei were assigned to previously published VISp cell type taxonomy [11] using a nearest centroid classifier based on a set of 563 markers that were detected in both datasets (expression > 0). To estimate the robustness of mapping, classification was repeated 100 times, each time using 80% of randomly sampled markers, and the probability for each cell to map to every reference cluster was computed. R (version 4.1.1) and Seurat (version 4.0) [22,23] were used for snRNA-seq analysis. Doublets were identified using DoubletFinder [39] and excluded from analysis. The percentage of mitochondrial transcripts for each nucleus was calculated and added as metadata to the Seurat object using *percent.mito*. Nuclei with less than 500 genes, more than 8000 genes, and greater than 0.5% of mitochondrial genes were excluded from analysis. After pre-filtering, AIBS and rabies datasets were normalized and scaled separately using the *SCTransform* function. Variable features were first identified in each dataset individually with *SCTransform* after removing sex-specific genes, immediate early genes, and predicted gene models (gene names that start with Gm or end with Rik). The top 5000 variable features identified independently across datasets were determined using *SelectIntegrationFeatures* and used as input for downstream joint clustering analysis. Datasets were merged and integration anchors identified using *FindIntegrationAnchors*. These anchors were used to integrate the two datasets using *IntegrateData*. Dimensionality reduction via principal component analysis (PCA) was performed on the integrated data using *RunPCA*. The top 50 PCs were used as input for clustering analysis

using *FindClusters* with a resolution of 0.5. For unsupervised annotations, clusters were assigned cell type annotations based on the expression of combination of known marker genes for major cell subclasses and DEGs. For the latter, Model-based Analysis of Single-Cell Transcriptomics (MAST) [20] was used to perform DE analysis by comparing nuclei in each cluster to the rest of the nuclear profiles, with DEGs being those with Bonferroni corrected, $p_{adj} < 0.05$; $\log_2 FC > 0.25$. For supervised cell type annotation, we used a weighted vote classifier derived from the reference cell identities to map rabies-infected nuclei to established neuronal cell types. The rabies dataset and the AIBS dataset were integrated using the *FindTransferAnchors* function with the AIBS dataset assigned as reference and the rabies dataset as query. Following integration, class, subclass, and subtype labels were transferred to the rabies dataset using the *TransferData* function, providing a prediction score ranging from 0 to 1 for each class, subclass, and subtype.

Differential expression analysis and GSEA

To identify genes differentially expressed in rabies-infected nuclei compared to control DE analysis was performed using MAST. P-values were adjusted using Bonferroni correction and filtered at $p_{adj} < 0.05$. Gene Set Enrichment Analysis (GSEA) was performed using the *GSEA* function in the R package ClusterProfiler version 4.2 [40]. DEGs were ranked according to their log fold change (rabies vs control) and the ranked list was used as input to the *GSEA* function. Gene ontology (GO) sets and pathways were obtained using the Molecular Signatures Database (MSigDB) [41,42]. $p_{adj} < 0.05$ (Benjamini-Hochberg correction) was considered significant.

In vivo validation of gene expression using Hybridization Chain Reaction RNA FISH

Animals were perfused transcardially using phosphate-buffered saline (PBS) followed by 4% paraformaldehyde (PFA). Brains were dissected out from skulls and post-fixed overnight with 2% PFA and 15% sucrose in PBS at 4°C, then immersed in 30% sucrose in PBS at 4°C for an additional 24 hours. Hybridization Chain Reaction (HCR) reagents and Sst probes were obtained from Molecular Instruments. Tissue was sectioned coronally at 50um on a freezing microtome under RNase free conditions and HCR was performed according to the manufacturer's instructions. Briefly, sections were mounted onto Fisherbrand™ Tissue Path Superfrost™ Plus Gold Slides, left to air dry for 3 hours, post-fixed again in 4% PFA, and dehydrated with a series of ethanol incubations. Sst probes (10nM) were hybridized overnight at 37°C in a humidified chamber and then amplified overnight at room temperature. Tissue was imaged on an Olympus BX63 microscope (Olympus Corporation, Tokyo, Japan) with a 20x objective and a 5um optical section. Images were processed and analyzed in NIH ImageJ software (FIJI). ROIs for Sst neurons were manually drawn based on sfGFP INTACT signal. Average background signal in V1 was calculated for each section and was subtracted from measured Sst mRNA mean gray value (MGV) fluorescence intensity for cells in that section. Wilcoxon rank-sum test was used for statistical analysis. ns: $p > 0.05$, *: $p <= 0.05$, **: $p <= 0.01$, ***: $p <= 0.001$, ****: $p <= 0.0001$

Appendix

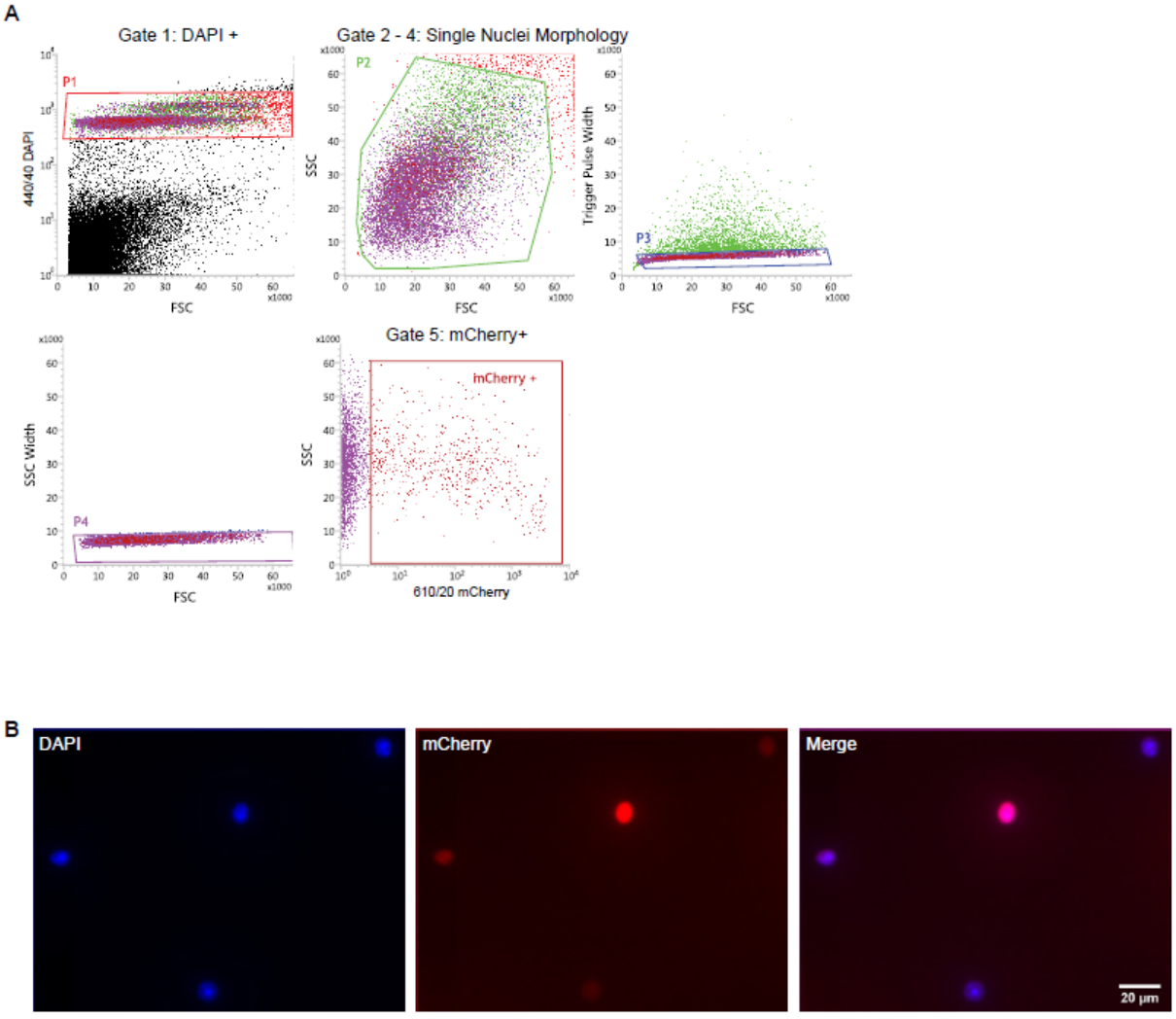

Figure 1.S1 Details on rabies-infected fluorescence-activated nuclei sorting. (A) Detailed gating strategy of fluorescence-activated nuclei sorting. Gate 1 selects for DAPI+ nuclei to exclude debris. Gate 2 -4 exclude cell doublets based on single nuclei morphology. Gate 5 selects for mCherry+ fluorescence. (B) Post-sorting visualization of sorted mCherry+ nuclei for quality control.

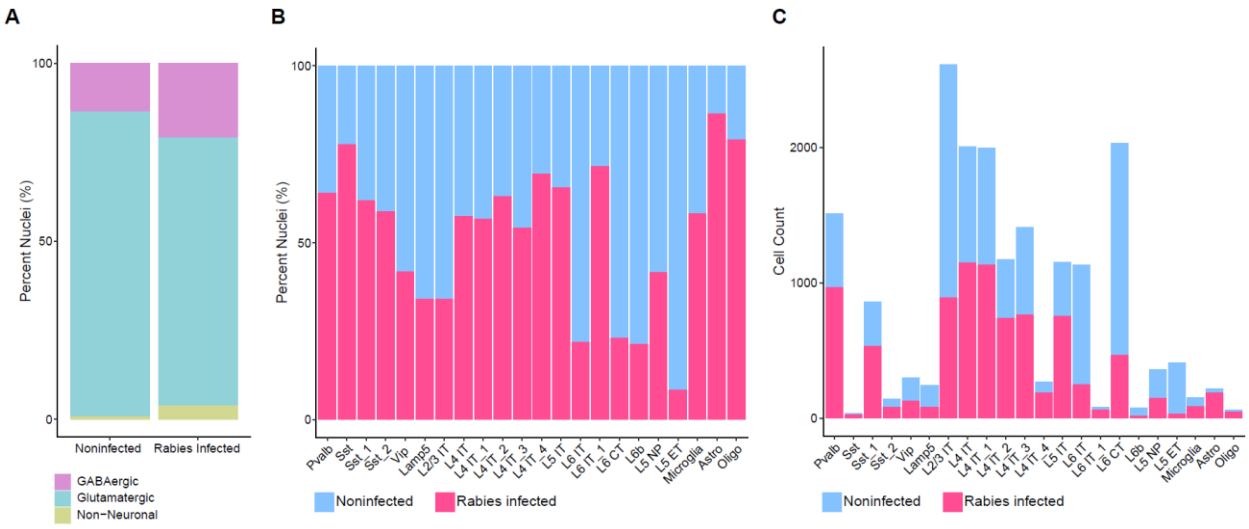

Figure 1.S2 Cell type composition of datasets. (A) Percent of excitatory, inhibitory, and non-neuronal nuclei across experimental groups. (B) Percent distribution of rabies-infected and uninfected nuclei in each cluster. (C) Absolute count of rabies-infected and uninfected nuclei in each cluster.

Acknowledgements

Chapter 1, in full, is a reprint of the material as it appears in: Patiño M, Lagos WN, Patne NS, Tasic B, Zeng H, & Callaway EM (2022). Single-cell transcriptomic classification of rabies-infected cortical neurons. *Proceedings of the National Academy of Sciences*, *119* (22), e2203677119. The dissertation author was the primary investigator and author of this paper.

References

1. Callaway EM, Luo L. Monosynaptic Circuit Tracing with Glycoprotein-Deleted Rabies Viruses. *J Neurosci*. 2015;35(24):8979-8985. doi:10.1523/JNEUROSCI.0409-15.2015

2. Wickersham IR, Finke S, Conzelmann KK, Callaway EM. Retrograde neuronal tracing with a deletion-mutant rabies virus. *Nat Methods*. 2007;4(1):47-49. doi:10.1038/nmeth999

3. Wall NR, Wickersham IR, Cetin A, Parra MDL, Callaway EM. Monosynaptic circuit tracing in vivo through Cre-dependent targeting and complementation of modified rabies virus. *PNAS*. 2010;107(50):21848-21853. doi:10.1073/pnas.1011756107

4. Marshel JH, Mori T, Nielsen KJ, Callaway EM. Targeting Single Neuronal Networks for Gene Expression and Cell Labeling In Vivo. *Neuron*. 2010;67(4):562-574. doi:10.1016/j.neuron.2010.08.001

5. Armand EJ, Li J, Xie F, Luo C, Mukamel EA. Single-Cell Sequencing of Brain Cell Transcriptomes and Epigenomes. *Neuron*. 2021;109(1):11-26. doi:10.1016/j.neuron.2020.12.010

6. Ährlund-Richter S, Xuan Y, van Lunteren JA, Kim H, Ortiz C, Pollak Dorocic I, Meletis K, Carlén M. A whole-brain atlas of monosynaptic input targeting four different cell types in the medial prefrontal cortex of the mouse. *Nat Neurosci*. 2019;22(4):657-668. doi:10.1038/s41593-019-0354-y

7. Yetman MJ, Washburn E, Hyun JH, Osakada F, Hayano Y, Zeng H, Callaway EM, Kwon HB, Taniguchi H. Intersectional Monosynaptic Tracing for Dissecting Subtype-Specific Organization of GABAergic Interneuron Inputs. *Nat Neurosci*. 2019;22(3):492-502. doi:10.1038/s41593-018-0322-y

8. Komarova AV, Real E, Borman AM, Brocard M, England P, Tordo N, Hershey JWB, Kean KM, Jacob Y. Rabies virus matrix protein interplay with eIF3, new insights into rabies virus pathogenesis. *Nucleic Acids Res*. 2007;35(5):1522-1532. doi:10.1093/nar/gkl1127

9. Yao Z, Liu H, Xie F, Fischer S, Adkins RS, Aldridge AI, Ament SA, Bartlett A, Behrens MM, Van den Berge K, Bertagnolli D, de Bézieux HR, Biancalani T, Booeshaghi AS, Bravo HC, Casper T, Colantuoni C, Crabtree J, Creasy H, Crichton K, Crow M, Dee N, Dougherty EL, Doyle WI, Dudoit S, Fang R, Felix V, Fong O, Giglio M, Goldy J, Hawrylycz M, Herb BR, Hertzano R, Hou X, Hu Q, Kancherla J, Kroll M, Lathia K, Li YE, Lucero JD, Luo C, Mahurkar A, McMillen D, Nadaf NM, Nery JR, Nguyen TN, Niu SY, Ntranos V, Orvis J, Osteen JK, Pham T, Pinto-Duarte A, Poirion O, Preissl S, Purdom E, Rimorin C, Risso D, Rivkin AC, Smith K, Street K, Sulc J, Svensson V, Tieu M, Torkelson A, Tung H, Vaishnav ED, Vanderburg CR, van Velthoven C, Wang X, White OR, Huang ZJ, Kharchenko PV, Pachter L, Ngai J, Regev A, Tasic B, Welch JD, Gillis J, Macosko EZ, Ren B, Ecker JR, Zeng H, Mukamel EA. A transcriptomic and epigenomic cell atlas of the mouse primary motor cortex. *Nature*. 2021;598(7879):103-110. doi:10.1038/s41586-021-03500-8

10. Yao Z, van Velthoven CTJ, Nguyen TN, Goldy J, Sedeno-Cortes AE, Baftizadeh F, Bertagnolli D, Casper T, Chiang M, Crichton K, Ding SL, Fong O, Garren E, Glandon A, Gouwens NW, Gray J, Graybuck LT, Hawrylycz MJ, Hirschstein D, Kroll M, Lathia K, Lee C, Levi B, McMillen D, Mok S, Pham T, Ren Q, Rimorin C, Shapovalova N, Sulc J, Sunkin SM, Tieu M, Torkelson A, Tung H, Ward K, Dee N, Smith KA, Tasic B, Zeng H. A taxonomy of transcriptomic cell types across the isocortex and hippocampal formation. *Cell*. 2021;184(12):3222-3241.e26. doi:10.1016/j.cell.2021.04.021

11. Tasic B, Yao Z, Graybuck LT, Smith KA, Nguyen TN, Bertagnolli D, Goldy J, Garren E, Economo MN, Viswanathan S, Penn O, Bakken T, Menon V, Miller J, Fong O, Hirokawa KE, Lathia K, Rimorin C, Tieu M, Larsen R, Casper T, Barkan E, Kroll M, Parry S, Shapovalova NV, Hirschstein D, Pendergraft J, Sullivan HA, Kim TK, Szafer A, Dee N, Groblewski P, Wickersham I, Cetin A, Harris JA, Levi BP, Sunkin SM, Madisen L, Daigle TL, Looger L, Bernard A, Phillips J, Lein E, Hawrylycz M, Svoboda K, Jones AR, Koch C, Zeng H. Shared and distinct transcriptomic cell types across neocortical areas. *Nature*. 2018;563(7729):72-78. doi:10.1038/s41586-018-0654-5

12. Gouwens NW, Sorensen SA, Berg J, Lee C, Jarsky T, Ting J, Sunkin SM, Feng D, Anastassiou CA, Barkan E, Bickley K, Blesie N, Braun T, Brouner K, Budzillo A, Caldejon S, Casper T, Castelli D, Chong P, Crichton K, Cuhaciyan C, Daigle TL, Dalley R, Dee N, Desta T, Ding SL, Dingman S, Doperalski A, Dotson N, Egdorf T, Fisher M, de Frates RA, Garren E, Garwood M, Gary A, Gaudreault N, Godfrey K, Gorham M, Gu H, Habel C, Hadley K, Harrington J, Harris JA, Henry A, Hill D, Josephsen S, Kebede S, Kim L, Kroll M, Lee B, Lemon T, Link KE, Liu X, Long B, Mann R, McGraw M, Mihalas S, Mukora A, Murphy GJ, Ng L, Ngo K, Nguyen TN, Nicovich PR, Oldre A, Park D, Parry S, Perkins J, Potekhina L, Reid D, Robertson M, Sandman D, Schroedter M, Slaughterbeck C, Soler-Llavina G, Sulc J, Szafer A, Tasic B, Taskin N, Teeter C, Thatra N, Tung H, Wakeman W, Williams G, Young R, Zhou Z, Farrell C, Peng H, Hawrylycz MJ, Lein E, Ng L, Arkhipov A, Bernard A, Phillips JW, Zeng H, Koch C. Classification of electrophysiological and morphological neuron types in the mouse visual cortex. *Nat Neurosci*. 2019;22(7):1182-1195. doi:10.1038/s41593-019-0417-0

13. Gouwens NW, Sorensen SA, Baftizadeh F, Budzillo A, Lee BR, Jarsky T, Alfiler L, Baker K, Barkan E, Berry K, Bertagnolli D, Bickley K, Bomben J, Braun T, Brouner K, Casper T, Crichton K, Daigle TL, Dalley R, de Frates RA, Dee N, Desta T, Lee SD, Dotson N, Egdorf T, Ellingwood L, Enstrom R, Esposito L, Farrell C, Feng D, Fong O, Gala R, Gamlin C, Gary A, Glandon A, Goldy J, Gorham M, Graybuck L, Gu H, Hadley K, Hawrylycz MJ, Henry AM, Hill D, Hupp M, Kebede S, Kim TK, Kim L, Kroll M, Lee C, Link KE, Mallory M, Mann R, Maxwell M, McGraw M, McMillen D, Mukora A, Ng L, Ng L, Ngo K, Nicovich PR, Oldre A, Park D, Peng H, Penn O, Pham T, Pom A, Popović Z, Potekhina L, Rajanbabu R, Ransford S, Reid D, Rimorin C, Robertson M, Ronellenfitch K, Ruiz A, Sandman D, Smith K, Sulc J, Sunkin SM, Szafer A, Tieu M, Torkelson A, Trinh J, Tung H, Wakeman W, Ward K, Williams G, Zhou Z, Ting JT, Arkhipov A, Sümbül U, Lein ES, Koch C, Yao Z, Tasic B, Berg J, Murphy GJ, Zeng H. Integrated Morphoelectric and

Transcriptomic Classification of Cortical GABAergic Cells. *Cell*. 2020;183(4):935-953.e19. doi:10.1016/j.cell.2020.09.057

14. Muñoz W, Tremblay R, Levenstein D, Rudy B. Layer-specific modulation of neocortical dendritic inhibition during active wakefulness. *Science*. 2017;355(6328):954-959. doi:10.1126/science.aag2599

15. Huang KW, Sabatini BL. Single-Cell Analysis of Neuroinflammatory Responses Following Intracranial Injection of G-Deleted Rabies Viruses. *Front Cell Neurosci*. 2020;14:65. doi:10.3389/fncel.2020.00065

16. Prosniak M, Hooper DC, Dietzschold B, Koprowski H. Effect of rabies virus infection on gene expression in mouse brain. *PNAS*. 2001;98(5):2758-2763.

17. Zhao P, Zhao L, Zhang T, Qi Y, Wang T, Liu K, Wang H, Feng H, Jin H, Qin C, Yang S, Xia X. Innate immune response gene expression profiles in central nervous system of mice infected with rabies virus. *Comparative Immunology, Microbiology and Infectious Diseases*. 2011;34(6):503-512. doi:10.1016/j.cimid.2011.09.003

18. Rudy B, Fishell G, Lee S, Hjerling-Leffler J. Three Groups of Interneurons Account for Nearly 100% of Neocortical GABAergic Neurons. *Dev Neurobiol*. 2011;71(1):45-61. doi:10.1002/dneu.20853

19. Seidler B, Schmidt A, Mayr U, Nakhai H, Schmid RM, Schneider G, Saur D. A Cre-loxP-based mouse model for conditional somatic gene expression and knockdown in vivo by using avian retroviral vectors. *PNAS*. 2008;105(29):10137-10142. doi:10.1073/pnas.0800487105

20. Finak G, McDavid A, Yajima M, Deng J, Gersuk V, Shalek AK, Slichter CK, Miller HW, McElrath MJ, Prlic M, Linsley PS, Gottardo R. MAST: a flexible statistical framework for assessing transcriptional changes and characterizing heterogeneity in single-cell RNA sequencing data. *Genome Biology*. 2015;16(1):278. doi:10.1186/s13059-015-0844-5

21. Faul EJ, Lyles DS, Schnell MJ. Interferon Response and Viral Evasion by Members of the Family Rhabdoviridae. *Viruses*. 2009;1(3):832-851. doi:10.3390/v1030832

22. Butler A, Hoffman P, Smibert P, Papalexi E, Satija R. Integrating single-cell transcriptomic data across different conditions, technologies, and species. *Nat Biotechnol*. 2018;36(5):411-420. doi:10.1038/nbt.4096

23. Stuart T, Butler A, Hoffman P, Hafemeister C, Papalexi E, Mauck WM, Hao Y, Stoeckius M, Smibert P, Satija R. Comprehensive Integration of Single-Cell Data. *Cell*. 2019;177(7):1888-1902.e21. doi:10.1016/j.cell.2019.05.031

24. Xu X, Roby KD, Callaway EM. Immunochemical characterization of inhibitory mouse cortical neurons: Three chemically distinct classes of inhibitory cells. *Journal of Comparative Neurology*. 2010;518(3):389-404. doi:10.1002/cne.22229

25. Goubau D, Deddouche S, Reis e Sousa C. Cytosolic Sensing of Viruses. *Immunity*. 2013;38(5):855-869. doi:10.1016/j.immuni.2013.05.007

26. Sui H, Hao M, Chang W, Imamichi T. The Role of Ku70 as a Cytosolic DNA Sensor in Innate Immunity and Beyond. *Frontiers in Cellular and Infection Microbiology*. 2021;11:1046. doi:10.3389/fcimb.2021.761983

27. Liu X, Luo D, Yang N. Cytosolic Low Molecular Weight FGF2 Orchestrates RIG-I-Mediated Innate Immune Response. *J Immunol*. 2015;195(10):4943-4952. doi:10.4049/jimmunol.1501503

28. Koncina E, Roth L, Gonthier B, Bagnard D. *Role of Semaphorins during Axon Growth and Guidance*. Landes Bioscience; 2013. Accessed October 18, 2021. https://www.ncbi.nlm.nih.gov/books/NBK6446/

29. Pfeffer CK, Xue M, He M, Huang ZJ, Scanziani M. Inhibition of inhibition in visual cortex: the logic of connections between molecularly distinct interneurons. *Nat Neurosci*. 2013;16(8):1068-1076. doi:10.1038/nn.3446

30. Tasic B, Menon V, Nguyen TN, Kim TK, Jarsky T, Yao Z, Levi B, Gray LT, Sorensen SA, Dolbeare T, Bertagnolli D, Goldy J, Shapovalova N, Parry S, Lee C, Smith K, Bernard A, Madisen L, Sunkin SM, Hawrylycz M, Koch C, Zeng H. Adult mouse cortical cell taxonomy revealed by single cell transcriptomics. *Nat Neurosci*. 2016;19(2):335-346. doi:10.1038/nn.4216

31. Mo A, Mukamel EA, Davis FP, Luo C, Henry GL, Picard S, Urich MA, Nery JR, Sejnowski TJ, Lister R, Eddy SR, Ecker JR, Nathans J. Epigenomic Signatures of Neuronal Diversity in the Mammalian Brain. *Neuron*. 2015;86(6):1369-1384. doi:10.1016/j.neuron.2015.05.018

32. Peng H, Xie P, Liu L, Kuang X, Wang Y, Qu L, Gong H, Jiang S, Li A, Ruan Z, Ding L, Yao Z, Chen C, Chen M, Daigle TL, Dalley R, Ding Z, Duan Y, Feiner A, He P, Hill C, Hirokawa KE, Hong G, Huang L, Kebede S, Kuo HC, Larsen R, Lesnar P, Li L, Li Q, Li X, Li Y, Li Y, Liu A, Lu D, Mok S, Ng L, Nguyen TN, Ouyang Q, Pan J, Shen E, Song Y, Sunkin SM, Tasic B, Veldman MB, Wakeman W, Wan W, Wang P, Wang Q, Wang T, Wang Y, Xiong F, Xiong W, Xu W, Ye M, Yin L, Yu Y, Yuan J, Yuan J, Yun Z, Zeng S, Zhang S, Zhao S, Zhao Z, Zhou Z, Huang ZJ, Esposito L, Hawrylycz MJ, Sorensen SA, Yang XW, Zheng Y, Gu Z, Xie W, Koch C, Luo Q, Harris JA, Wang Y, Zeng H. Morphological diversity of single neurons in molecularly defined cell types. *Nature*. 2021;598(7879):174-181. doi:10.1038/s41586-021-03941-1

33. DeNardo LA, Berns DS, DeLoach K, Luo L. Connectivity of mouse somatosensory and prefrontal cortex examined with trans-synaptic tracing. *Nat Neurosci*. 2015;18(11):1687-1697. doi:10.1038/nn.4131

34. Kim EJ, Juavinett AL, Kyubwa EM, Jacobs MW, Callaway EM. Three Types of Cortical Layer 5 Neurons That Differ in Brain-wide Connectivity and Function. *Neuron*. 2015;88(6):1253-1267. doi:10.1016/j.neuron.2015.11.002

35. Wall NR, De La Parra M, Sorokin JM, Taniguchi H, Huang ZJ, Callaway EM. Brain-Wide Maps of Synaptic Input to Cortical Interneurons. *J Neurosci*. 2016;36(14):4000-4009. doi:10.1523/JNEUROSCI.3967-15.2016

36. Zhang D, He F, Bi S, Guo H, Zhang B, Wu F, Liang J, Yang Y, Tian Q, Ju C, Fan H, Chen J, Guo X, Luo Y. Genome-Wide Transcriptional Profiling Reveals Two Distinct Outcomes in Central Nervous System Infections of Rabies Virus. *Front Microbiol*. 2016;7:751. doi:10.3389/fmicb.2016.00751

37. Reardon TR, Murray AJ, Turi GF, Wirblich C, Croce KR, Schnell MJ, Jessell TM, Losonczy A. Rabies Virus CVS-N2cΔG Strain Enhances Retrograde Synaptic Transfer and Neuronal Viability. *Neuron*. 2016;89(4):711-724. doi:10.1016/j.neuron.2016.01.004

38. Lacar B, Linker SB, Jaeger BN, Krishnaswami SR, Barron JJ, Kelder MJE, Parylak SL, Paquola ACM, Venepally P, Novotny M, O'Connor C, Fitzpatrick C, Erwin JA, Hsu JY, Husband D, McConnell MJ, Lasken R, Gage FH. Nuclear RNA-seq of single neurons reveals molecular signatures of activation. *Nat Commun*. 2016;7(1):11022. doi:10.1038/ncomms11022

39. McGinnis CS, Murrow LM, Gartner ZJ. DoubletFinder: Doublet Detection in Single-Cell RNA Sequencing Data Using Artificial Nearest Neighbors. *cels*. 2019;8(4):329-337.e4. doi:10.1016/j.cels.2019.03.003

40. Yu G, Wang LG, Han Y, He QY. clusterProfiler: an R Package for Comparing Biological Themes Among Gene Clusters. *OMICS: A Journal of Integrative Biology*. 2012;16(5):284-287. doi:10.1089/omi.2011.0118

41. Liberzon A, Birger C, Thorvaldsdóttir H, Ghandi M, Mesirov JP, Tamayo P. The Molecular Signatures Database (MSigDB) hallmark gene set collection. *Cell Syst*. 2015;1(6):417-425. doi:10.1016/j.cels.2015.12.004

42. Subramanian A, Tamayo P, Mootha VK, Mukherjee S, Ebert BL, Gillette MA, Paulovich A, Pomeroy SL, Golub TR, Lander ES, Mesirov JP. Gene set enrichment analysis: A knowledge-based approach for interpreting genome-wide expression profiles. *PNAS*. 2005;102(43):15545-15550. doi:10.1073/pnas.0506580102

Chapter 2. Laminar connectivity of mouse primary visual cortex examined using Single Transcriptome Assisted Rabies Tracing (START)

Abstract

The complex functions of the neocortex rely on networks of interconnected excitatory and inhibitory interneurons. A plethora of studies have explored the diversity of cortical neurons, their connectivity patterns, and their role in information processing. Still, the advent of single-cell genomic technologies has unveiled that the extent of neuronal diversity may be much greater than originally imagined, raising new questions about the connectivity patterns of these more precisely defined cell subtypes. Here we present a method, Single Transcriptome Assisted Rabies Tracing (START), which combines monosynaptic rabies tracing and single-nuclei RNA sequencing (snRNA-seq) to identify the transcriptomic cell types that provide monosynaptic inputs to defined populations of neurons. We employed START to transcriptomically characterize the monosynaptic connections to layer 2/3 (L2/3) and layer 6 corticothalamic (L6 CT) neurons in mouse V1. At the subclass level, consistent with established circuit models, we found that L2/3 receives extensive input from L4 and to a smaller degree L5 intratelencephalic (IT) neurons, while L6 CT receives input from L5 intratelencephalic (IT) neurons. More importantly, with the improved cell type granularity achieved with transcriptomic characterization of inputs, we were able to uncover subtypes of somatostatin and parvalbumin interneurons that provide input to L2/3 and L6 CT excitatory neurons. Overall, this novel circuit tracing can help disentangle cortical circuits at transcriptomic resolution and expands the repertoire of tools available to neuroscientists studying circuit organization across all cortical areas in both health and disease.

Introduction

The neocortex is composed of a multitude of neuronal cell types thought to serve unique functional roles in cortical processing. Different cell types can be described based on distinct morphological, molecular, and physiological properties. In addition to intrinsic properties, the functional roles of neurons are derived from their excitatory and inhibitory inputs. Thus, to understand cortical processing it is necessary to investigate the precise ways that neurons connect to one another. Prior work has revealed that the majority of synaptic connections in the neocortex are made between neighboring neurons that make up local cortical microcircuits [1] and canonical principles of local microcircuit connectivity have been proposed [2–4].

Derived largely from experiments investigating cat primary visual cortex (V1), the canonical model follows as such: thalamic information arrives at layer 4 (L4), whose neurons send axonal projections to L2/3, which then projects to L5 and L6. Furthermore, principles governing the role of inhibitory neurons in cortical microcircuits are increasingly becoming well understood. For example, the rise of genetic tools for optogenetic manipulation, activity monitoring, and circuit tracing [5] has allowed for the study of the connectivity and functional roles of non-overlapping groups of inhibitory cortical neurons. Such studies have suggested that parvalbumin (Pvalb) neurons primarily connect to pyramidal cells and each other, somatostatin (Sst) neurons to other inhibitory neurons, but not themselves, and vasoactive intestinal peptide (Vip) neurons to Sst interneurons [6].

Despite progress in unraveling local cortical connectivity motifs, considerable variability across studies exists and outstanding questions regarding cell-type specific principles remain. For example, a study [7] investigating the role of barrel cortex Sst interneurons during active whisking described five distinct types of Sst interneurons, each with unique morphology, connectivity, and

activity, demonstrating the importance of characterizing neurons at a much granular resolution. Furthermore, the advent of single-cell genomic technologies has unveiled that the extent of neuronal diversity may be much greater than originally imagined [8–10], raising new questions about the connectivity patterns of these more precisely defined cell subtypes. Thus, our understanding of the specialized connectivity patterns underlying cortical networks remains rudimentary and many aspects of cortical circuit organization remain unknown.

Here we introduce a method, Single Transcriptome Assisted Rabies Tracing (START), which combines monosynaptic rabies tracing [11,12] and single-nuclei RNA sequencing (snRNA-seq) to identify the transcriptomic cell types that provide monosynaptic inputs to defined populations of neurons. We employ START to characterize the interlaminar synaptic connectivity of mouse V1 at the transcriptomic level. We conduct retrograde transsynaptic tracing to identify inputs to L2/3, L4, L5 intratelencephalic (IT), L5 extratelencephalic (ET), and L6 cortical thalamic (CT) excitatory neurons. Using the transcriptome-wide profile of input neurons we are able to classify them at much finer resolution compared to rabies-based circuit tracing methods that rely on antibody staining or intersectional approaches [13,14].

Results

Transcriptomic characterization of rabies labeled input cells

To investigate subtype specific inputs to excitatory neurons in distinct cortical layers of mouse V1 we conducted monosynaptic rabies tracing across multiple Cre-driver mouse lines followed by snRNA-seq. To restrict initial RVdG infection to excitatory neurons in specific layers, we first injected a Cre-dependent helper adeno-associated virus (AAV) into Sepw1-Cre, Scnn1a-Tg3-Cre, Tlx3-Cre, Npr3-IRES-Cre, and Ntsr1-Cre mice to target L2/3, L4, L5

intratelencephalic (IT), L5 extratelencephalic (ET), and L6 cortical thalamic (CT) excitatory neurons respectively. Pairing of AAV-DIO-TC66T-2A-oG with the Cre-driver mouse lines allows for the selective expression of a mutant TVA receptor, TVA^{66T}, and optimized rabies glycoprotein (oG) in layer specific Cre^{+} neurons (Figure 2.1A). TVA is a receptor for the avian sarcoma leucosis virus envelope protein, EnvA, and is necessary for entry of pseudotyped $EnvA^{+}$ RVdG into Cre^{+} cells. The use of mutant TVA^{66T}, with 10% efficiency for viral entry, eliminates Cre-independent background labeling [15], thus making it more suitable for tracing local monosynaptic inputs. Expression of oG in Cre^{+} neurons allows for trans-complementation in $EnvA^{+}$ RVdG infected neurons, also termed starter cells, allowing the virus to spread retrogradely into presynaptically connected inputs [16]. Importantly, because input neurons lack the glycoprotein required for further spread retrograde spread is halted and monosynaptically restricted. Three weeks after helper virus injection, a variant of EnvA+ RVdG that expresses the mCherry fluorophore tagged with the histone H2B nuclear targeting sequence (EnvA+ RVdG-H2B-mCherry) was injected and allowed to express for 10 days (Figure 2.1A). Following retrograde spread of RVdG into input neurons, V1 tissue was dissected and individual rabies-labeled nuclei sorted by flow cytometry (FANS). Individual nuclei were subjected to snRNAseq using the 10X genomics V3.1 platform (Figure 2.1A).

To transcriptomically classify rabies-labeled input neurons according to established transcriptomic cortical cell types we used SingleR to transfer the taxonomy cell type labels from a reference dataset to the rabies-labeled input neurons. We used a transcriptomic reference dataset, composed of uninfected nuclei collected from V1 with cell type annotations established according to the Allen Institute for Brain Science (AIBS) cell type taxonomy [9], that has been previously shown to allow accurate characterization of rabies-infected cortical neurons [17].

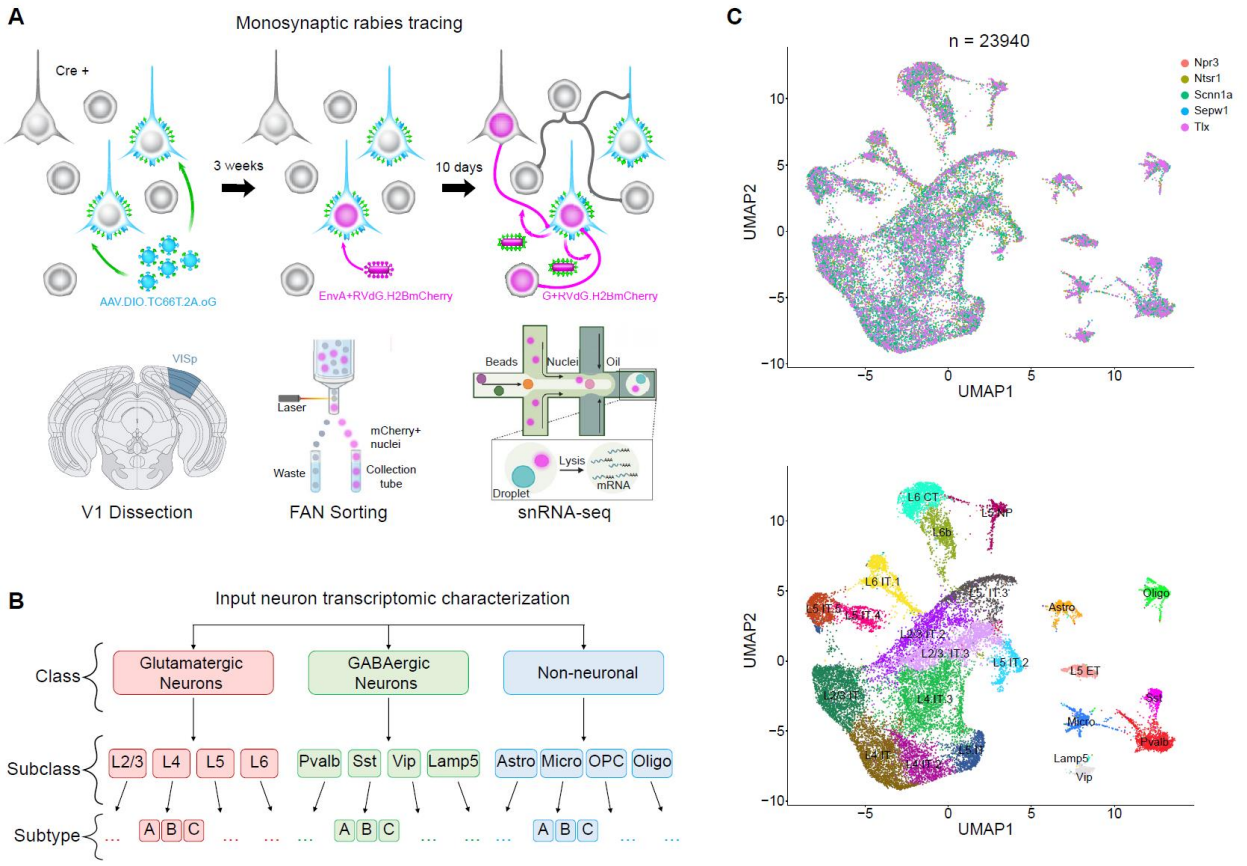

Figure 2.1 Transcriptomic characterization of rabies labeled input cells. (A) Schematic of experiment workflow. Monosynaptic rabies tracing was performed in Sepw1, Scnn1a, Tlx, Npr3, and Ntsr1 Cre driver mouse lines. Four mice per line were injected with AAV-DIO-TC66T-2A-oG in V1. Three weeks after helper virus injection, EnvA+ RVdG-H2B-mCherry was injected into the same region. 10 days after injection, V1 was dissected and mCherry+ nuclei collected using FANS. snRNA-seq of FANS–sorted rabies-infected nuclei was performed using the 10× Genomics platform. (B) Levels of taxonomy used to transcriptomically classify input neurons. (C) UMAP of 23,940 rabies-labeled nuclei color coded by the Cre-line tracing experiment they were collected from (top) or by subclass identity (bottom). Data from each line and tracing experiment were analyzed separately and then merged for visualization purposes.

SingleR was used to conduct supervised label transfer annotation of cell types for it's robustness against cell type similarity and increased cell type number compared to other computational methods [18,19]. Input neurons were classified at the class level (glutamatergic, GABAergic, or non-neuronal), subclass level (Sst, Pvalb, ect), and at the subtype level (Sst Chodl, Sst Esm1, ect) (Figure 2.1B and 2.1C).

Transcriptomic inputs to L2/3 excitatory neurons of mouse V1

A benefit of mapping transcriptomic inputs to L2/3 excitatory neurons is that we can compare the finding revealed using START to other methods that been used to examine this circuitry across distinct cortical areas, albeit at more coarse resolutions [14,20–24]. We conducted rabies tracing as described above using Sepw1-Cre to restrict starter cells to L2/3 excitatory neurons. After transcriptomically characterizing input cells, for each experimental animal (n=4, 1 male, 3 females) we calculated the number of inputs belonging to distinct neuronal subclasses as a fraction of the total neuronal inputs. At this resolution, we can better compare the proportions of inputs to prior findings. Furthermore, to determine whether certain subclass and subtypes were over or underrepresented in inputs to L2/3 we compared the proportions obtained to a computed estimate of the prevalence of distinct cell types in wild-type control mouse V1. To obtain a measure of the likely prevalence of cell types we performed 10,000 iterations of random sampling from the control dataset (methods).

We found that excitatory L4 IT excitatory neurons were significantly overrepresented in rabies-labeled inputs to L2/3 compared to baseline prevalence (39.38% vs 30.21% respectively, $p = 0.002$; Figure 2.2A), largely in agreement with previously reported connectivity [21–23]. Conflicting findings have been reported regarding excitatory projections from L5 to L2/3, with

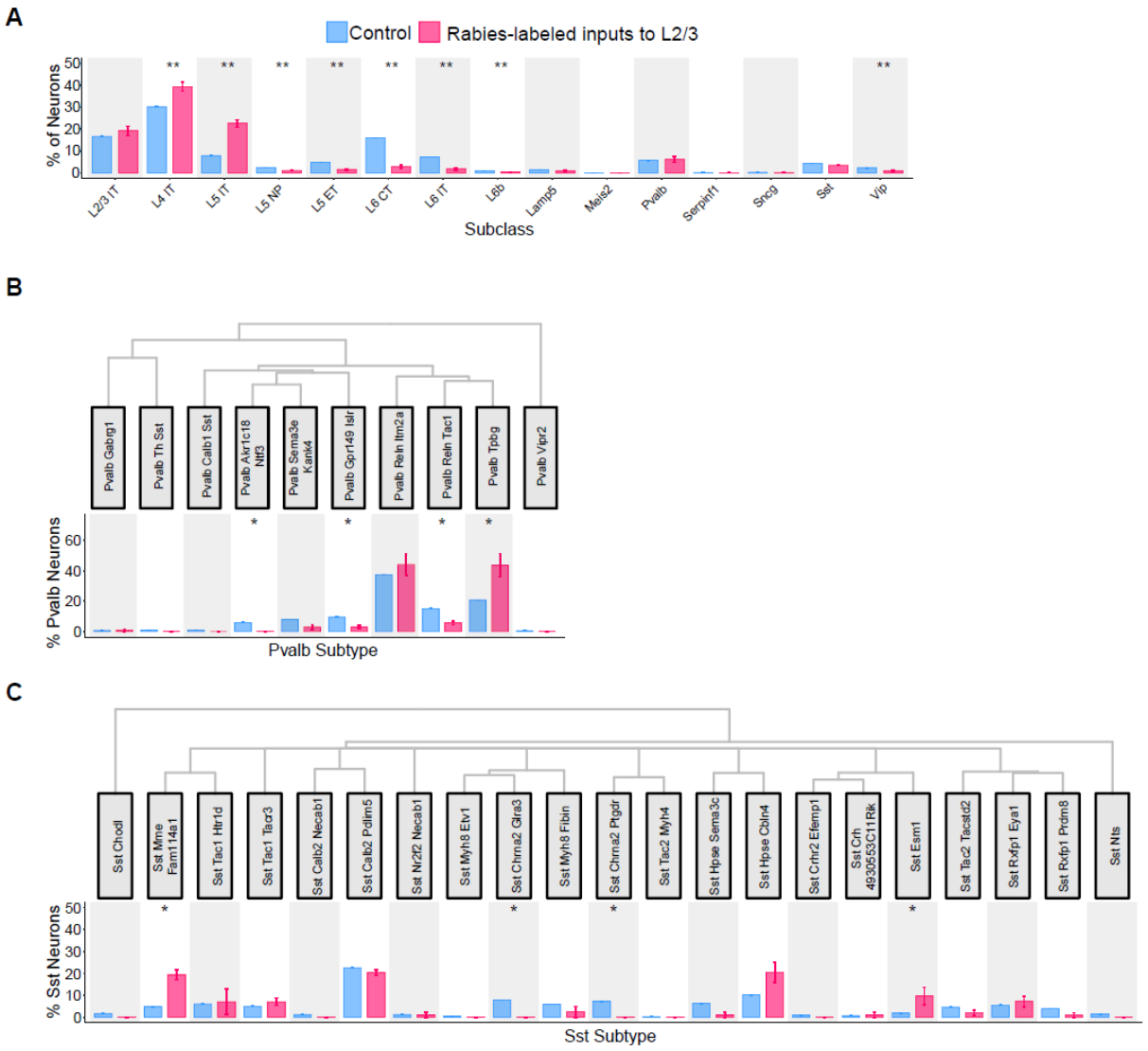

Figure 2.2 Transcriptomic inputs to L2/3 excitatory neurons of mouse V1. (A) Plot of the proportion of rabies-labeled input neurons to L2/3 belonging to distinct transcriptomic subclasses (red). In blue are the proportions of neurons belonging to each of the transcriptomic subclasses in control mouse V1 as determined by 10,000 iterations of random sampling from the control dataset. (B) Plot of the proportion of Pvalb rabies-labeled input neurons to L2/3 belonging to distinct Pvalb transcriptomic subtypes (red). In blue are the proportions of Pvalb neurons belonging to each Pvalb transcriptomic subtypes in control mouse V1 as determined by 10,000 iterations of random sampling from the control dataset. (C) Plot of the proportion of Sst rabies-labeled input neurons to L2/3 belonging to distinct Sst transcriptomic subtypes (red). In blue are the proportions of Sst neurons belonging to each Sst transcriptomic subtypes in control mouse V1 as determined by 10,000 iterations of random sampling from the control dataset. Values are reported as mean ± SEM. Statistics were calculated from Wilcoxon rank-sum test for non-parametric comparisons, with Benjamini–Hochberg correction for multiple comparisons. *$p \leq 0.05$, **$p \leq 0.01$

certain studies observing sparse connectivity [22,25,26] and others reporting a high number of excitatory L5 projections to L2/3 [21,24]. We observed an overrepresentation of L5 IT neurons (22.56% vs 7.84%. p = 0.002; Figure 2.2A) in rabies-labeled inputs to L2/3. On the other hand, L5 ET and L5 near-projecting (NP) neurons were underrepresented (1.51% vs 4.88%. p = 0.002 and 1.06% vs 2.44%, p = 0.003 respectively; Figure 2.2A). Excitatory L6 CT, L6 IT, and L6b were all underrepresented in rabies-label input neurons (2.8% vs 16%, p = 0.002; 1.64% vs 7.22%, p = 0.002; 0.31% vs 0.97%, p = 0.0048 respectively; Figure 2.2A).

Descriptions of inhibitory cell subclasses to L2/3 pyramidal neurons have previously been reported; however, these approaches largely fail to separate the major inhibitory cell subclasses (Sst, Pvalb, Vip) into more distinct inhibitory cell types [14,21]. We therefore sought to comprehensively examine inhibitory inputs to L2/3 at the much more precise resolution conferred by transcriptomic characterization. Specifically, we investigated whether L2/3 excitatory neurons receive differential input from distinct inhibitory subtypes. We calculated the number of inputs belonging to distinct inhibitory subtypes as a fraction of the total inputs from the corresponding subclass. Within the Pvalb subclass, we found one subtype that was overrepresented and three subtypes that were underrepresented. The Pvalb Tpbg subtype was significantly enriched compared to its prevalence in control mouse V1 (43.65% vs 20.7%, p = 0.015; Figure 2.2B). Pvalb Tpbg interneurons have been show to predominantly reside in and send extensive axonal projections to L2/3 [27]. Pvalb Akr1c18 Ntf3, Pvalb Gpr149 Islr, and Pvalb Reln Tac1 were all underrepresented in Pvalb inputs to L2/3 (0% vs 5.99%, p = 0.015; 2.94% vs 9.55%, p = 0.022; and 5.67% vs 15.07%, p = 0.015; Figure 2.2B). Pvalb Reln Tac1 has been found to correspond to fast-spiking cells with L5-dominant axon innervation. Similarly Pvalb

Akr1c18 Ntf3 and Pvalb Gpr149 Islr send extensive axonal projections to deep layers, but largely avoid L2/3 [27].

Within the Sst subclass, we found 2 subtypes that were overrepresented and two subtypes that were underrepresented. Sst Mme Fam114a1, one of the enriched Sst subtypes (19.26% vs 4.81%, p = 0.013; Figure 2.2C), has been found to send axons to L1 (Martinotti-like), but additionally is characterized as having axonal projections that split evenly across two distinct layers [27]. Sst Esm1, the other overrepresented subtype (9.67% vs 1.9%, p = 0.048; Figure 2.2C), is found primarily in L5 and interestingly sends projections primarily to deeper layers and have few projections to superficial layers [27]. Sst Chrna2 Glra3 and Sst Chrna2 Ptgdr were both underrepresented in Sst inputs (0% vs 7.89%, p = 0.039 and 0% vs 7.28%, p = 0.039; Figure 2.2C).

Transcriptomic inputs to L6 CT neurons of mouse V1

Similar to our current understanding of L2/3 local connectivity, our knowledge of local inputs to L6 CT excitatory neurons is limited to broad classifications of inputs [14,20,24]. At the subclass level, we observed an overrepresentation of L5 IT neurons (22.83% vs 7.85%, p = 0.0023) and an underrepresentation of L4 IT (20.17% vs 30.21%, p = 0.0023) and most inhibitory neuron subclasses (Figure 2.3A). At the subtype level two Pvalb subtypes and one Sst subtype were enriched in inputs to L6 CT (Figure 2.3B and 2.3C). Both enriched Pvalb subtypes, Pvalb Sema3e Kank4 (18.68% vs 7.97%, p = 0.01) and Pvalb Gpr149 Islr (17.95% vs 9.53%, p = 0.03) have axons targeting deep cortical layers [27]. Conversely, Pvalb Tpbg, which was overrepresented in inputs to L2/3, was underrepresented in inputs to L6 CT (12.16% vs 20.7%, p = 0.03). The Sst Chodl subtype was the only Sst subtype significantly overrepresented in input to

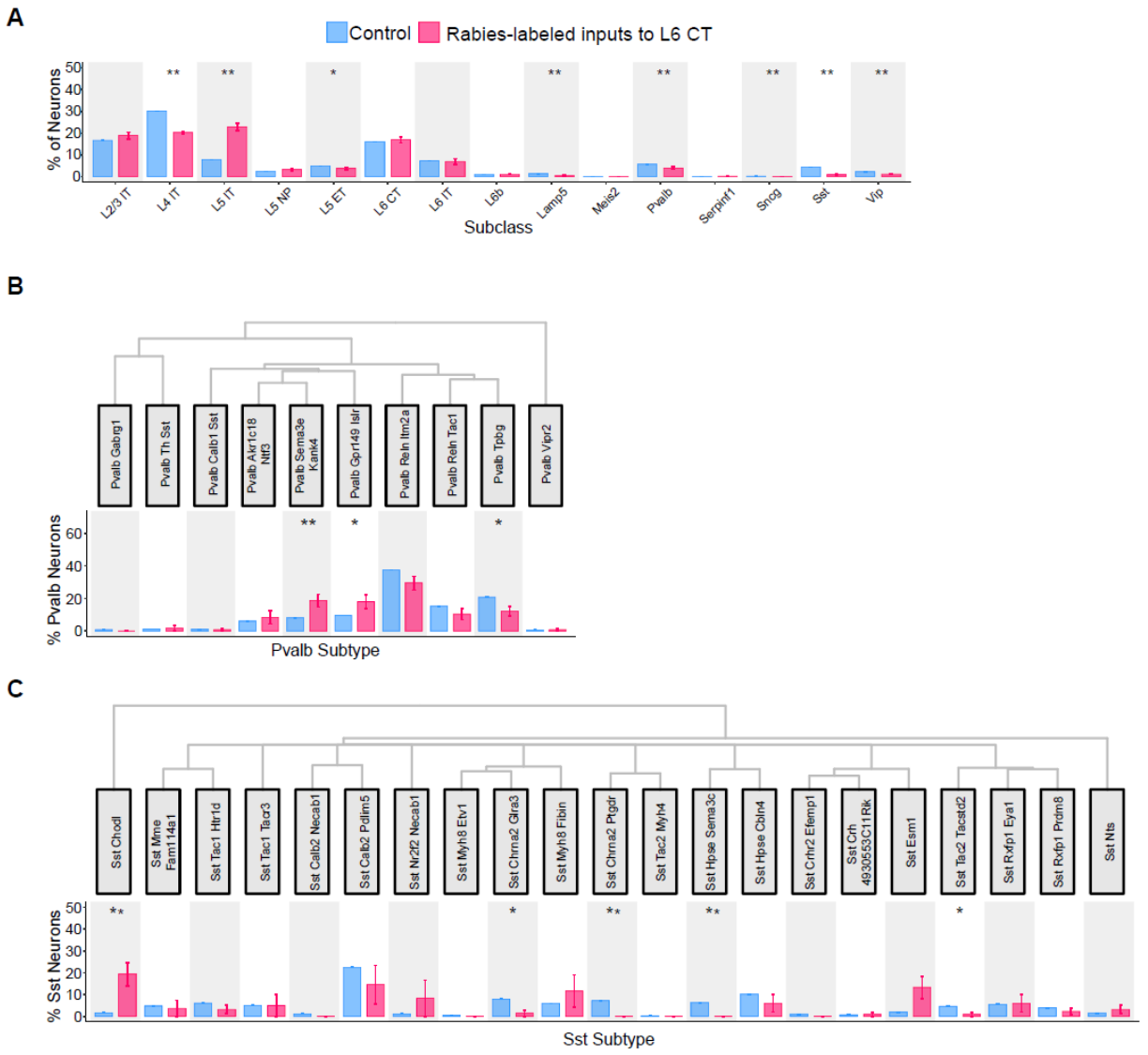

Figure 2.3 Transcriptomic inputs to L6 CT excitatory neurons of mouse V1. (A) Plot of the proportion of rabies-labeled input neurons to L6 CT belonging to distinct transcriptomic subclasses (red). In blue are the proportions of neurons belonging to each of the transcriptomic subclasses in control mouse V1 as determined by 10,000 iterations of random sampling from the control dataset. (B) Plot of the proportion of Pvalb rabies-labeled input neurons to L6 CT belonging to distinct Pvalb transcriptomic subtypes (red). In blue are the proportions of Pvalb neurons belonging to each Pvalb transcriptomic subtypes in control mouse V1 as determined by 10,000 iterations of random sampling from the control dataset. (C) Plot of the proportion of Sst rabies-labeled input neurons to L6 CT belonging to distinct Sst transcriptomic subtypes (red). In blue are the proportions of Sst neurons belonging to each Sst transcriptomic subtypes in control mouse V1 as determined by 10,000 iterations of random sampling from the control dataset. Values are reported as mean ± SEM. Statistics were calculated from Wilcoxon rank-sum test for non-parametric comparisons, with Benjamini–Hochberg correction for multiple comparisons. *$p \leq 0.05$, **$p \leq 0.01$

L6 CT (19.35% vs 1.68%, p = 0.005). The Sst Chodl subtype corresponds to long-range projecting non-Martinotti inhibitory interneurons that are found primarily in deeper layers [9,27–30]. Multiple Sst subtypes had sparse representation in L6 CT inputs including: Sst Chrna2 Glra3, Sst Chrna2 Ptgdr, Sst Hpse Cbln4, and Sst Tac2 Tacstd2.

Discussion

The recent explosion of genomic technologies has enabled our ability to characterize neural cell types based on their gene expression patterns [8], facilitating work towards the creation of a catalogue of the cellular building blocks that make up the mammalian brain [31]. However, cells do not function in isolation and our newfound understanding of neural diversity has generated new questions regarding connectivity properties at the level of transcriptomic cell types. Here we present START, a new technical approach for coupling circuit connectivity tracing with transcriptomic classification of neural cells. We use START to investigate interlaminar synaptic connectivity of mouse V1. By conducting our analysis at multiple levels of cell type granularity (subclass and subtype) we were able to compare subclass level results to prior published work and establish the utility of START as a circuit tracing tool. More importantly, with the more precise neural characterization achievable with START we were able to uncover new circuit connectivity motifs between inhibitory subtypes and excitatory neurons in distinct laminar layers.

Methods

Mouse Transgenic Lines

All experimental procedures were approved by the Salk Institute Animal Care and Use Committee. C57BL/6J mice were used as wild-type. GENSAT BAC transgenic Sepw1-Cre NP39, Scnn1a-Tg3-Cre, Tlx3-Cre PL56, Npr3-IRES-Cre-neo, and Ntsr1-Cre GN220 mice have been previously described [32–34]. Transgenic mice were maintained on C57BL/6J backgrounds. Mice were housed with a 12-hour light and 12-hour dark cycle and *ad libitum* access to food and water. Both male and female mice were used for RNA sequencing experiments.

Virus Preparation

AAV8-DIO-TC66T-2A-oG (4.31E+13 GC/mL) and EnvA+RVdG-H2BmCherry (7.43E+07) were produced by the Salk GT3 Viral Core.

Animal Surgery for Virus Injection

For rabies input tracing transgenic mice received AAV helper injections at P49 – P60. Mice were initially anesthetized with 2% isoflurane and maintained at 1.5% isoflurane after placement on a stereotax (David Kopf Instruments, Model 940 series) for surgery and stereotaxic injections. A small craniotomy was made with a mounted drill over the primary visual cortex of the left hemisphere using the following coordinates: 3.4 mm posterior and 2.6 mm lateral relative to bregma. 100 nl of diluted AAV8-DIO-TC66T-2A-oG (4.31E+12 GC/mL) was injected into the center of V1 0.5–0.7 mm ventral from the pia using a pulled glass pipette with a tip size of 30 um connected to a 1ml syringe with 18G tubing adaptor and tubing. To prevent backflow, the pipette was left in the brain for 5 minutes after injection. Three weeks after AAV helper virus

injection, 200 nl of EnvA+RVdG-H2BmCherry (7.43E+07 IU/ml) was injected into the same site in V1. After recovery, mice were given water with ibuprofen (30mg/kg) and housed for 10 days before tissue harvest to allow for fluorescent protein expression.

Brain Dissection and Single Nuclei Isolation

Ten days after rabies injection, animals were euthanized with an overdose of isoflurane. Brains were extracted and immediately submerged in ice-cold slicing solution (2.5mM KCl, 0.5mM CaCl2, 7mM MgCl2, 1.25mM NaH2PO4, 110mM sucrose, 10mM glucose and 25mM NaHCO3) that was bubbled with carbogen. Coronal brain slices (400um thick) were cut using VF-300 CompresstomeTM (Precisionary Instruments, Greenville,NC) and submerged in ice-cold slicing solution. Subregions of V1 containing mCherry+ nuclei in brain slices were micro-dissected out under a fluorescent dissection microscope (Olympus SZX6) and transferred to microcentrifuge tubes and immediately frozen in dry ice, and subsequently stored at -80°C. The remaining brain slices after dissection were collected, fixed with ice-cold 4% PFA overnight, stained with DAPI, and scanned with a 10x objective to validate correct V1 dissection using an Olympus BX63 Microscope.

Single nuclei preparations were performed following a published protocol [35] with modification. In summary, the frozen brain tissues were transferred to pre-chilled dounce homogenizers with 1ml NIM buffer (0.25M sucrose, 25mM KCl, 5mM MgCl2, 10mM Tris-HCl (pH7.4), 1mM DTT (Sigma 646563), 10ul of protease inhibitor (Sigma P8340), 1.5ul of RNasin Plus RNase inhibitor (Promega, N2611)), 0.1% Triton X-100, and 10 uM DAPI, and gently homogenized on ice with ice-cold pestles 10 - 15 times. The homogenate was transferred to pre-chilled microcentrifuge tubes and centrifuged at 1000 rcf for 8 min at 4°C to pellet the nuclei.

The supernatant was aspirated, the pellet gently resuspended in ice-cold 1ml NIM buffer, and again centrifuged at 1000 rcf for 8 min at 4°C. The pellet was then resuspended in 450ul of nuclei storage buffer (0.25M sucrose, 5mM MgCl2, 10mM Tris-HCl (pH7.4), 1mM DTT, 9ul of Protease inhibitor), and filtered through a 40μM cell strainer. The sample was incubated with 50ul of nuclease-free BSA to prevent nuclei clumping.

Fluorescence-activated nuclei sorting of single nuclei was performed using a FACS Aria Fusion sorter with a 70 μM nozzle at 22.5 PSI sheath pressure. DAPI+/mCherry+ rabies-infected nuclei were sorted into 0.2ml Eppendorf PCR tubes and immediately loaded onto the 10X Genomics Chromium Controller. Biological replicates were processed on different days.

10x Chromium RNA-Sequencing

For 10x processing, we used Chromium Next GEM single-cell 3' Kit (v3.1 Dual Index) and Chromium Next GEM single-cell 3' LT Kit (v3.1 Dual Index) (10x Genomics, PN-1000127 and PN-1000325). We followed the manufacturer's instructions for single-cell capture, barcoding, reverse transcription, cDNA amplification, and library construction. We targeted sequencing depth of about 100,000 reads per cell. Pooled libraries were sequenced on Illumina NovaSeq^{TM} 6000 Sequencing System (S4) and raw read (fastq) files were aligned to the mouse pre-mRNA reference transcriptome (mm10) using the 10x Genomics CellRanger pipeline (version 6.0.). Intronic reads were included in expression quantification using the include-introns parameter.

RNA-seq data quality control and cell-type annotation

Reference data used in this study includes 10x v3 single nucleus RNA-seq from primary visual cortex obtained from the Allen Institute for Brain Science (AIBS, GSE196771). Reference 10x v3 nuclei were assigned to previously published VISp cell type taxonomy [9] using a nearest centroid classifier based on a set of 563 markers that were detected in both datasets (expression > 0). To estimate the robustness of mapping, classification was repeated 100 times, each time using 80% of randomly sampled markers, and the probability for each cell to map to every reference cluster was computed. R (version 4.1.1), Seurat (version 4.0) [36,37], and SingleR (version 4.1) [18] were used for snRNA-seq analysis. Doublets were identified using DoubletFinder [38] and excluded from analysis. The percentage of mitochondrial transcripts for each nucleus was calculated and added as metadata to the Seurat object using percent.mito. Nuclei with less than 500 genes, more than 8000 genes, and greater than 0.5% of mitochondrial genes were excluded from analysis.

SingleR was used for supervised labeled transfer of class, subclass, and subtype taxonomy from the reference dataset to rabies-labeled input neurons. To decrease supervised annotation performance susceptibility to the effects of large subtype numbers, cell type similarity, and rare cell type detection we employed pseudo-bulk aggregation of reference cells within specific subtype labels [19]. After log-normalization and principal components analysis, k-means clustering within each subtype label is performed to create pseudo-bulk reference samples that preserve the label's internal distribution. To classify rabies-labeled input neurons the Spearman correlation between each rabies-labeled input neuron's expression profile and that of each reference sample is computed. This process is performed iteratively, rerunning the correlation analysis but using only the top cell types from the previous step until only one cell

type annotation remains. At each iteration only the variable genes between the top cell types are used to differentiate between closely related cell types. Poor quality or ambiguous assignments were determined according to the per-cell delta score, which is the difference between the score for the assigned label and the median across all labels for each cell. Low deltas indicate an uncertain assignment and high deltas score indicate a high confidence assignment. Cells with small deltas that were outliers compared to other annotated cells in that label were excluded from further analysis.

We compared the proportion of rabies-labeled input neurons corresponding to distinct transcriptomic subtypes to the prevalence of those subtypes in wild-type control mouse V1. To obtain a comparable measure of the likely prevalence of any given subtype we first performed random sampling from the control dataset, where the number of cells sampled (n) = the average number of input cells obtained across mice within a Cre-mouse line (4 mice per line). 10,000 iterations of random sampling of n cells were performed independently for each Cre-mouse line. The prevalence of a given subtype was reported as the mean of the subtype proportion across all 10,000 iterations. This mean was compared to the proportion mean obtained across 4 animals in each set of rabies tracing experiments. Statistical significance was assessed by Wilcoxon rank-sum test with Benjamini–Hochberg correction for multiple comparison using R. Not significant (ns): $P > 0.05$, *$P \leq 0.05$, **$P \leq 0.01$, ***$P \leq 0.001$, ****$P \leq 0.0001$.

Appendix

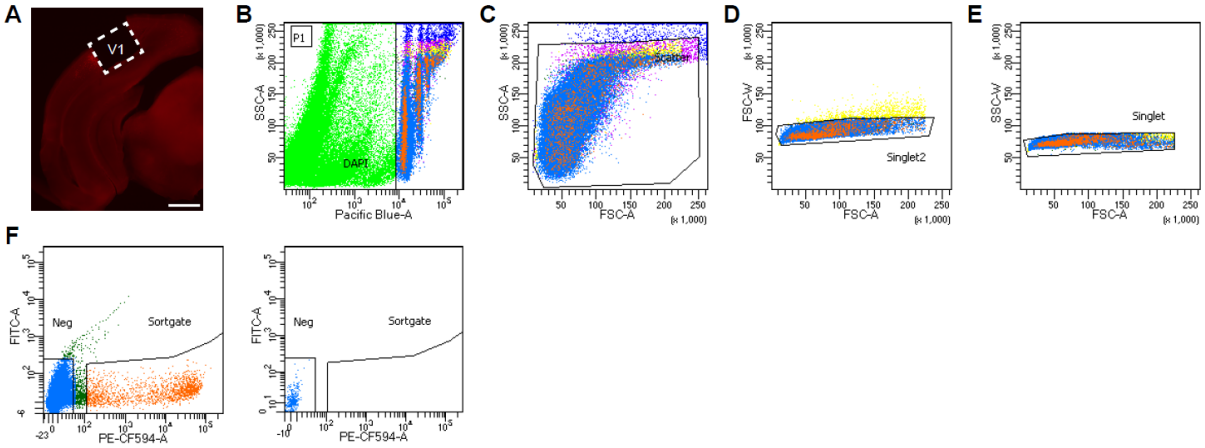

Figure 2.S1 Details on rabies-labeled presynaptic input nuclei sorting, related to Figure 1. (A) Example image of coronal brain slice from a monosynaptic rabies tracing experiment after V1 dissection. Dashed box indicates dissected region. Long-range rabies-labeled input neurons to V1 found in non-dissected brain regions are visible outside of V1 boundary. (B-F) Detailed gating strategy of fluorescence-activated nuclei sorting used for sorting mCherry$^+$ rabies-labeled nuclei. Gate 1 (B) selects for DAPI$^+$ nuclei to exclude debris. Gate 2-4 (C-E) exclude cell doublets based on single nuclei morphology. Gate 5 (F) selects for mCherry$^+$ fluorescence.

Acknowledgements

Chapter 2, in full, is currently being prepared for submission for publication and will include Marley Rossa, Will N. Lagos, and Neelakshi Patne, as co-authors and Professor Edward Callaway as the senior author. The dissertation author will be the first author of this work.

References

1. Douglas RJ, Koch C, Mahowald M, Martin KAC, Suarez HH. Recurrent Excitation in Neocortical Circuits. *Science*. 1995;269(5226):981-985. doi:10.1126/science.7638624

2. Douglas RJ, Martin KAC. Neuronal circuits of the neocortex. *Annu Rev Neurosci*. 2004;27:419-451. doi:10.1146/annurev.neuro.27.070203.144152

3. Douglas RJ, Martin KAC. Mapping the Matrix: The Ways of Neocortex. *Neuron*. 2007;56(2):226-238. doi:10.1016/j.neuron.2007.10.017

4. Kätzel D, Zemelman BV, Buetfering C, Wölfel M, Miesenböck G. The columnar and laminar organization of inhibitory connections to neocortical excitatory cells. *Nat Neurosci*. 2011;14(1):100-107. doi:10.1038/nn.2687

5. Luo L, Callaway EM, Svoboda K. Genetic Dissection of Neural Circuits: A Decade of Progress. *Neuron*. 2018;98(2):256-281. doi:10.1016/j.neuron.2018.03.040

6. Pfeffer CK, Xue M, He M, Huang ZJ, Scanziani M. Inhibition of inhibition in visual cortex: the logic of connections between molecularly distinct interneurons. *Nat Neurosci*. 2013;16(8):1068-1076. doi:10.1038/nn.3446

7. Muñoz W, Tremblay R, Levenstein D, Rudy B. Layer-specific modulation of neocortical dendritic inhibition during active wakefulness. *Science*. 2017;355(6328):954-959. doi:10.1126/science.aag2599

8. Armand EJ, Li J, Xie F, Luo C, Mukamel EA. Single-Cell Sequencing of Brain Cell Transcriptomes and Epigenomes. *Neuron*. 2021;109(1):11-26. doi:10.1016/j.neuron.2020.12.010

9. Tasic B, Yao Z, Graybuck LT, Smith KA, Nguyen TN, Bertagnolli D, Goldy J, Garren E, Economo MN, Viswanathan S, Penn O, Bakken T, Menon V, Miller J, Fong O, Hirokawa KE, Lathia K, Rimorin C, Tieu M, Larsen R, Casper T, Barkan E, Kroll M, Parry S, Shapovalova NV, Hirschstein D, Pendergraft J, Sullivan HA, Kim TK, Szafer A, Dee N, Groblewski P, Wickersham I, Cetin A, Harris JA, Levi BP, Sunkin SM, Madisen L, Daigle TL, Looger L, Bernard A, Phillips J, Lein E, Hawrylycz M, Svoboda K, Jones AR, Koch C, Zeng H. Shared and distinct transcriptomic cell types across neocortical areas. *Nature*. 2018;563(7729):72-78. doi:10.1038/s41586-018-0654-5

10. Yao Z, van Velthoven CTJ, Nguyen TN, Goldy J, Sedeno-Cortes AE, Baftizadeh F, Bertagnolli D, Casper T, Chiang M, Crichton K, Ding SL, Fong O, Garren E, Glandon A, Gouwens NW, Gray J, Graybuck LT, Hawrylycz MJ, Hirschstein D, Kroll M, Lathia K, Lee C, Levi B, McMillen D, Mok S, Pham T, Ren Q, Rimorin C, Shapovalova N, Sulc J, Sunkin SM, Tieu M, Torkelson A, Tung H, Ward K, Dee N, Smith KA, Tasic B, Zeng H. A taxonomy of transcriptomic cell types across the isocortex and hippocampal formation. *Cell*. 2021;184(12):3222-3241.e26. doi:10.1016/j.cell.2021.04.021

11. Wall NR, Wickersham IR, Cetin A, Parra MDL, Callaway EM. Monosynaptic circuit tracing in vivo through Cre-dependent targeting and complementation of modified rabies virus. *PNAS*. 2010;107(50):21848-21853. doi:10.1073/pnas.1011756107

12. Wickersham IR, Finke S, Conzelmann KK, Callaway EM. Retrograde neuronal tracing with a deletion-mutant rabies virus. *Nat Methods*. 2007;4(1):47-49. doi:10.1038/nmeth999

13. Ährlund-Richter S, Xuan Y, van Lunteren JA, Kim H, Ortiz C, Pollak Dorocic I, Meletis K, Carlén M. A whole-brain atlas of monosynaptic input targeting four different cell types in the medial prefrontal cortex of the mouse. *Nat Neurosci*. 2019;22(4):657-668. doi:10.1038/s41593-019-0354-y

14. Yetman MJ, Washburn E, Hyun JH, Osakada F, Hayano Y, Zeng H, Callaway EM, Kwon HB, Taniguchi H. Intersectional Monosynaptic Tracing for Dissecting Subtype-Specific Organization of GABAergic Interneuron Inputs. *Nat Neurosci*. 2019;22(3):492-502. doi:10.1038/s41593-018-0322-y

15. Miyamichi K, Shlomai-Fuchs Y, Shu M, Weissbourd BC, Luo L, Mizrahi A. Dissecting Local Circuits: Parvalbumin Interneurons Underlie Broad Feedback Control of Olfactory Bulb Output. *Neuron*. 2013;80(5):1232-1245. doi:10.1016/j.neuron.2013.08.027

16. Kim EJ, Jacobs MW, Ito-Cole T, Callaway EM. Improved Monosynaptic Neural Circuit Tracing Using Engineered Rabies Virus Glycoproteins. *Cell Reports*. 2016;15(4):692-699. doi:10.1016/j.celrep.2016.03.067

17. Patiño M, Lagos WN, Patne NS, Tasic B, Zeng H, Callaway EM. Single-cell transcriptomic classification of rabies-infected cortical neurons. *Proceedings of the National Academy of Sciences*. 2022;119(22):e2203677119. doi:10.1073/pnas.2203677119

18. Aran D, Looney AP, Liu L, Wu E, Fong V, Hsu A, Chak S, Naikawadi RP, Wolters PJ, Abate AR, Butte AJ, Bhattacharya M. Reference-based analysis of lung single-cell sequencing reveals a transitional profibrotic macrophage. *Nat Immunol*. 2019;20(2):163-172. doi:10.1038/s41590-018-0276-y

19. Huang Q, Liu Y, Du Y, Garmire LX. Evaluation of Cell Type Annotation R Packages on Single-cell RNA-seq Data. *Genomics, Proteomics & Bioinformatics*. 2021;19(2):267-281. doi:10.1016/j.gpb.2020.07.004

20. DeNardo LA, Berns DS, DeLoach K, Luo L. Connectivity of mouse somatosensory and prefrontal cortex examined with trans-synaptic tracing. *Nat Neurosci*. 2015;18(11):1687-1697. doi:10.1038/nn.4131

21. Hage TA, Bosma-Moody A, Baker CA, Kratz MB, Campagnola L, Jarsky T, Zeng H, Murphy GJ. Synaptic connectivity to L2/3 of primary visual cortex measured by two-photon

optogenetic stimulation. Mao T, Calabrese RL, eds. *eLife*. 2022;11:e71103. doi:10.7554/eLife.71103

22. Rossi MA, Basiri ML, Liu Y, Hashikawa Y, Hashikawa K, Fenno LE, Kim YS, Ramakrishnan C, Deisseroth K, Stuber GD. Transcriptional and functional divergence in lateral hypothalamic glutamate neurons projecting to the lateral habenula and ventral tegmental area. *Neuron*. Published online October 7, 2021. doi:10.1016/j.neuron.2021.09.020

23. Wertz A, Trenholm S, Yonehara K, Hillier D, Raics Z, Leinweber M, Szalay G, Ghanem A, Keller G, Rózsa B, Conzelmann KK, Roska B. Single-cell–initiated monosynaptic tracing reveals layer-specific cortical network modules. *Science*. 2015;349(6243):70-74. doi:10.1126/science.aab1687

24. Yao S, Wang Q, Hirokawa KE, Ouellette B, Ahmed R, Bomben J, Brouner K, Casal L, Caldejon S, Cho A, Dotson NI, Daigle TL, Egdorf T, Enstrom R, Gary A, Gelfand E, Gorham M, Griffin F, Gu H, Hancock N, Howard R, Kuan L, Lambert S, Lee EK, Luviano J, Mace K, Maxwell M, Mortrud MT, Naeemi M, Nayan C, Ngo NK, Nguyen T, North K, Ransford S, Ruiz A, Seid S, Swapp J, Taormina MJ, Wakeman W, Zhou T, Nicovich PR, Williford A, Potekhina L, McGraw M, Ng L, Groblewski PA, Tasic B, Mihalas S, Harris JA, Cetin A, Zeng H. *A Whole-Brain Monosynaptic Input Connectome to Neuron Classes in Mouse Visual Cortex*.; 2021:2021.09.29.459010. doi:10.1101/2021.09.29.459010

25. Jiang X, Shen S, Cadwell CR, Berens P, Sinz F, Ecker AS, Patel S, Tolias AS. Principles of connectivity among morphologically defined cell types in adult neocortex. *Science*. 2015;350(6264):aac9462. doi:10.1126/science.aac9462

26. Lefort S, Tomm C, Sarria JCF, Petersen CCH. The Excitatory Neuronal Network of the C2 Barrel Column in Mouse Primary Somatosensory Cortex. *Neuron*. 2009;61(2):301-316. doi:10.1016/j.neuron.2008.12.020

27. Gouwens NW, Sorensen SA, Baftizadeh F, Budzillo A, Lee BR, Jarsky T, Alfiler L, Baker K, Barkan E, Berry K, Bertagnolli D, Bickley K, Bomben J, Braun T, Brouner K, Casper T, Crichton K, Daigle TL, Dalley R, de Frates RA, Dee N, Desta T, Lee SD, Dotson N, Egdorf T, Ellingwood L, Enstrom R, Esposito L, Farrell C, Feng D, Fong O, Gala R, Gamlin C, Gary A, Glandon A, Goldy J, Gorham M, Graybuck L, Gu H, Hadley K, Hawrylycz MJ, Henry AM, Hill D, Hupp M, Kebede S, Kim TK, Kim L, Kroll M, Lee C, Link KE, Mallory M, Mann R, Maxwell M, McGraw M, McMillen D, Mukora A, Ng L, Ng L, Ngo K, Nicovich PR, Oldre A, Park D, Peng H, Penn O, Pham T, Pom A, Popović Z, Potekhina L, Rajanbabu R, Ransford S, Reid D, Rimorin C, Robertson M, Ronellenfitch K, Ruiz A, Sandman D, Smith K, Sulc J, Sunkin SM, Szafer A, Tieu M, Torkelson A, Trinh J, Tung H, Wakeman W, Ward K, Williams G, Zhou Z, Ting JT, Arkhipov A, Sümbül U, Lein ES, Koch C, Yao Z, Tasic B, Berg J, Murphy GJ, Zeng H. Integrated Morphoelectric and Transcriptomic Classification of Cortical GABAergic Cells. *Cell*. 2020;183(4):935-953.e19. doi:10.1016/j.cell.2020.09.057

28. He M, Tucciarone J, Lee S, Nigro MJ, Kim Y, Levine JM, Kelly SM, Krugikov I, Wu P, Chen Y, Gong L, Hou Y, Osten P, Rudy B, Huang ZJ. Strategies and Tools for Combinatorial Targeting of GABAergic Neurons in Mouse Cerebral Cortex. *Neuron*. 2016;91(6):1228-1243. doi:10.1016/j.neuron.2016.08.021

29. Kilduff TS, Cauli B, Gerashchenko D. Activation of Cortical Interneurons During Sleep: An Anatomical Link to Homeostatic Sleep Regulation? *Trends Neurosci*. 2011;34(1):10-19. doi:10.1016/j.tins.2010.09.005

30. Paul A, Crow M, Raudales R, He M, Gillis J, Huang ZJ. Transcriptional Architecture of Synaptic Communication Delineates GABAergic Neuron Identity. *Cell*. 2017;171(3):522-539.e20. doi:10.1016/j.cell.2017.08.032

31. Callaway EM, Dong HW, Ecker JR, Hawrylycz MJ, Huang ZJ, Lein ES, Ngai J, Osten P, Ren B, Tolias AS, White O, Zeng H, Zhuang X, Ascoli GA, Behrens MM, Chun J, Feng G, Gee JC, Ghosh SS, Halchenko YO, Hertzano R, Lim BK, Martone ME, Ng L, Pachter L, Ropelewski AJ, Tickle TL, Yang XW, Zhang K, Bakken TE, Berens P, Daigle TL, Harris JA, Jorstad NL, Kalmbach BE, Kobak D, Li YE, Liu H, Matho KS, Mukamel EA, Naeemi M, Scala F, Tan P, Ting JT, Xie F, Zhang M, Zhang Z, Zhou J, Zingg B, Armand E, Yao Z, Bertagnolli D, Casper T, Crichton K, Dee N, Diep D, Ding SL, Dong W, Dougherty EL, Fong O, Goldman M, Goldy J, Hodge RD, Hu L, Keene CD, Krienen FM, Kroll M, Lake BB, Lathia K, Linnarsson S, Liu CS, Macosko EZ, McCarroll SA, McMillen D, Nadaf NM, Nguyen TN, Palmer CR, Pham T, Plongthongkum N, Reed NM, Regev A, Rimorin C, Romanow WJ, Savoia S, Siletti K, Smith K, Sulc J, Tasic B, Tieu M, Torkelson A, Tung H, van Velthoven CTJ, Vanderburg CR, Yanny AM, Fang R, Hou X, Lucero JD, Osteen JK, Pinto-Duarte A, Poirion O, Preissl S, Wang X, Aldridge AI, Bartlett A, Boggeman L, O'Connor C, Castanon RG, Chen H, Fitzpatrick C, Luo C, Nery JR, Nunn M, Rivkin AC, Tian W, Dominguez B, Ito-Cole T, Jacobs M, Jin X, Lee CT, Lee KF, Miyazaki PA, Pang Y, Rashid M, Smith JB, Vu M, Williams E, Biancalani T, Booeshaghi AS, Crow M, Dudoit S, Fischer S, Gillis J, Hu Q, Kharchenko PV, Niu SY, Ntranos V, Purdom E, Risso D, de Bézieux HR, Somasundaram S, Street K, Svensson V, Vaishnav ED, Van den Berge K, Welch JD, An X, Bateup HS, Bowman I, Chance RK, Foster NN, Galbavy W, Gong H, Gou L, Hatfield JT, Hintiryan H, Hirokawa KE, Kim G, Kramer DJ, Li A, Li Xiangning, Luo Q, Muñoz-Castañeda R, Stafford DA, Feng Z, Jia X, Jiang S, Jiang T, Kuang X, Larsen R, Lesnar P, Li Yaoyao, Li Yuanyuan, Liu L, Peng H, Qu L, Ren M, Ruan Z, Shen E, Song Y, Wakeman W, Wang P, Wang Yimin, Wang Yun, Yin L, Yuan J, Zhao S, Zhao X, Narasimhan A, Palaniswamy R, Banerjee S, Ding L, Huilgol D, Huo B, Kuo HC, Laturnus S, Li Xu, Mitra PP, Mizrachi J, Wang Q, Xie P, Xiong F, Yu Y, Eichhorn SW, Berg J, Bernabucci M, Bernaerts Y, Cadwell CR, Castro JR, Dalley R, Hartmanis L, Horwitz GD, Jiang X, Ko AL, Miranda E, Mulherkar S, Nicovich PR, Owen SF, Sandberg R, Sorensen SA, Tan ZH, Allen S, Hockemeyer D, Lee AY, Veldman MB, Adkins RS, Ament SA, Bravo HC, Carter R, Chatterjee A, Colantuoni C, Crabtree J, Creasy H, Felix V, Giglio M, Herb BR, Kancherla J, Mahurkar A, McCracken C, Nickel L, Olley D, Orvis J, Schor M, Hood G, Dichter B, Grauer M, Helba B, Bandrowski A, Barkas N, Carlin B, D'Orazi FD, Degatano K, Gillespie TH, Khajouei F, Konwar K, Thompson C, Kelly K, Mok S, Sunkin S. A

multimodal cell census and atlas of the mammalian primary motor cortex. *Nature*. 2021;598(7879):86-102. doi:10.1038/s41586-021-03950-0

32. Daigle TL, Madisen L, Hage TA, Valley MT, Knoblich U, Larsen RS, Takeno MM, Huang L, Gu H, Larsen R, Mills M, Bosma-Moody A, Siverts LA, Walker M, Graybuck LT, Yao Z, Fong O, Nguyen TN, Garren E, Lenz GH, Chavarha M, Pendergraft J, Harrington J, Hirokawa KE, Harris JA, Nicovich PR, McGraw MJ, Ollerenshaw DR, Smith KA, Baker CA, Ting JT, Sunkin SM, Lecoq J, Lin MZ, Boyden ES, Murphy GJ, Costa NM da, Waters J, Li L, Tasic B, Zeng H. A Suite of Transgenic Driver and Reporter Mouse Lines with Enhanced Brain-Cell-Type Targeting and Functionality. *Cell*. 2018;174(2):465-480.e22. doi:10.1016/j.cell.2018.06.035

33. Gerfen CR, Paletzki R, Heintz N. GENSAT BAC Cre-Recombinase Driver Lines to Study the Functional Organization of Cerebral Cortical and Basal Ganglia Circuits. *Neuron*. 2013;80(6):1368-1383. doi:10.1016/j.neuron.2013.10.016

34. Madisen L, Zwingman TA, Sunkin SM, Oh SW, Zariwala HA, Gu H, Ng LL, Palmiter RD, Hawrylycz MJ, Jones AR, Lein ES, Zeng H. A robust and high-throughput Cre reporting and characterization system for the whole mouse brain. *Nat Neurosci*. 2010;13(1):133-140. doi:10.1038/nn.2467

35. Lacar B, Linker SB, Jaeger BN, Krishnaswami SR, Barron JJ, Kelder MJE, Parylak SL, Paquola ACM, Venepally P, Novotny M, O'Connor C, Fitzpatrick C, Erwin JA, Hsu JY, Husband D, McConnell MJ, Lasken R, Gage FH. Nuclear RNA-seq of single neurons reveals molecular signatures of activation. *Nat Commun*. 2016;7(1):11022. doi:10.1038/ncomms11022

36. Butler A, Hoffman P, Smibert P, Papalexi E, Satija R. Integrating single-cell transcriptomic data across different conditions, technologies, and species. *Nat Biotechnol*. 2018;36(5):411-420. doi:10.1038/nbt.4096

37. Stuart T, Butler A, Hoffman P, Hafemeister C, Papalexi E, Mauck WM, Hao Y, Stoeckius M, Smibert P, Satija R. Comprehensive Integration of Single-Cell Data. *Cell*. 2019;177(7):1888-1902.e21. doi:10.1016/j.cell.2019.05.031

38. McGinnis CS, Murrow LM, Gartner ZJ. DoubletFinder: Doublet Detection in Single-Cell RNA Sequencing Data Using Artificial Nearest Neighbors. *cels*. 2019;8(4):329-337.e4. doi:10.1016/j.cels.2019.03.003

Chapter 3. Quantification of monosynaptic rabies tracing efficiency

Abstract

Retrograde monosynaptic tracing using genetically modified rabies virus is an important component of the growing toolkit available for the investigation of neural circuit structure and connectivity. It allows for the identification of first-order presynaptic connections to cell populations of interest across both the central and peripheral nervous system, helping to decipher the complex connectivity patterns of the neural networks that give rise to brain function. However, despite its utility, the efficiency with which genetically modified rabies virus spreads retrogradely across synapses remains uncertain. Currently, it is unknown what proportion of total inputs to a start cell of interest are labeled using this method. Here we use a new rabies virus construct that allows for the simultaneous labeling of pre and postsynaptic densities to investigate spread efficiency at the synapse level. We demonstrate that less than half of first-order presynaptic excitatory inputs to excitatory or inhibitory starter cell types are labeled. Furthermore, we find evidence that spread efficiency is not dependent on the subcellular location of the synaptic input.

Introduction

Monosynaptic rabies tracing using glycoprotein (G) – deleted rabies virus (RVdG) is a powerful tool for the study of neural circuit connectivity. This method enables scientists to label, genetically manipulate, or monitor the activity of brain-wide monosynaptic inputs to cell populations of interest. Since its introduction [1,2] it has been widely used for the identification of presynaptic inputs to single neurons [3–5], projection-defined neurons [6,7], adult-born neurons [8,9], transplanted neurons [10,11], hPSC-derived organoid neurons [12,13], and genetically defined

excitatory neurons [14,15], inhibitory neurons [16,17], and non-neuronal cell types [18,19]. In addition to being used for the identification of inputs, the incorporation of Ca^{2+} indicators and light-activated opsins into rabies reagents [20] now allow rabies tracing experiments to probe the relationship between function and connectivity [5,21,22]. The ability of genetically modified RVdG to selectively spread retrogradely between synaptically connected cells allows for the identification of presynaptic partners regardless of their distance from one another and has led to novel insights throughout brain regions of the central nervous system.

Despite the utility and widespread use of monosynaptic rabies tracing to study neural connectivity, there is uncertainty about the efficiency of transsynaptic spread from starter cells to input neurons. Although studies quantifying inputs to single neurons have provided some insight into the efficiency of spread [3,4,23], results vary widely across experimental conditions and no direct measurements of spread efficiency are available. Furthermore, using the convergence index, recent studies have shown that the number of input neurons labeled per starter cell can be improved about 10-fold by modifying the rabies glycoprotein [24] or replacing the rabies virus strain [25]. The convergence index is defined as the number of rabies-labeled input neurons divided by the number of starter cells. Despite making quantitative comparisons these studies relied on methods that result in large animal to animal variability and require tedious counting across many animals. Most importantly, these methods fail to quantify what proportion of all inputs are labeled. Additionally, the use of convergence index fails to address questions of the influence of biological factors on rabies spread efficiency, such as distance of synapses to the starter cell soma or differences of spread from different starter cell types.

In this study we examine the efficiency of RVdG retrograde spread from starter cell to input neurons at the synaptic level. We designed a new genetically modified rabies virus that

labels presynaptic and excitatory postsynaptic densities. This construct allows us to quantify the proportion of excitatory synapses on a starter cell that have their corresponding input neuron labeled with rabies virus. We found that rabies retrogradely labels about 35% to 40% of excitatory inputs to cell populations of interest. Furthermore, we found that efficiency of spread does not vary by the proximity or distance of synapses to the starter cell soma or by the type of neuronal dendrite. Overall, this study provides insight into some long-standing questions about the efficiency of monosynaptic rabies tracing.

Results

RVdG-PSD95GFP-SynPhRFP viral construct allows simultaneous fluorescent labeling of pre and postsynaptic densities

To investigate the efficiency of rabies transsynaptic spread from starter cells to input neurons we developed a high throughput and precise method to directly measure transsynaptic spread at the synapse level. We created a new deletion-mutant rabies virus construct that expresses two synaptic fusion protein transgenes from the rabies G locus (Figure 3.1A) modeled after existing rabies constructs known to label multiple subcellular compartments of neurons [26]. One gene encodes for a fusion protein of the postsynaptic marker, postsynaptic density 95 (PSD-95), and enhanced green fluorescent protein (eGFP). The other encodes for a fusion protein of the presynaptic marker synaptophysin (SynPh) and the brighter and more photostable red fluorescent protein TagRFP-T [27]. We chose the synaptophysin-TagRFP-T (SynPhRFP) fusion protein as it has previously been shown to result in a punctate red fluorescent pattern that colocalizes with varicosities on axons when expressed from the rabies genome [26]. Injection of RVdG-PSD95GFP-SynPhRFP in mouse primary visual cortex (V1) resulted in strong punctate

Figure 3.1 RVdG-PSD95GFP-SynPhRFP allows simultaneous fluorescent labeling of pre and postsynaptic densities. (A) Schematic of RVdG-PSD95GFP-SynPhRFP viral construct design. Two transgenes were inserted into the G locus of the rabies genome. One encodes a presynaptically-targeted fluorescent fusion protein, synaptophysin TagRFP-T (SynPhRFP), and the other a postsynaptically targeted fluorescent fusion protein, PSD-95 eGFP (PSD95GFP). (B) Coronal sections of mouse V1 infected with EnvA+ RVdG-PSD95GFP-SynPhRFP imaged at 20X with confocal microscopy. Top row shows neurons expressing both PSD95GFP and SynPhRFP fusion proteins. Bottom row shows a zoomed in image of the region enclosed by the dashed square in the top row. White arrows point to PSD-95 puncta, blue arrows to synaptophysin puncta, and gray arrows to large non-specific nuclear fluorescent aggregates. Scale bars represent 100 um (top row) or 10 um (bottom row). (C) Airyscan super-resolution images taken at 63X showing co-localization of PSD95GFP fusion protein expressed from the rabies genome with anti-PSD95 antibody staining in magenta. Scale bar = 1 um.

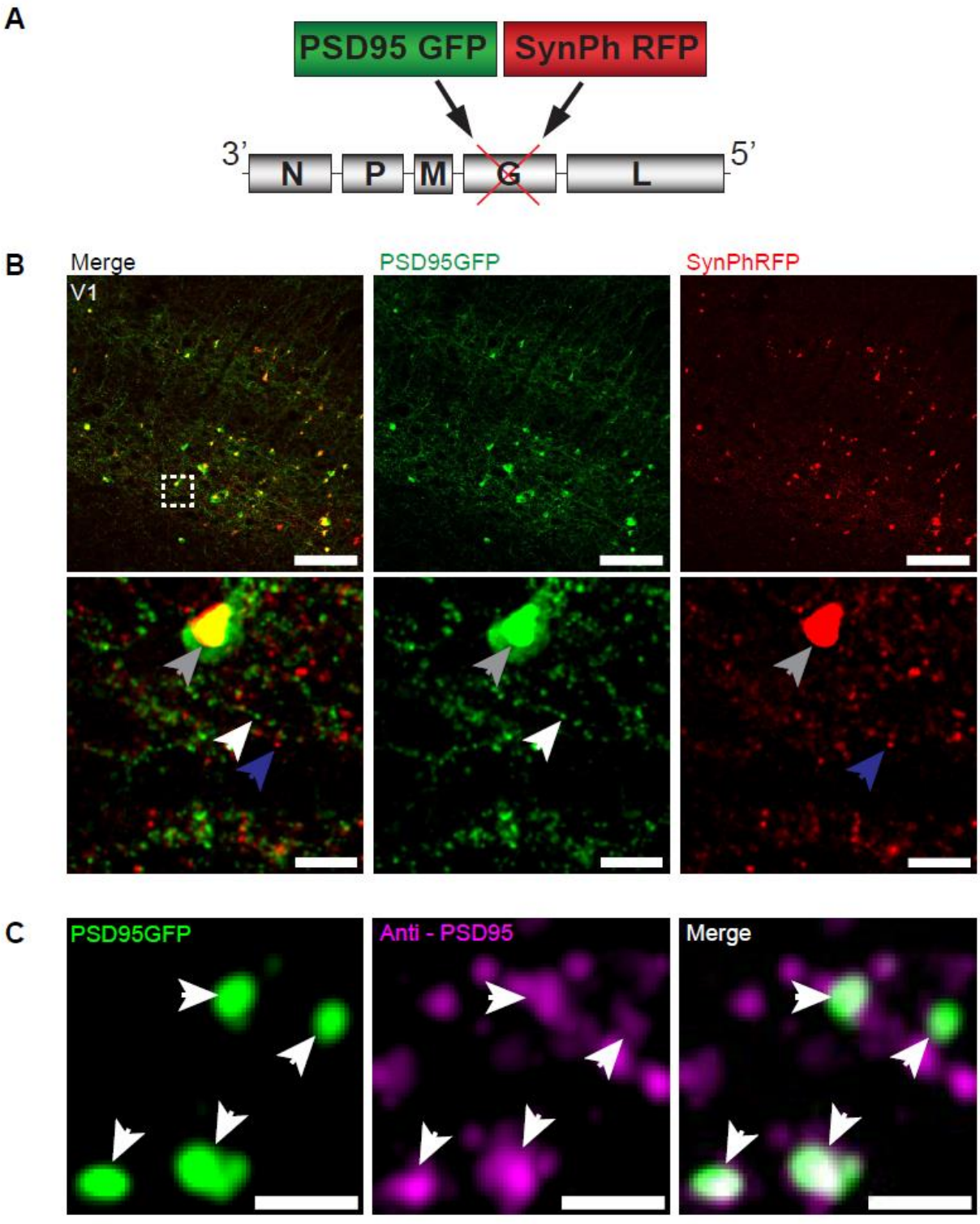
A
PSD95 GFP
SynPh RFP
3'
N
P
M
G
L
5'
B
Merge
V1
PSD95GFP
SynPhRFP
C
PSD95GFP
Anti - PSD95
Merge

green and red fluorescent labeling (Figure 3.1B), with green labeling prominent on dendrites and dendritic spine (Figure 3.2E, 3.2F) that colocalized with antibody staining against endogenous PSD-95 (Figure 3.1C).

Rabies transsynaptic spread efficiency across excitatory synapses from excitatory starter neurons

To quantify the proportion of inputs labeled with rabies virus we injected three Cre-dependent helper adeno-associated virus (AAV) into Nr5a1-Cre mice to sparsely target initial rabies infection to L4 excitatory neurons (Figure 3.2A, 3.2B). AAV8-nef-AO-66/71-TVA950 (AAV-CIAO-TVA), expresses the TVA receptor for the avian sarcoma leukosis virus envelope protein, EnvA, which is necessary for entry of pseudotyped $EnvA^+$ RVdG into Cre^+ cells. However, recombinant-independent off-target leak expression of transgenes is common in recombinase-dependent DIO and FLEX AAV constructs. Because even miniscule quantities of TVA leak expression is sufficient for pseudotyped rabies to enter off-target cells and confound results [28], it was necessary to minimize leak expression of TVA. We therefore used the novel cross-over insensitive ATG-out (CIAO) AAV construct, which has been shown to eliminate leak expression and provide reliable and targeted transgene expression [29], to express TVA in our population of interest. AAV8-hSyn-FLEX-H2BBFP-oG expresses optimized rabies glycoprotein (oG) [24], which allows for trans-complementation in EnvA+ RVdG infected neurons, also termed starter cells, allowing the rabies to spread retrogradely into presynaptically connected inputs. Co-expression of nuclear mTagBFP2 (BFP), a brighter and more photostable blue fluorescent protein [30], and oG allows for the unambiguous identification of starter cells (Figure 3.2C, 3.2E). Because H2BBFP only labels the nucleus of starter cells, we used AAV-CAG-FLEX-smFP_myc

to trace their dendrites. This AAV expresses spaghetti monster fluorescent protein (smFP), which consists of dark non-fluorescent GFP fused to 10 Myc epitope tags that can be combined with anti-Myc antibody staining to attain bright fluorescent labeling of subcellular structures [31]. Infection of L4 excitatory neurons with AAV-CAG-FLEX-smFP_myc resulted in strong dendritic labeling that improved the ability to accurately trace apical and basal dendrites of starter cells (Figure 3.2C, 3.2E, 3.2F). After 3 weeks, $EnvA^+$ RVdG-PSD95GFP-SynPhRFP was injected into the same location in V1 and allowed to express for 7 days. We observed that dorsal lateral geniculate nucleus (dLGN) long-distance inputs to L4 excitatory neurons were reliably labeled with RVdG-PSD95GFP-SynPhRFP (Figure 3.2D).

Starter neurons that also expressed smFP were first identified using wide-field fluorescence microscopy. Select areas of starter neuron dendrites were imaged using Airyscan super-resolution microscopy [32] to increase the resolution and signal-to-noise and allow visualization of single synaptic puncta (Figure 3.2F). To assess the transsynaptic spreading efficiency, we quantified the proportion of starter cell excitatory postsynaptic specializations, labeled with PSD95GFP, that were directly opposed with rabies-labeled presynaptic terminals, labeled with SynPhRFP (Figure 3.2F). Because L4 excitatory neurons connect to one another, we also calculated the proportion of PSD95GFP puncta opposed to SynPhRFP in experiments that omitted oG (Figure 3.S1A, 3.S1B, 3.S1C). The omission of oG prevents retrograde spread of rabies virus and labeling of input neurons (Figure 3.2D), therefore observed SynPhRFP colocalization with PSD95GFP are presumed to be a result of L4 to L4 excitatory neuron connections. We found that neurons in which oG was used for trans-complementation displayed significantly higher proportions of PSD95GFP puncta colocalized with SynPhRFP compared to neurons in which oG was omitted (50.61 ± 3.92% versus 8.86 ± 1.79% respectively, Wilcoxon

Figure 3.2 Efficiency of transsynaptic spread from excitatory L4 Nr5a1+ starter cells to excitatory inputs. (A) Schematic illustration of experimental design and timeline for monosynaptic rabies tracing. Nr5a1-Cre mice were injected in V1 with a mixture of AAV-CIAO-TVA, AAV-FLEX-H2BBFP-oG, and AAV-FLEX-smFP_myc. 3 weeks later EnvA+ RVdG-PSD95GFP-SynPhRFP was injected into the same site and allowed to express for 7 days. (B) Schematic of rabies retrograde spread efficiency quantification paradigm. Starter neurons are distinguished from input neurons based on expression of nuclear BFP from AAV-FLEX-H2BBFP-oG in addition to fusion proteins from EnvA+ RVdG-PSD95GFP-SynPhRFP. Starter neurons expressing smFP_myc are used for synaptic quantification to allow tracing of distal dendrites. Retrograde spread efficiency is measured by quantifying the proportion of postsynaptic densities (PSD95GFP) on the starter neuron opposed with rabies-labeled presynaptic terminals (SynPhRFP). (C) Representative example images of V1 injection site, obtained using widefield fluorescence microscopy at 10X. Scale bar = 200um. (D) Coronal section example images obtained using widefield fluorescence microscopy at 10X showing long range monosynaptic input neurons in dLGN to Nr5a1+ L4 neurons in V1 when using the new RVdG construct (top). No retrograde spread is observed when glycoprotein is omitted, see Figure 3.S1 for additional information. Insets are zoomed in images of dashed box regions. Scale bar represents 1 mm in hemisection image or 200 um in inset. (E) Images obtained using Airyscan super-resolution imaging at 63X. Left, example image of starter neuron (H2BBFP+,PSD95GFP+, and SynPhRFP+) labeled with smFP_myc. Middle, example image of the distal domain of an apical dendrite of a starter neuron. Right, example image of the proximal domain of a basal dendrite. Scale bar = 20um (all three). (F) Spatial resolution using Airyscan imaging is sufficient to quantify rabies transsynaptic spread at the synapse level. Zoomed in image of boxed region in (E) right, illustrating PSD-95 puncta co-colocalized with cytoplasmic smFP_myc. Top, yellow boxed region highlights a spine with PSD-95 puncta without an opposed rabies-labeled presynaptic density. White boxed region highlights a spine with PSD-95 puncta with an opposed rabies-labeled presynaptic density. Middle row, zoomed in images of yellow boxed regions and bottom row are zoomed in images of white boxed regions. Top, scale bar = 2um and middle and bottom scale bar = 0.5 um. (G) Percent of postsynaptic densities (PSD95GFP) on Nr5a1+ starter cells opposed with rabies-labeled presynaptic terminals (SynPhRFP). Left, quantification of colocalization at baseline (no glycoprotein) due to L4 to L4 connections compared to colocalization from transsynaptic spread (with glycoprotein). Middle, colocalization on apical vs basal dendrites. Right, colocalization on the distal vs proximal domains of apical dendrites. Values are reported as mean ± SEM. Statistics were calculated from the Wilcoxon rank-sum test for non-parametric comparisons. Individual data points (circles) indicate values for each neuron. ns, not significant, ***$p \leq 0.001$

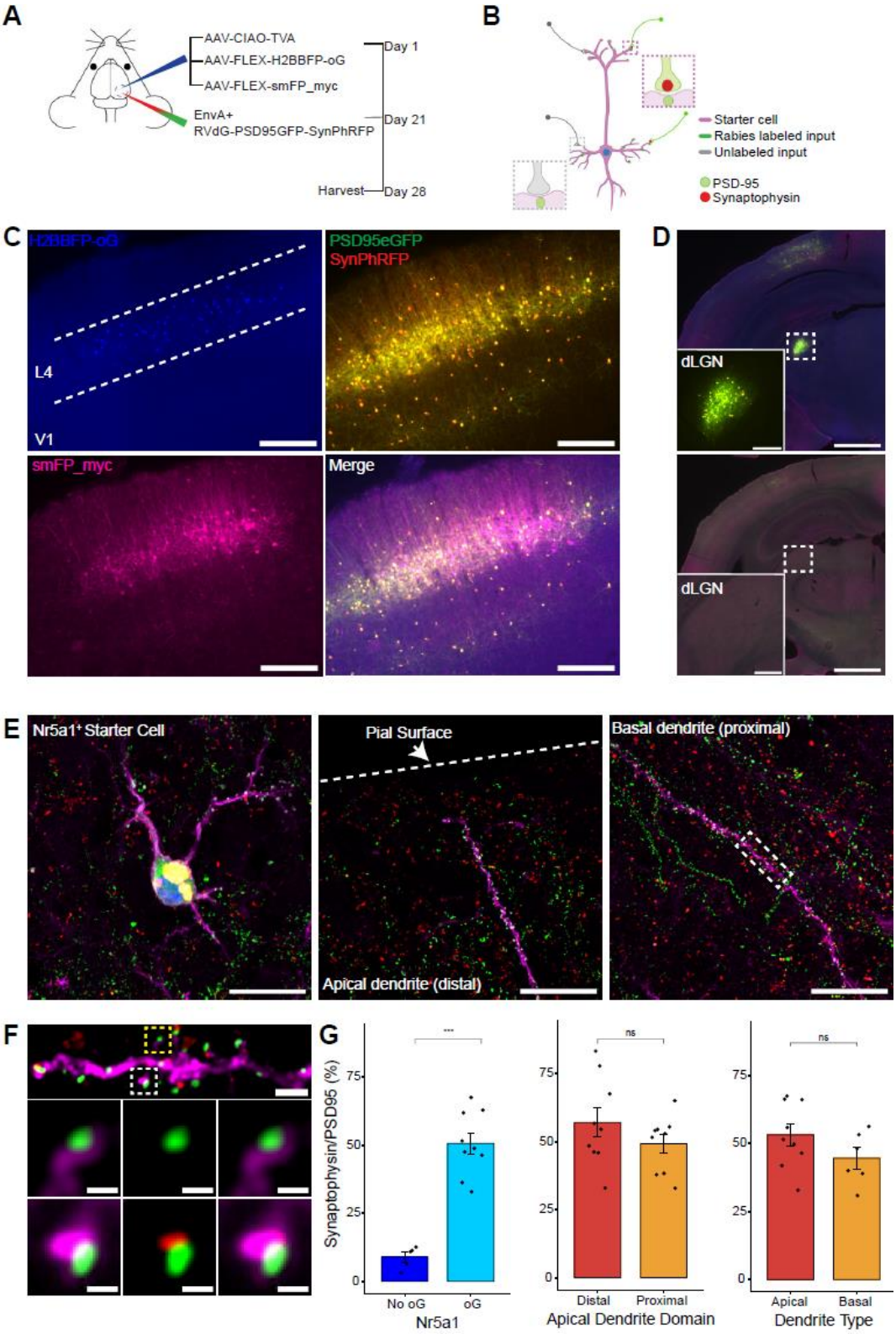
A
AAV-CIAO-TVA
AAV-FLEX-H2BBFP-oG
AAV-FLEX-smFP_myc
EnvA+
RVdG-PSD95GFP-SynPhRFP
Day 1
Day 21
Harvest
Day 28
B
Starter cell
Rabies labeled input
Unlabeled input
PSD-95
Synaptophysin
C
H2BBFP-oG
L4
V1
PSD95eGFP
SynPhRFP
smFP_myc
Merge
D
dLGN
dLGN
E
Nr5a1+ Starter Cell
Pial Surface
Apical dendrite (distal)
Basal dendrite (proximal)
F
G
Synaptophysin/PSD95 (%)
***
ns
ns
No oG
oG
Nr5a1
Distal
Proximal
Apical Dendrite Domain
Apical
Basal
Dendrite Type

rank-sum test, p = 0.001, n= 9 neurons across 3 mice and n=5 neurons across 2 mice; Figure 3.2G). Within experimental condition groups, puncta colocalization did not vary significantly across neurons from distinct experimental animals.

To determine how efficiency of spread is related to distance from the cell body we sampled from different portions of the dendritic arbors of starter cells. Sampled areas within 75um of the soma were classified as proximal dendritic domains and areas within 75um of the pial surface were considered distal domains. We found no significance difference between efficiency of spread at proximal regions of apical dendrites compared to the distal regions as determined by PSD95GFP and SynPhRFP puncta colocalization (49.14 ± 3.49% versus 57 ± 5.43% respectively, Wilcoxon rank-sum test, p = 0.34; Figure 3.2G). We also compared retrograde spread efficiency at basal dendrites to apical dendrites and observed no significant difference (44.52 ± 3.96% versus 53.05 ± 3.99% respectively, Wilcoxon rank-sum test, p = 0.22; Figure 3.2G).

Rabies transsynaptic spread efficiency across excitatory synapses from inhibitory starter neurons

To assess possible differences in rabies retrograde spread efficiency for different starter cell types, we conducted monosynaptic rabies tracing using RVdG-PSD95GFP-SynPhRFP as described above using mouse lines that express Cre recombinase in two distinct types of inhibitory neurons. We used the knock-in Som-IRES-Cre and Vip-IRES-Cre lines to target initial infection to either somatostatin (Sst)-expressing or vasoactive intestinal peptide (Vip)-expressing inhibitory neurons (Figure 3.3A). We selected Sst and Vip interneurons as both exhibit very low levels of recurrent connections compared to parvalbumin (Pvalb)-expressing neurons, which

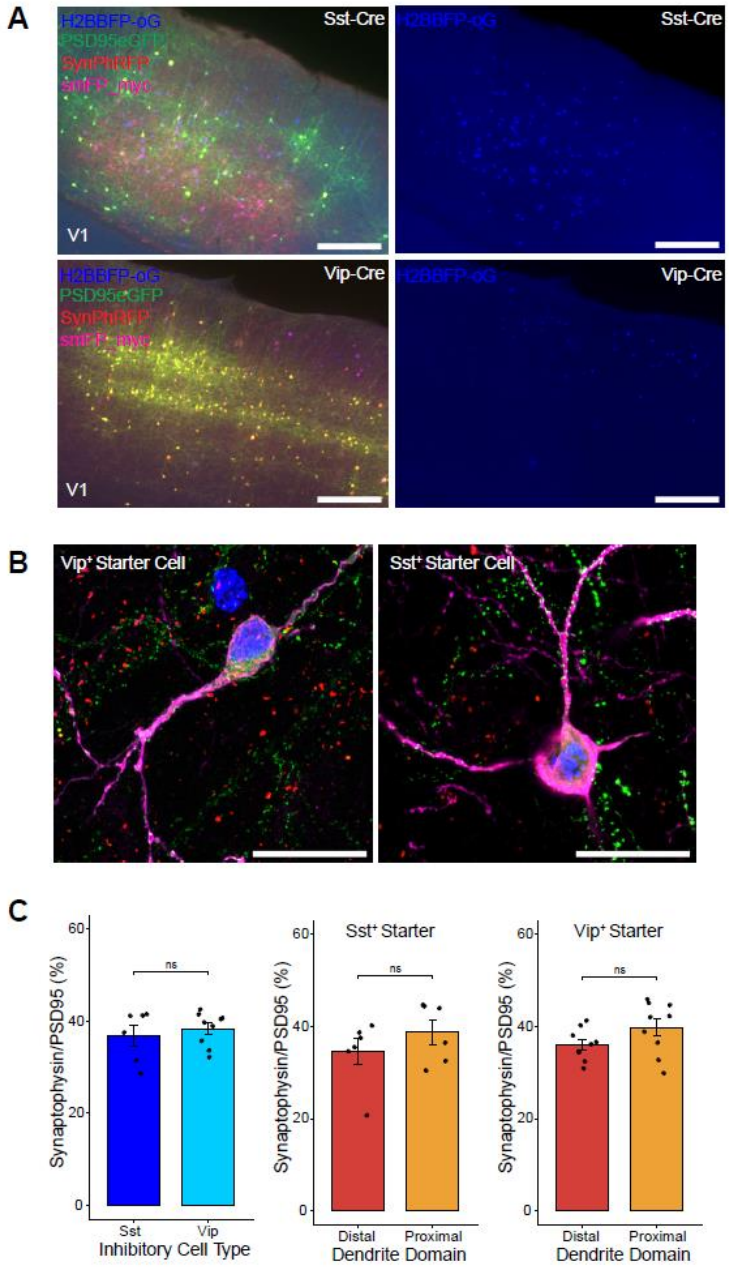

Figure 3.3 Efficiency of transsynaptic spread from inhibitory starter cells to excitatory inputs. (A) Representative example images of V1 injection site for Sst-Cre mouse line (top) and Vip-Cre mouse line (bottom), obtained using widefield fluorescence microscopy at 10X. Scale bar = 200um. (B) Images obtained using Airyscan super-resolution imaging at 63X. Example image of Vip+ (right) and Sst+ (left) starter neurons (H2BBFP+,PSD95GFP+, and SynPhRFP+) labeled with smFP_myc. Scale bar = 20um. (C) Left, percent of postsynaptic densities (PSD95GFP) on VIP+ and Sst+ starter cells opposed with rabies-labeled presynaptic terminals (SynPhRFP). Middle, colocalization on the distal vs proximal domains of Sst+ dendrites. Right, colocalization on the distal vs proximal domains of Vip+ dendrites. Values are reported as mean ± SEM. Statistics were calculated from Wilcoxon rank-sum test for non-parametric comparisons. Individual data points (circles) indicate values for each neuron. ns, not significant.

connect extensively to each other [33,34]. We found no significant difference between the percent of PSD95GFP puncta opposed with SynPhRFP on Sst dendrites compared to Vip dendrites (36.93 ± 2.29% versus 38.38± 1.22% respectively, Wilcoxon rank-sum test, p = 0.86, n = 6 neurons across 2 mice and n = 9 neurons across 3 mice; Figure 3.3C). We also assessed whether retrograde spread efficiency varied based on distance from the cell body. For Sst starter cells, colocalization of PSD95GFP with SynPhRFP on proximal dendritic domains did no differ significantly from distal dendritic domains (38.803 ± 2.65% versus 34.612 ± 2.88% respectively, Wilcoxon rank-sum test, p = 0.48). We observed similar results for Vip starter cells, with no difference between retrograde spread efficiency at proximal versus distal domains (39.80 ± 1.90% versus 36.122 ± 1.14% respectively, Wilcoxon rank-sum test, p = 0.11)

Discussion

Genetically modified RVdG has proven instrumental in deciphering the intricate connectivity patterns of neural networks. Here we investigated the efficiency with which RVdG spreads retrogradely across excitatory synapses and report, for the first time, direct measurements of the proportion of presynaptic inputs to a starter neuron of interest that are labeled using the monosynaptic rabies tracing system. Our results demonstrate that only a fraction of presynaptic inputs to starter cells are labeled, with about 35% to 40% of excitatory inputs to examined cell types labeled when using oG and the SAD-B19 rabies strain. Furthermore, we found that efficiency of spread did not vary depending on the distance of synapses to the cell body or across dendrite types.

Considering the finding that rabies labels less than half of synaptic inputs, it is likely that differential spread of rabies virus leads to differences in the probability of distinct input types

being labeled. Although we found evidence that the subcellular location of synaptic contacts of input cells onto the dendrites of starter cells does not affect spread efficiency it remains unknown what leads to the observed incomplete labeling. It is possible that this is affected by the number of synaptic contacts a presynaptic neuron makes onto the starter cell or differences in uptake receptors on the axon of distinct input cell types [28]. It is important to note that we only examined spread efficiency at excitatory synapses, labeled with the excitatory postsynaptic density marker PSD-95, and did not quantify the efficiency of spread to inhibitory presynaptic inputs.

Prior studies suggest that maximizing glycoprotein expression, either through the use of strong promoters [16] or optimized helper virus concentration [35], increases spread efficiency. Importantly, the use of 2A linker elements has been implicated to reduce expression levels of glycoprotein [36,37]. Thus, the use of separate AAVs, with one expressing glycoprotein independently from other genes, is recommended to improve efficiency. In the described experiments we utilized a 2A linker element to incorporate both nuclear BFP and oG into the same helper virus to achieve unambiguous identification of starter cells expressing oG, which was required for the measurement of transsynaptic spread. We therefore expect that efficiency of spread may be higher in experiments using AAVs that express glycoprotein independently compared to values reported here. Overall, we report the efficiency of spread achieved in multiple conditions consisting of distinct starter neuron types. Additionally, the described approach can be used by other researchers to test efficiency of spread across different rabies reagents, distinct input cell types, and starter neuron types not tested in this study.

Methods

Mouse Transgenic Lines

All experimental procedures were approved by the Salk Institute Animal Care and Use Committee. C57BL/6J mice were used as wild-type. GENSAT BAC transgenic Nr5a1-Cre, knock-in Som-IRES-Cre, and knock-in Vip-IRES-Cre mice have been previously described [38,39]. Transgenic mice were maintained on C57BL/6J backgrounds. Mice were housed with a 12-hour light and 12-hour dark cycle and *ad libitum* access to food and water. Both male and female mice were used for experiments.

Virus Preparation

The following AAVs were produced by the Salk GT3 Viral Core: AAV8-hSyn-FLEX-H2BmTagBFP2-oG (3.57E+13 GC/ml) and AAV8-nef-AO-66/71-TVA950 (5.25E+13 GC/mL). AAV1-CAG.FLEX.GFPsm_myc.WPRE.SV40 (1.12E+13 GC/ml) was purchased from Addgene. EnvA+ RVdG-5PSD95eGFP-SynPhRFP (1.55E+08 IU/ml) was produced by the Salk GT3 Viral Core.

Animal Surgery for Virus Injection

For rabies transsynaptic spread efficiency experiments mice received AAV helper injections at postnatal day (P) 50. Mice were initially anesthetized with 2% isoflurane and maintained at 1.5% isoflurane after placement on a stereotax (David Kopf Instruments, Model 940 series) for surgery and stereotaxic injections. A small craniotomy was made with a mounted drill over the primary visual cortex of the left hemisphere using the following coordinates: 3.4 mm posterior and 2.6 mm lateral relative to bregma. The following viruses AAV8-hSyn-FLEX-

H2BmTagBFP2-oG, AAV8-nef-AO-66/71-TVA950, and AAV1-CAG.FLEX.GFPsm_myc.WPRE.SV40 were mixed at a ratio of 1:40, 1:100, and 1:2 respectively. 100nl of mixture was injected into the center of V1 0.5–0.7 mm ventral from the pia using a pulled glass pipette with a tip size of 30um connected to a 1ml syringe with 18G tubing adapter and tubing. To prevent backflow, the pipette was left in the brain for 5 minutes after injection. Three weeks after AAV helper injection, 150 nl of EnvA+ RVdG-5PSD95eGFP-SynPhRFP was injected into the same site in V1. Mice were housed for 10 days to allow for transsynaptic rabies spread and fluorescent protein expression. After recovery, mice were given water with ibuprofen (30mg/kg) and housed for 10 days to allow for transsynaptic rabies spread and fluorescent protein expression.

Histology

Ten days after rabies injection, brains were harvested after transcardial perfusion using PBS followed by 4% paraformaldehyde (PFA). Brains were dissected out from skulls and post-fixed with 2% PFA and 15% sucrose in PBS at 4°C for 16–20 hours, then immersed in 30% sucrose in PBS at 4°C before sectioning. 50 um coronal brain sections were prepared using a freezing microtome and stored in PBS with 0.01% sodium azide at 4°C. Free-floating sections were incubated at 4°C for 16 hours with rabbit anti-Myc (1:500, C3956; Sigma-Aldrich) primary antibody in PBS/0.5% normal donkey serum/0.1% Triton X-100, followed by donkey anti-rabbit conjugated to Alexa 647 (A-21206, ThermoFisher) at room temperature for 2–3 hours. Immunostained tissue sections were mounted on slides with polyvinyl alcohol mounting medium containing DABCO and allowed to air-dry overnight.

Image Acquisition and Analysis

Individual sections were first scanned at 10x magnification using an Olympus BX63 wide-field fluorescent microscope to detect starter neurons triple positive for H2BBFP-oG, smFP_myc, and RVdG-PSD95GFP-SynPhRFP. Individual starter neurons were then imaged using a Zeiss LSM 880 Airyscan FAST Microscope with a Plan-Apochromat 63x/1.4 Oil DIC M27 objective. First, neurons were confirmed to be starter neurons by checking for expression of nuclear BFP. Z-stacks of images were acquired with a step interval of 500 nm for select dendritic domains. Dendrites immediately next to the soma and spanning 75um away were defined as proximal dendrites and representative images were acquired. Using expression of smFP_myc, dendrites were traced from the soma up to the pial surface. Dendritic regions spanning 75um from the pial surface were acquired and designated as distal domains. Images were processed and analyzed using NIH ImageJ software (FIJI). Images were first analyzed with only the far-red (smFP_myc) and green channel visible to count all PSD95GFP labeled postsynaptic densities colocalized with the far-red labeled dendritic region. After postsynaptic counts for that region were quantified, the red channel was turned on to quantify the amount of presynaptic densities colocalized with postsynaptic densities. Due to the abundance of synapses across a 50um coronal section, puncta were counted manually one z-plane at a time. Wilcoxon rank-sum test for non-parametric comparisons was used for statistical analysis. For all figures: ***, $p < 0.001$; ns = not significant, $p > 0.05$.

Appendix

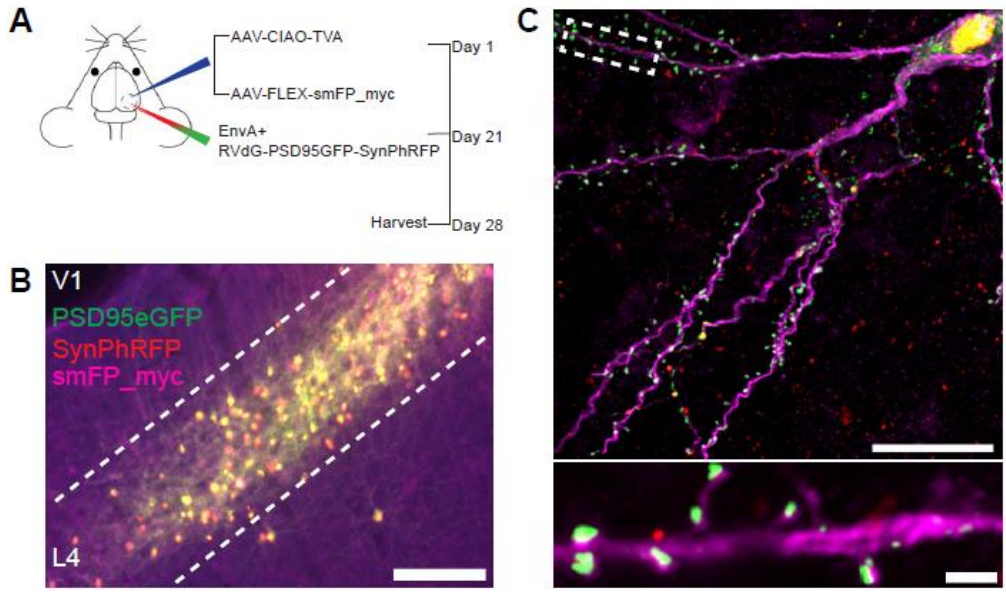

Figure 3.S1 (A) Schematic illustration of experimental design and timeline for control experiments without glycoprotein. Nr5a1-Cre mice were injected in V1 with a mixture of AAV-CIAO-TVA and AAV-FLEX-smFP-myc. 3 weeks later EnvA+ RVdG-PSD95GFP-SynPhRFP was injected into the same site and allowed to express for 7 days. (B) Representative image of V1 injection site, obtained using widefield fluorescence microscopy at 10X. Scale bar = 200um. (C) Images obtained using Airyscan super-resolution imaging at 63X. Top, example image of rabies-infected neuron labeled with smFP_myc, without glycoprotein. Bottom, zoomed in image of boxed region in top image, illustrating PSD-95 puncta colocalized with cytoplasmic smFP_myc. Scale bar = 20um (top) and scale bar = 2um (bottom).

Acknowledgements

Chapter 3, in full, is currently being prepared for submission for publication and will include Will N. Lagos, and Neelakshi Patne, as co-authors and Professor Edward Callaway as the senior author. The dissertation author will be the first author of this work.

References

1. Wickersham IR, Finke S, Conzelmann KK, Callaway EM. Retrograde neuronal tracing with a deletion-mutant rabies virus. *Nat Methods*. 2007;4(1):47-49. doi:10.1038/nmeth999

2. Wickersham IR, Lyon DC, Barnard RJO, Mori T, Finke S, Conzelmann KK, Young JAT, Callaway EM. Monosynaptic Restriction of Transsynaptic Tracing from Single, Genetically Targeted Neurons. *Neuron*. 2007;53(5):639-647. doi:10.1016/j.neuron.2007.01.033

3. Marshel JH, Mori T, Nielsen KJ, Callaway EM. Targeting Single Neuronal Networks for Gene Expression and Cell Labeling In Vivo. *Neuron*. 2010;67(4):562-574. doi:10.1016/j.neuron.2010.08.001

4. Rancz EA, Franks KM, Schwarz MK, Pichler B, Schaefer AT, Margrie TW. Transfection via whole-cell recording in vivo: bridging single-cell physiology, genetics and connectomics. *Nat Neurosci*. 2011;14(4):527-532. doi:10.1038/nn.2765

5. Wertz A, Trenholm S, Yonehara K, Hillier D, Raics Z, Leinweber M, Szalay G, Ghanem A, Keller G, Rózsa B, Conzelmann KK, Roska B. Single-cell–initiated monosynaptic tracing reveals layer-specific cortical network modules. *Science*. 2015;349(6243):70-74. doi:10.1126/science.aab1687

6. Cruz-Martín A, El-Danaf RN, Osakada F, Sriram B, Dhande OS, Nguyen PL, Callaway EM, Ghosh A, Huberman AD. A dedicated circuit links direction-selective retinal ganglion cells to the primary visual cortex. *Nature*. 2014;507(7492):358-361. doi:10.1038/nature12989
7. Levine AJ, Hinckley CA, Hilde KL, Driscoll SP, Poon TH, Montgomery JM, Pfaff SL. Identification of a cellular node for motor control pathways. *Nat Neurosci*. 2014;17(4):586-593. doi:10.1038/nn.3675

8. Deshpande A, Bergami M, Ghanem A, Conzelmann KK, Lepier A, Götz M, Berninger B. Retrograde monosynaptic tracing reveals the temporal evolution of inputs onto new neurons in the adult dentate gyrus and olfactory bulb. *Proceedings of the National Academy of Sciences*. 2013;110(12):E1152-E1161. doi:10.1073/pnas.1218991110

9. Garcia I, Quast KB, Huang L, Herman AM, Selever J, Deussing JM, Justice NJ, Arenkiel BR. Local CRH Signaling Promotes Synaptogenesis and Circuit Integration of Adult-Born Neurons. *Developmental Cell*. 2014;30(6):645-659. doi:10.1016/j.devcel.2014.07.001

10. Doerr J, Schwarz MK, Wiedermann D, Leinhaas A, Jakobs A, Schloen F, Schwarz I, Diedenhofen M, Braun NC, Koch P, Peterson DA, Kubitscheck U, Hoehn M, Brüstle O. Whole-brain 3D mapping of human neural transplant innervation. *Nat Commun*. 2017;8(1):14162. doi:10.1038/ncomms14162

11. Grealish S, Heuer A, Cardoso T, Kirkeby A, Jönsson M, Johansson J, Björklund A, Jakobsson J, Parmar M. Monosynaptic Tracing using Modified Rabies Virus Reveals Early

and Extensive Circuit Integration of Human Embryonic Stem Cell-Derived Neurons. *Stem Cell Reports*. 2015;4(6):975-983. doi:10.1016/j.stemcr.2015.04.011

12. Andersen J, Revah O, Miura Y, Thom N, Amin ND, Kelley KW, Singh M, Chen X, Thete MV, Walczak EM, Vogel H, Fan HC, Paşca SP. Generation of Functional Human 3D Cortico-Motor Assembloids. *Cell*. 2020;183(7):1913-1929.e26. doi:10.1016/j.cell.2020.11.017

13. Miura Y, Li MY, Birey F, Ikeda K, Revah O, Thete MV, Park JY, Puno A, Lee SH, Porteus MH, Pașca SP. Generation of human striatal organoids and cortico-striatal assembloids from human pluripotent stem cells. *Nat Biotechnol*. 2020;38(12):1421-1430. doi:10.1038/s41587-020-00763-w

14. DeNardo LA, Berns DS, DeLoach K, Luo L. Connectivity of mouse somatosensory and prefrontal cortex examined with trans-synaptic tracing. *Nat Neurosci*. 2015;18(11):1687-1697. doi:10.1038/nn.4131

15. Kim EJ, Juavinett AL, Kyubwa EM, Jacobs MW, Callaway EM. Three Types of Cortical Layer 5 Neurons That Differ in Brain-wide Connectivity and Function. *Neuron*. 2015;88(6):1253-1267. doi:10.1016/j.neuron.2015.11.002

16. Miyamichi K, Shlomai-Fuchs Y, Shu M, Weissbourd BC, Luo L, Mizrahi A. Dissecting Local Circuits: Parvalbumin Interneurons Underlie Broad Feedback Control of Olfactory Bulb Output. *Neuron*. 2013;80(5):1232-1245. doi:10.1016/j.neuron.2013.08.027

17. Wall NR, De La Parra M, Sorokin JM, Taniguchi H, Huang ZJ, Callaway EM. Brain-Wide Maps of Synaptic Input to Cortical Interneurons. *J Neurosci*. 2016;36(14):4000-4009. doi:10.1523/JNEUROSCI.3967-15.2016

18. Clark IC, Gutiérrez-Vázquez C, Wheeler MA, Li Z, Rothhammer V, Linnerbauer M, Sanmarco LM, Guo L, Blain M, Zandee SEJ, Chao CC, Batterman KV, Schwabenland M, Lotfy P, Tejeda-Velarde A, Hewson P, Manganeli Polonio C, Shultis MW, Salem Y, Tjon EC, Fonseca-Castro PH, Borucki DM, Alves de Lima K, Plasencia A, Abate AR, Rosene DL, Hodgetts KJ, Prinz M, Antel JP, Prat A, Quintana FJ. Barcoded viral tracing of single-cell interactions in central nervous system inflammation. *Science*. 2021;372(6540):eabf1230. doi:10.1126/science.abf1230

19. Mount CW, Yalçın B, Cunliffe-Koehler K, Sundaresh S, Monje M. Monosynaptic tracing maps brain-wide afferent oligodendrocyte precursor cell connectivity. Nave KA, Westbrook GL, Lyons DA, eds. *eLife*. 2019;8:e49291. doi:10.7554/eLife.49291

20. Osakada F, Mori T, Cetin AH, Marshel JH, Virgen B, Callaway EM. New Rabies Virus Variants for Monitoring and Manipulating Activity and Gene Expression in Defined Neural Circuits. *Neuron*. 2011;71(4):617-631. doi:10.1016/j.neuron.2011.07.005

21. Tian J, Huang R, Cohen JY, Osakada F, Kobak D, Machens CK, Callaway EM, Uchida N, Watabe-Uchida M. Distributed and Mixed Information in Monosynaptic Inputs to Dopamine Neurons. *Neuron*. 2016;91(6):1374-1389. doi:10.1016/j.neuron.2016.08.018

22. Wester JC, Mahadevan V, Rhodes CT, Calvigioni D, Venkatesh S, Maric D, Hunt S, Yuan X, Zhang Y, Petros TJ, McBain CJ. Neocortical Projection Neurons Instruct Inhibitory Interneuron Circuit Development in a Lineage-Dependent Manner. *Neuron*. 2019;102(5):960-975.e6. doi:10.1016/j.neuron.2019.03.036

23. Miyamichi K, Amat F, Moussavi F, Wang C, Wickersham I, Wall NR, Taniguchi H, Tasic B, Huang ZJ, He Z, Callaway EM, Horowitz MA, Luo L. Cortical representations of olfactory input by trans-synaptic tracing. *Nature*. 2011;472(7342):191-196. doi:10.1038/nature09714

24. Kim EJ, Jacobs MW, Ito-Cole T, Callaway EM. Improved Monosynaptic Neural Circuit Tracing Using Engineered Rabies Virus Glycoproteins. *Cell Reports*. 2016;15(4):692-699. doi:10.1016/j.celrep.2016.03.067

25. Reardon TR, Murray AJ, Turi GF, Wirblich C, Croce KR, Schnell MJ, Jessell TM, Losonczy A. Rabies Virus CVS-N2cΔG Strain Enhances Retrograde Synaptic Transfer and Neuronal Viability. *Neuron*. 2016;89(4):711-724. doi:10.1016/j.neuron.2016.01.004

26. Wickersham IR, Sullivan HA, Seung HS. Axonal and subcellular labelling using modified rabies viral vectors. *Nat Commun*. 2013;4(1):2332. doi:10.1038/ncomms3332

27. Shaner NC, Lin MZ, McKeown MR, Steinbach PA, Hazelwood KL, Davidson MW, Tsien RY. Improving the photostability of bright monomeric orange and red fluorescent proteins. *Nat Methods*. 2008;5(6):545-551. doi:10.1038/nmeth.1209

28. Callaway EM, Luo L. Monosynaptic Circuit Tracing with Glycoprotein-Deleted Rabies Viruses. *J Neurosci*. 2015;35(24):8979-8985. doi:10.1523/JNEUROSCI.0409-15.2015
29. Fischer KB, Collins HK, Callaway EM. Sources of off-target expression from recombinase-dependent AAV vectors and mitigation with cross-over insensitive ATG-out vectors. *PNAS*. 2019;116(52):27001-27010. doi:10.1073/pnas.1915974116

30. Subach OM, Gundorov IS, Yoshimura M, Subach FV, Zhang J, Grüenwald D, Souslova EA, Chudakov DM, Verkhusha VV. Conversion of red fluorescent protein into a bright blue probe. *Chem Biol*. 2008;15(10):1116-1124. doi:10.1016/j.chembiol.2008.08.006

31. Viswanathan S, Williams ME, Bloss EB, Stasevich TJ, Speer CM, Nern A, Pfeiffer BD, Hooks BM, Li WP, English BP, Tian T, Henry GL, Macklin JJ, Patel R, Gerfen CR, Zhuang X, Wang Y, Rubin GM, Looger LL. High-performance probes for light and electron microscopy. *Nat Methods*. 2015;12(6):568-576. doi:10.1038/nmeth.3365

32. Huff J, Bergter A, Birkenbeil J, Kleppe I, Engelmann R, Krzic U. The new 2D Superresolution mode for ZEISS Airyscan. *Nat Methods*. 2017;14(12):1223-1223. doi:10.1038/nmeth.f.404

33. Campagnola L, Seeman SC, Chartrand T, Kim L, Hoggarth A, Gamlin C, Ito S, Trinh J, Davoudian P, Radaelli C, Kim MH, Hage T, Braun T, Alfiler L, Andrade J, Bohn P, Dalley R, Henry A, Kebede S, Mukora A, Sandman D, Williams G, Larsen R, Teeter C, Daigle TL, Berry K, Dotson N, Enstrom R, Gorham M, Hupp M, Dingman Lee S, Ngo K, Nicovich PR, Potekhina L, Ransford S, Gary A, Goldy J, McMillen D, Pham T, Tieu M, Siverts L, Walker M, Farrell C, Schroedter M, Slaughterbeck C, Cobb C, Ellenbogen R, Gwinn RP, Keene CD, Ko AL, Ojemann JG, Silbergeld DL, Carey D, Casper T, Crichton K, Clark M, Dee N, Ellingwood L, Gloe J, Kroll M, Sulc J, Tung H, Wadhwani K, Brouner K, Egdorf T, Maxwell M, McGraw M, Pom CA, Ruiz A, Bomben J, Feng D, Hejazinia N, Shi S, Szafer A, Wakeman W, Phillips J, Bernard A, Esposito L, D'Orazi FD, Sunkin S, Smith K, Tasic B, Arkhipov A, Sorensen S, Lein E, Koch C, Murphy G, Zeng H, Jarsky T. Local connectivity and synaptic dynamics in mouse and human neocortex. *Science*. 2022;375(6585):eabj5861. doi:10.1126/science.abj5861

34. Pfeffer CK, Xue M, He M, Huang ZJ, Scanziani M. Inhibition of inhibition in visual cortex: the logic of connections between molecularly distinct interneurons. *Nat Neurosci*. 2013;16(8):1068-1076. doi:10.1038/nn.3446

35. Lavin TK, Jin L, Lea NE, Wickersham IR. Monosynaptic Tracing Success Depends Critically on Helper Virus Concentrations. *Frontiers in Synaptic Neuroscience*. 2020;12. Accessed May 24, 2022. https://www.frontiersin.org/article/10.3389/fnsyn.2020.00006

36. Wall NR, Wickersham IR, Cetin A, Parra MDL, Callaway EM. Monosynaptic circuit tracing in vivo through Cre-dependent targeting and complementation of modified rabies virus. *PNAS*. 2010;107(50):21848-21853. doi:10.1073/pnas.1011756107

37. Watabe-Uchida M, Zhu L, Ogawa SK, Vamanrao A, Uchida N. Whole-Brain Mapping of Direct Inputs to Midbrain Dopamine Neurons. *Neuron*. 2012;74(5):858-873. doi:10.1016/j.neuron.2012.03.017

38. Harris JA, Hirokawa KE, Sorensen SA, Gu H, Mills M, Ng LL, Bohn P, Mortrud M, Ouellette B, Kidney J, Smith KA, Dang C, Sunkin S, Bernard A, Oh SW, Madisen L, Zeng H. Anatomical characterization of Cre driver mice for neural circuit mapping and manipulation. *Front Neural Circuits*. 2014;8:76. doi:10.3389/fncir.2014.00076

39. Taniguchi H, He M, Wu P, Kim S, Paik R, Sugino K, Kvitsani D, Fu Y, Lu J, Lin Y, Miyoshi G, Shima Y, Fishell G, Nelson SB, Huang ZJ. A Resource of Cre Driver Lines for Genetic Targeting of GABAergic Neurons in Cerebral Cortex. *Neuron*. 2011;71(6):995-1013. doi:10.1016/j.neuron.2011.07.026